Spring 5-8-2021

Multimodal Neuroimaging of HIV and Aging

Brandon Lew
University of Nebraska Medical Center

MULTIMODAL NEUROIMAGING OF HIV AND AGING

By

Brandon J. Lew

A DISSERTATION

Presented to the Faculty of

The Graduate College at the University of Nebraska

In Partial Fulfillment of Requirements

For the Degree of Doctor of Philosophy

Interdisciplinary Graduate Program in Biomedical Sciences

(Neuroscience)

Under the Supervision of Dr. Tony W. Wilson

University of Nebraska Medical Center

Omaha, Nebraska

February, 2021

Supervisory Committee:

Max J. Kurz, Ph.D.	Elizabeth Heinrichs-Graham Ph.D.
David E. Warren, Ph.D.	Alëna A. Balasanova, M.D.

ACKNOWLEDGEMENTS

There is a long list of people who have influenced and supported my journey throughout graduate school, all of whom I cannot thank enough. First and foremost I am thankful for my family. Principally, my wife Christina, who has supported me through far more than just graduate school. We have been together since high school and she has held my hand every step of the way since. I am also beyond thankful for our wonderful son, Oliver, whose endless smiles reminds me every day what is really important in life. I am thankful for my parents, Maria and David Lew, whom I now appreciate much more since becoming one, as well as my siblings, Samantha, Joseph, and Kayla, and all of the other members of my family for their support.

Secondly, I attribute much of my successes throughout graduate school towards having the greatest mentor, Dr. Tony Wilson. An outstanding mentor not only guides students toward their goals with encouragement and enthusiasm, but also serves as a role model and goes out of their way to support students in all aspects of their career. Tony has done all of this for me and more. It truly has been the pleasure of a lifetime to work under and learn from Tony, and I know I will always cherish my time in his lab and I will continue to look up to him as a lifelong mentor.

Many others played significant roles in my graduate training. For my MEG training, Dr. Elizabeth Heinrichs-Graham, Dr. Alex Wiesman, Dr. Amy Proskovec, and Tim McDermott were lab members before me who gave me wonderful and thorough training in MEG methodology. I also cannot underestimate the value of learning from and alongside Christine Embury and Rachel Spooner, whose graduate training paralleled mine. For my MRI training, I credit the fMRI course at MRN run by Dr. Vince Calhoun and others for giving a groundwork in fMRI research, Dr. Dave Warren's journal clubs for giving me an understanding of fMRI literature, and most critically, Dr. Gaelle Doucet, who gave me the one-on-one, hands on data processing instruction that made the

fMRI portion of this project possible. I would also like to thank Alex again for helping me learn Matlab code, which gave me the skills in computer programming that made this work possible.

With regard to these dissertation data specifically, there are a number of people who have helped make this project possible. Firstly, the research assistants and lab members who performed the recruitment and data acquisition for this project, some of whom included Jennifer O'Neill, Nichole Knott, Mackenzie Mills, Michael Rezich and Mikki Schantell. Secondly, for the data analysis of structural MRI data, I would like to thank Dr. Amy Proskovec for introducing me to the structural analysis pipeline used for this project. For analysis of functional MRI data, much of the credit goes to Dr. Gaelle Doucet and Marie McCusker. Marie and I embarked on the journey of analyzing resting state fMRI data, and she did the majority of the groundwork in preprocessing the data. Dr. Doucet then led us through the process after we ultimately ran into multiple road blocks, teaching us along the way. They deserve much of the credit for the fMRI portion of this project. For the resting state MEG data analysis, I must acknowledge Nicholas Christopher-Hayes's astounding computer programming work in making an artifact rejection toolbox, which was an integral part of the resting state MEG processing pipeline. Additionally, I'd like to thank Lauren Ott who helped with Figure 1, and Samantha Penhale and Emily Fitzgerald helped with Figure 2 of this dissertation. Finally, for the epigenetic age advancement calculations, I give full credit to those in other labs who processed these data, including Dr. Howard Fox, Brenda Morsey, Dr. Trey Ideker, and Dr. Tina Wang.

Working in such a productive and collaborative lab also cannot be underestimated. In addition to the members mentioned previously, I'd like to thank all of the other lab members during my graduate training, including but not limited to: other graduate students Yasra Arif, Chloe Meehan, Abraham Killanin and Seth Springer, postdoctoral fellows Dr. Brittany Taylor and Dr. Mason Price, and other members Jacob Eastman, Michaela Frenzel, Rebecca Losh, Maddie

Fung, Chloe Casagrande, Hallie Johnson, Madelyn Willett, Lisa Houseman, Sam Koshy, Abril Rangel-Pacheco, Anabel Salimian, Boman Groff, and Nathan Coolidge.

I would also like to specifically thank the participants included in this study, who generously volunteered their time and effort to make this science possible. Additionally, I would like to thank Dr. Susan Swindells, Dr. Sara Bares, and the entire team at the UNMC HIV specialty care clinic, who are not only wonderful research collaborators, but also astounding healthcare providers as I saw in my preceptorship time in the clinic.

And finally, I would like to thank my committee members, Dr. Max Kurz, Dr. Elizabeth Heinrichs-Graham, Dr. David Warren, Dr. Alëna Balasanova, who supervised my graduate training and this dissertation.

This work was financially supported by grants to my advisor, Tony W. Wilson, from then ational Institutes of Health (R01-MH103220; R01-MH116782; R01-MH118013; R01-DA DA041917), and the National Science Foundation (1539067). Additionally, my training was supported by a Ruth L. Kirschstein Predoctoral Fellowship from the National Institute on Drug Abuse (F30- DA048713), and supplemented by a research awards from the Office of Graduate Studies at the University of Nebraska Medical Center.

ABSTRACT

HIV infection remains a significant contributor to disease burden, and with the success of antiretroviral therapies, the population of people with HIV is aging. A growing literature suggests a relationship between HIV-infection and a profile of age advancement, most notably in molecular studies of epigenetics. However, despite the widely-known high prevalence of HIV-related brain atrophy, functional deficits, and HIV-associated neurocognitive disorder (HAND), epigenetic age advancement has not been linked to HIV-related changes in neuroimaging metrics. We applied three neuroimaging methods, structural MRI, resting state functional MRI, and resting state MEG, to study the brain structure and function of 121 virally-suppressed participants with HIV infection and 133 uninfected controls age 22-72. All participants were assessed for cognitive impairment, and blood samples were collected from a subset of participants to estimate epigenetic age. We examined the group-level interactive effects of HIV and chronological age, and then used individual estimations of epigenetic age to understand the relationship between age advancement and brain structure. Finally, we studied the effects of HIV-associated neurocognitive disorder. In brain structure, HIV-infection was related to grey matter reductions, independent of age. Using epigenetic age as a biomarker for age advancement, individual HIV-related age advancement was associated with reductions in total grey matter. HIV-associated neurocognitive disorder was associated with decreases in thalamic and hippocampal grey matter. Examining functional resting state networks, HIV-infection and age were independently associated with broad increases in between-network connectivity. In contrast to the structural results however, changes in resting state functional connectivity were not significantly associated with epigenetic age advancement. With respect to HAND, increases in functional connectivity with the ventral attention network appeared to be driven by PWH with HAND. Finally, in resting state oscillatory activity, while independent age related changes were identified in delta power, beta power, and

alpha peak frequency, no effects of HIV were identified. Exploring these null results, post-hoc Bayesian analyses showed evidence that many oscillatory metrics were equivalent between PWH and uninfected controls. In conclusion, despite viral suppression, accentuated grey matter loss and resting state functional network reorganization is evident with HIV-infection, while resting oscillatory activity is largely preserved. Greater biological age advancement appears to specifically relate to grey matter loss. These findings are a critical step towards understanding and treating the aging brain of PWH.

TABLE OF CONTENTS

LIST OF FIGURES

LIST OF TABLES

LIST OF ABBREVIATIONS

AIDS	Acquired Immune Deficiency Syndrome
ANCOVA	Analysis of Covariance
BF	Bayes Factor
BOLD	Blood Oxygen Level Dependent
cART	Combination Antiretroviral Therapy
CAT12	Computational Anatomy Toolbox
CDC	Center for Disease Control and Prevention
CNS	Central Nervous System
CpG	Cytosine-Phosphate-Guanine
DAN	Dorsal Attention Network
DMN	Default Mode Network
dSPM	Dynamical Statistical Parametric Mapping
EEG	Electroencephalography
fMRI	Functional Magnetic Resonance Imaging
FWHM	Full Width at Half Maximum
HAART	Highly Active Antiretroviral Therapy
HAND	HIV-Associated Neurocognitive Disorder
HIV	Human Immunodeficiency Virus
ICBM	International Consortium for Brain Mapping
MEG	Magnetoencephalography
MNI	Montreal Neurological Institute
MRI	Magnetic Resonance Imaging
NMR	Nuclear Magnetic Resonance
PWH	People with HIV
PSD	Power Spectrum Density
SPM	Statistical Parametric Mapping
SBM	Surface Based Morphometry

VAN	Ventral Attention Network
VBM	Voxel Based Morphometry

CHAPTER 1: Background

A Brief History of HIV

The history of Human Immunodeficiency Virus (HIV) represents one of the most significant scientific struggles, and at the same time one of the most significant scientific successes, in modern history. While the virus still remains prevalent today, discrete and incremental scientific progress since the discovery of the virus has allowed treatment of HIV to become highly effective. Such treatment is also becoming readily available across the world,[1] and we are now at a time where research (and dissertations) are beginning to focus on aging people with HIV (PWH), a point that might have been unimaginable decades ago.

The first documented cases of HIV in the US occurred in 1981 with a Center for Disease Control and Prevention (CDC) report of a rare lung infection, pneumocystis carinii pneumonia. Reports of severe immunodeficiency then became more recognized, and the term AIDS (Acquired Immune Deficiency Syndrome) was adopted by the CDC in 1982. At the time, life expectancy following a diagnosis was approximately two years,[2] essentially labeled as a terminal illness. Then, in 1983, Dr. Françoise Barré-Sinoussi and Dr. Luc Montagnier successfully identified the retrovirus that causes AIDS (HIV). Its identification allowed for the development of blood tests and further characterization of the virus. While the first antiretroviral therapy, zidovudine (a nucleoside reverse transcriptase inhibitor originally made for cancer therapy) was approved by the US Food and Drug Administration in 1987, the AIDS epidemic continued to grow, with AIDS becoming the leading cause of death for all Americans ages 25-44 in 1994. Scientific advances however continued to comprehend the biology of HIV, including contributions made by the director of the National Institute of Allergy and Infectious Diseases, Dr. Anthony Fauci.[3] This ultimately allowed for the development of further targeted antiretrovirals, including the development of the first

protease inhibitor in 1995, and then the first non-nucleoside reverse transcriptase inhibitor in 1996, ushering in an era of highly active antiretroviral therapy (HAART).[4] HAART become the new standard of care for PWH, and soon after in 1997, the CDC reported the first substantial decline in AIDS related deaths in the United States.[4]

Since then, over 30 different antiretrovirals have been developed as they have continued to be refined, targeting a diverse array of molecular targets. The combined use of multiple antiretrovirals (cART) has proven to be highly effective, allowing PWH to achieve and maintain viral suppression. Now today, these successes of cART have substantially increased life expectancy in PWH, and HIV infection has largely become a non-life threatening disease.

Now that PWH can achieve a life expectancy similar to that of uninfected individuals in the resource-rich countries,[5] HIV is often seen as a chronic disease. HIV eradication remains elusive, and PWH represent a significant portion of people with chronic illness. HIV infection continues to be a significant contributor to disease burden, being one of the leading causes of disability adjusted life years.[6] Additionally, with aging and long-term chronic disease, age-related co-morbidities have become a key concern in PWH.[7,8] Studies have noticed that there is an increased incidence of age-related comorbidities in PWH compared to uninfected individuals.[9] These comorbidities include cardiovascular disease,[10] liver disease,[11] renal disease,[12] and neurologic diseases such as HIV-associated neurocognitive disorder (HAND).[13] This profile of increased age related disease in PWH has led to theories of advanced aging related to HIV, whereby HIV infection propagates age-related changes in PWH.

HIV and Advanced Aging

There has been some debate in the literature on the manner in which HIV infection propagates pathologic aging. That is, multiple different terms have been utilized across studies to

describe this pathologic aging, including accelerated aging, premature aging, and accentuated aging.[9,14] These terms all refer to a process by which HIV propagates biological aging mechanisms, but it has been proposed that accelerated aging should be used to describe a process of continual, progressive cellular senescence caused by HIV, while premature or accentuated aging refers to a more singular "hit" in biological aging.[9] These definitions are not however universal, as other studies have distinguished between the phrases in terms of cross-sectional versus longitudinal interaction effects.[15] Here we use the more neutral term, age advancement, as used in Gross et al., 2016,[16] to encompass the multiple potential mechanisms by which HIV-related aging occurs.

Beyond this debate, studies agree that a biomarker of HIV-related advanced aging is needed.[9] One promising method that has been used to measure HIV-related age advancement is through the epigenetic clock. This method involves the quantification of specific CpG (cytosine phosphate guanines) sites from human cells.[17,18] These pre-determined sites have been identified in genes associated with development and aging, and examining epigenetic methylation at these sites allows for modeling of an individual's biological age. Age advancement can then be determined as the difference between an individual's chronological and biological age. Notably, this metric has shown to be predictive of all-cause mortality in older age,[19] and has been utilized in multiple fields. In the context of HIV specifically, advanced aging has been detected in both blood and brain tissue using the epigenetic clock,[16,20] and such HIV-related epigenetic aging has been linked to HAND.[21] Advanced epigenetic age has even been found in adolescents with perinatally acquired HIV infection.[22] However, it remains unclear how such advanced epigenetic aging relates to the changes in brain structure and function seen in HIV.

HIV and Advanced Aging in the Brain

When it comes to HIV's effects on the brain, HIV-associated neurocognitive disorder (HAND) is the most prevalent neurological comorbidity related to HIV infection. While cART has sharply reduced the most severe forms of HAND (i.e., HIV-associated dementia), milder forms of HAND remain quite common with estimates ranging from 35-70% of all HIV-infected patients.[13,23,24] These neurologic HIV-associated comorbidities are thought to be a result of viral invasion past the blood brain barrier into the CNS via infected monocytes, leading to widespread inflammation in the brain.[25] Chronic inflammation may also play a role in weakening the blood brain barrier,[26] and regardless the neuroinflammation is thought to be an important driving factor in neural injury and development of neurologic complications.[27,28] Relating this back to aging, the hypothesis of "inflammaging" is a key explanation for understanding the aging process.

Inflammaging refers to a low grade, chronic inflammation that characterizes aging.[29,30] It is thought to be related to a wide array of mechanisms, including pro-inflammatory cytokine production, mitochondrial dysfunction, and cellular waste and senescence.[31] Given that the brain acts as a viral reservoir for HIV, and that the presence of HIV leads to chronic neuroinflammation, inflammaging is an intuitive mechanism by which HIV may advance aging in the brain. Therefore, a biomarker of advanced aging could represent a discrete mechanistic measure to index how HIV affects the brain. Despite this, few studies have attempted to relate HIV-associated changes in brain structure and function to a biomarker of HIV-related age advancement, and even aging more broadly.

Central Research Question

To summarize, HIV infection remains highly prevalent, and the population of PWH is gradually aging. HIV may be related to even further advanced aging related to chronic

inflammatory processes, which are known to be present in the brain under HIV infection. However, relatively few studies have fully characterized the brain in the context of HIV infection, aging and advanced aging. Therefore, the central research question we aim to address is: how does HIV infection affect the brain in the context of aging, and how do such changes relate to advanced aging? To address this question, we aim to utilize multiple neuroimaging techniques and epigenetic age estimations to examine a large group of participants, with and without HIV, across the span of adulthood.

CHAPTER 2: Literature Review

Noninvasive neuroimaging may be able to clarify the relationships between HIV infection and aging in the brain, as it allows differences in brain structure and function to be identified in PWH. Neuroimaging of HIV has led to the rapid advancement of markers associated with HIV infection, HAND, and aging.[32,33] Here we will discuss these advances in three neuroimaging modalities: structural magnetic resonance imaging (sMRI), resting state functional MRI (fMRI), and magnetoencephalography (MEG).

HIV and Aging's Effects on Brain Structure

The aberrations in brain structure seen with HIV infection is potentially the most established of the three modalities proposed here. HIV-related brain atrophy was well recognized in the 1990's, often described as global brain atrophy related to clinical decline and neurocognitive deficits.[34–36] Today however, despite viral suppression being readily achievable, multiple studies continue to indicate that such atrophy remains present even in those treated with cART for extended periods of time.[37,38] Therefore, changes in the brain structure of PWH remain a persistent issue that cART has yet to fully address. Additionally, while such atrophy has been well-characterized, the relationship between aging, advanced aging, and HIV related atrophy remains relatively understudied.

Some evidence has suggested that HIV-related advanced aging may be linked to gross changes in brain structure [32], which some studies suggest reflect those seen in normative aging although accentuated [39,40]. Multiple studies have examined how these structural changes are differentially modulated by aging in HIV infection [41–46], but the overall findings in PWH have been inconsistent, with some studies showing that other health factors such as adipose tissue[47] and hypertension[48] may also be associated with the brain atrophy seen in PWH. Additionally, none of

these studies have included a biomarker of age advancement, which could help quantify age advancement at the individual level, beyond conventional gross measures like chronological age, and clarify the nature of these changes in local brain structure.

Therefore, in the structural neuroimaging portion of the project, we aim to examine the relationship between aging and multiple measurements brain structure in the context of HIV infection. Given that the majority of diagnosed PWH in the United States are virally-suppressed,[49] we aimed to study virally-suppressed PWH. Briefly, we will apply advanced computational methods on high-resolution structural MRIs from a large group of PWH and uninfected controls, sampled evenly from 22 to 72 years old. Additionally, we will measure epigenetic age from peripheral blood to determine each participant's age advancement, and then related such aging to our MRI-derived measures of brain structure. We hypothesized that structural MRI metrics would show evidence of advanced aging in PWH, and that these metrics would relate to our independent epigenetic age advancement estimations. Finally, we studied how these metrics differ in participants with HAND relative to cognitively-unimpaired participants, hypothesizing that those with HAND would show larger degrees of atrophy and age advancement.

HIV and Aging in fMRI: Alterations in Brain Networks

Beyond these structural studies, functional neuroimaging investigations, which can more directly probe the aberrant neural activity related to HIV infection, have been far less common. Functional MRI (fMRI) is one neuroimaging technique that has been used to study the functional brain changes related to a wide variety of neurologic and psychiatric diseases. This technique relies on the blood oxygen level dependent (BOLD) signal, which is an indirect measurement of neural activity (see chapter 3). Importantly however, despite the measurement relying on the hemodynamic response, the BOLD signal has been thoroughly studied and is closely tied to

underlying neural activity.[50–52] Changes in the BOLD signal in certain regions of the brain have also been found to correlate with other regions of the brain.[53] These correlations have been shown to be functionally relevant and has given rise to a rich field of functional connectivity literature, showing organized networks of activity across the brain.[54,55] Using these techniques, research examining PWH have begun to identify changes in brain function related to HIV infection.

Task based studies using fMRI have broadly identified hyperactivity related to HIV.[56] Specifically, a series of papers by Chang et al., utilized a tracking ball task identify attention related increases in prefrontal and cingulate activity.[57–59] Similar increases in activity in the prefrontal cortex were also detected during working memory tasks.[60,61] Separately, subcortical function has been shown to be altered with HIV infection, including a greater recruitment of the basal ganglia during a lexical retrieval task.[62] Overall, aberrations of the frontal cortex and striatum appear to be the most consistent across studies, as shown in meta-analysis of task-based fMRI studies of HIV, which specifically pointed towards dysfunction of the fronto-striatal circuit.[63]

While these task based studies have given significant insight into specific cognitive functions in PWH, resting state fMRI offers the opportunity to study the functional connectivity of multiple networks. A number of resting state fMRI studies of HIV have found altered functional connectivity in PWH. The most consistent findings in these studies have been alterations in connectivity with the frontal cortices, including the executive network.[64–66] A pair of studies specifically identified altered cortico-striatal connectivity related to HIV infection.[65,66] Additionally, studies have also identified HIV related reduced functional connectivity within the default mode network (DMN).[64,67] Functional connectivity between subcortical regions however do not appear to differ in PWH on long term cART compared to uninfected controls.[68]

Some of these studies have begun to examine the added impact of aging in addition to HIV on these functional networks. These studies have been somewhat inconsistent, with the majority failing to identify an HIV by age interaction.[41,64,65,69,70] Other studies have identified specific age by HIV interactions including one study examining an attention task, and identified an HIV specific increase in activity with age related to cognitive reserve,[59] and another noting a significant HIV by age interaction in the motor network.[71] Overall however, the studies with the largest samples, including longitudinal studies,[67] seem to indicate that age and HIV have independent effects on functional connectivity.

In uninfected individuals, normative aging appears to be related to decreased brain modularity in functional networks.[72] That is, with increasing age, within-network connectivity appears to decrease, while between-network connectivity increases.[72–74] This pattern is also noted with measures of network efficiency, which show increasing network efficiency with development, and then subsequent decreases in efficiency and modularity with aging.[75] Overall, this global pattern of decreasing network segregation with aging provides a concise framework to understand how functional connectivity changes with normative aging.

With this framework, we can extend these network-level changes towards the study of HIV infection. That is, while the effect of HIV may be independent of age, the alterations seen with HIV can be examined through the lens of the aging phenotype. Indeed, a recent study identified decreases in network modularity related to HIV.[76] Few studies however have examined how HIV related changes fit into this aging framework, and no studies have probed whether these changes relate to independent epigenetic measures of advanced aging.

Therefore, in the fMRI portion of this project, we aim to examine the relationship between aging and resting state functional connectivity in the context of HIV infection. Briefly, we

will compute network-level estimates of functional connectivity in the same large group of PWH and uninfected controls, sampled evenly from 22 to 72 years old. Additionally, we will measure epigenetic age from peripheral blood to determine each participant's age advancement, and then related such aging to our measures of functional connectivity. We hypothesized that PWH would show evidence of advanced aging in the form of increased between-network connectivity, and decreased within-network connectivity relative to uninfected controls. We also hypothesized that these metrics would relate to our independent epigenetic age advancement estimations. Finally, we studied how these metrics differ in participants with HAND relative to cognitively-unimpaired participants, hypothesizing that those with HAND would show larger functional aberrations and age advancement.

Studies of HIV and Aging with MEG and Neurophysiology

From a different functional perspective, magnetoencephalography (MEG) allows for the direct quantification of neural activity at a much more precise timescale. This allows for the examination of oscillatory activity, which broadly refers to population-level neural activity at distinct frequencies (see chapter 3). Oscillatory activity is known to be important in cognition,[77] and has been shown to be critical in a wide array of disorders.[78–80] Investigations into how the brain's oscillatory activity changes with HIV infection are far less common, which leaves a significant gap in the literature.

Task based studies utilizing MEG to examine oscillatory activity and HIV infection have shown multiple functional deficits in both primary sensory activity as well as in higher order functioning.[81] In somato-motor studies, MEG investigations have identified HIV-related increases in beta event-related desynchronizations at the motor cortex during finger tapping,[82] differential alpha and theta processing,[83] and decreased gamma responses during tactile stimulation.[84]

Examining visual processing, PWH have been shown to have altered alpha activity in dorsolateral prefrontal cortex,[85] and decreased occipital theta responses during early visual processing.[86] In visual attentional processing, one study also identified altered frontal theta activity specific to PWH with HAND.[87] Finally, during working memory processing, PWH were shown to have aberrant alpha responses specifically during the memory maintenance portion of the task.[88]

Interestingly among these task based studies, there have been multiple findings of altered oscillatory power during the baseline (non-task relevant) portion of the paradigms being used. These findings include increased visual gamma power related to HIV during the baseline of a visual-spatial processing task,[89] and increased somatosensory gamma during the baseline of a somatosensory processing task.[84] Increased alpha power during the baseline of both visual processing and attentional processing tasks was also shown to be specifically related to HAND.[87,89] On an attentional task, baseline theta power was also shown to be increased specifically in those with HAND.[87] Overall, these studies seem to indicate a broad increase in spontaneous oscillatory activity related to HIV.

Resting state studies of HIV using MEG are also relatively rare. One study reported an HIV-related decrease in resting beta power.[90] A smaller pilot resting state study identified reduced gamma power associated with HIV infection.[91] Another small study found sensor-level connectivity differences in PWH,[92] but did not investigate oscillatory power. Resting state EEG studies of HIV on the other hand have generally identified decreases in alpha power related to HIV infection.[93–95] Therefore, resting oscillatory activity in PWH shows some evidence of HIV-related aberrant activity, however the subject remains largely understudied.

Adding in the effect of aging, even fewer studies have examined the impact of both aging and HIV. For reference, in normative aging, neural oscillatory activity shows distinct alterations in

specific frequency bands. In the lower frequency bands, some studies have shown decreases in delta and theta power with increasing age.[96] The alpha rhythm is most studied of these changes, which consistently shows slowing (ie decrease in peak frequency) with age.[97–100] Some studies have also reported that alpha power decreases with age as well,[96,100–102] although these findings are somewhat less consistent and may be influenced by the changes seen in peak alpha frequency.[103] Beta power is known to robustly increase with age,[96,100,104,105] typically at the somato-motor cortices where beta activity is most prominent.[104,105] Finally, gamma activity is least frequently reported in the resting state, with a select few studies reporting an increase in power with age.[106]

The studies that have utilized MEG to study HIV and aging include a few task based studies that specifically examined for interactive effects of HIV by age. These findings include HIV by age interactions in theta, alpha and beta activity during attentional processing.[107,108] Additionally, HAND-status by age interactions have been found in frontal gamma during somatosensory processing,[109] and parieto-occipital gamma during visual processing,[110] and frontal and parietal gamma during attentional processing.[107] However, no MEG studies have examined HIV and aging during the resting state.

Additionally, none of these studies have examined the relationship between HIV-associated epigenetic advanced aging and neural oscillatory measures. One study of uninfected controls has successfully identified a relationship between anterior cingulate gamma activity during an attention task and epigenetic age estimations.[111] Therefore, given PWH exhibit both altered oscillatory activity and advanced epigenetic age, epigenetic aging could index altered oscillatory activity seen in PWH.

To summarize, task based MEG studies show multiple oscillatory aberrations in PWH, while the resting state oscillatory activity of PWH is highly understudied and contains relatively inconsistent results. Spontaneous activity during task-based paradigms have shown an increase in power in gamma activity related to HIV infection and increased theta and alpha activity related to HAND. At the same time, resting state neurophysiological studies have shown decreased power in alpha, beta, and gamma frequencies. Broadly, aging is normally associated with a decrease in lower frequency power (delta, theta, alpha), and an increase in higher frequency power (beta, gamma), although the strongest effects appear to be the increase in beta power, and a slowing of alpha peak frequency.

Therefore, in the MEG portion of this project, we aim to examine the relationship between aging and oscillatory activity in the context of HIV infection. Briefly, we will compute source-level estimates of oscillatory power in canonical frequency bands, as well as peak alpha and beta frequencies. As before, we will study the same large group of PWH and uninfected controls, sampled evenly from 22 to 72 years old, and then relate oscillatory measures to epigenetic advanced aging estimates. We hypothesized that PWH will have decreased resting low frequency power, increased beta power, and decreased peak alpha frequency relative to controls, in an additive fashion to the changes seen with aging. Additionally, as before, we hypothesized that these changes would be related to epigenetic advanced aging seen in PWH. Finally, we studied how these metrics differ in participants with HAND relative to cognitively-unimpaired participants, hypothesizing that those with HAND would show larger functional aberrations.

Hypotheses

In summary, given these previous studies, our central hypothesis is that HIV infection precipitates structural and functional brain damage in a manner similar to, and additive to, the

aging process. Such aberrations may also directly relate to epigenetic measures of advanced aging, which is a relationship that has yet to be studied. Specifically, we have hypothesized that, relative to controls: 1) PWH have accentuated grey matter loss, independent of aging, and related to advanced aging, 2) PWH have decreased network modularity in the form of decreased within-network and increased between-network functional connectivity, independent of aging, and such changes will be related to advanced aging, and 3) PWH have decreased resting low frequency power, increased beta power, and decreased peak alpha frequency, also independent of aging, and associated with epigenetic advanced aging.

CHAPTER 3: Methodology

Here we aim to use multimodal neuroimaging techniques to understand the combined impact of HIV and aging in the brain. Specifically, we will be examining structural MRI data, resting state functional MRI data, and resting state MEG data. This chapter will cover the background for these different neuroimaging techniques and how they are implemented, with a focus on the outcome measures utilized in this project. We will then lay out the specific analysis pipelines utilized in each method. Finally, we will cover the statistical modeling that will be used uniformly across all three studies.

MRI Background

Magnetic resonance imaging works based on the principles of nuclear magnetic resonance (NMR). That is, nuclear, referring to the nuclei of hydrogen atoms, magnetic, referring to the creation of a net magnetization in these atoms, and resonance, the alignment of the nuclear spins to manipulate and measure the net magnetization. In short, the nuclei of hydrogen atoms naturally give off a magnetic field, due to the rotation of the protons, or more accurately "spin". When placed in a large magnetic field, many of these protons will align with (low energy) or against (high energy) the direction of the magnetic field, precessing at a rate of the Larmor frequency. Inside an MRI, the net magnetization is in the direction of the external field, termed the longitudinal magnetization. A radio frequency pulse can then be applied to align the magnetic moments, resulting in the loss of the longitudinal magnetization, and the generation of a transverse magnetization that can be measured by the coils.[112]

Then, the radio frequency signal is removed, and the relaxation of the magnetic moments begins. Loss of the transverse magnetization is called the T2, or spin-spin relaxation, and restoration of the longitudinal magnetization is called the T1, or spin-lattice relaxation. Different

tissues have different T1 and T2 relaxation times, and manipulation of the timing of radio frequency pulses allows for the enhancement of these differences. Principally, the relaxation time of lipid molecules is highly different from that of free water molecules, ultimately allowing different tissues (ie grey matter, white matter, and cerebrospinal fluid) to be contrasted.

To perform measurements throughout space, gradients in the magnetic field are utilized to alter the Larmor frequency of the atoms by space. Utilization of a phase encoding gradient and frequency encoding gradient allow for signal measurement at different spatial locations. In all, these techniques allow for a 3D picture of the brain to be generated, such that grey matter, white matter, and CSF have relatively contrasted values, ultimately resulting in a high resolution structural volume.

Analysis of this structural image can involve segmentation of the image into different tissue types. That is, the grey and white matter boundary can be delineated across the entire cortical ribbon. Knowing these boundaries, we can then obtain estimates of grey matter volume, white matter volume, and CSF volume. For a better spatial representation, the amount of grey matter per voxel in the brain can also be quantified. This is the metric used in voxel based morphometry (VBM) and is generally interpreted to be a measure of grey matter "content."[113] Similarly, with the grey and white matter boundary defined, a cortical surface can be generated with estimates of cortical thickness at each region of the cortex. This is the result that is generated through a surface based morphometry (SBM) approach. All of these metrics are quantitative values that can be utilized to study the brain structure of different populations.

In functional MRI, the differences in magnetic signal of oxygenated blood versus deoxygenated blood are examined. Deoxyhemoglobin is paramagnetic, which acts as a suppressor of the MR signal, while oxyhemoglobin is diamagnetic, resulting in a higher MR signal. Contrasting

these two signals is called the blood oxygen level dependent (BOLD) contrast. This contrast is relevant to neural activity because increases in neural activity results in a hemodynamic response, causing an increase in oxygenated blood relative to deoxygenated blood. Ultimately, this allows us to generate an indirect measure of neural activity. Importantly however, although this measurement is indirect, studies have shown a correspondence between BOLD signal and neuronal activity.[51,114]

Unlike in a structural scan, where one volume is sufficient, fMRI requires the measurement of multiple volumes over time to allow for the study of brain function. In task based MRI, participants perform a cognitive task, which elicits BOLD changes in regions associated with processing of that task. In resting state fMRI however, the natural fluctuations in that signal are what is studied. That is, the signal in certain regions of the brain are known to fluctuate in a similar manner to other regions of the brain. This can be quantified via a correlation of signal between brain regions.

The spatial patterns of these correlations have revealed organized brain networks called resting state networks, which are thought to reflect functional systems that support cognitive processes. The number of networks identified is relatively arbitrary, as networks can be continually subparcellated into smaller and smaller networks. That said, seven of the most consistent resting state networks in the brain include the visual, somato-motor, dorsal attention (DAN), ventral attention (VAN), limbic, executive control, and default mode (DMN) networks.[115] Ultimately, the degree of correlation, or functional connectivity, within, and also between, these networks can be quantified and contrasted between different populations.

MEG Background

Compared to the physics of MRI, the concepts behind how MEG works is relatively straightforward. MEG utilizes highly sensitive magnetic sensors (magnetometers/gradiometers) to measure the magnetic fields that emanate from the brain. These fields originate from neural activity, which consists of electrical currents flowing down the cellular membranes of neural cells. Such currents inherently generate a magnetic field in a manner according to Ampere's right hand grip rule, allowing the MEG sensors to give a direct measurement of neural activity. Importantly, the activity which generates a strong enough field to be measured by these external MEG sensors needs to be summative over a large population of neurons. Thus, the activity measured by MEG is not considered to be from neuronal action potentials, but rather dendritic potentials, which are slower and allow for a temporal summation in magnetic field.[116]

Practically, MEG is a noninvasive and totally silent neuroimaging technique that has excellent temporal (i.e., milliseconds) and spatial precision (i.e., millimeters). The neuromagnetic fields generated by population level neural activity are ultra-minute (i.e., roughly one billion times smaller than the Earth's steady-state field), thus MEG recordings are generally conducted in highly-shielded rooms using superconducting technology, unique sensors, and noise cancellation methods. The strength of these neuromagnetic fields is proportional to the amplitude of the underlying electrical currents. However, unlike electrical fields (as in EEG), magnetic fields are not distorted nor attenuated by the cerebrospinal fluid, skull, scalp, or other intervening tissues, which enables MEG to be much more spatially precise than electrically-based methods with comparable temporal resolution.[116]

This high temporal resolution allows for the inquiry of frequency-specific activity (ie oscillatory activity), which can be quantified through analysis of the MEG data. In task based

designs, where there is an event of interest, data around the event of interest can be examined via a time domain, or time-frequency domain analysis. In resting state data however, there are no events of interest to examine. This limits analysis of these data to a pure frequency domain analysis, which can be done by calculating a power spectrum density (PSD; Figure 1). This plots the power seen across the data by frequency, notably eliminating the time domain. Naturally, without measured activity, power decreases with increasing frequency, which can still be seen in the PSD. After adding human brain neurophysiological activity, canonical frequency bands are thought to be relevant towards neural activity and cognitive function: delta (2–4 Hz), theta (4–8 Hz), alpha (8–12 Hz), beta (15–30 Hz), and gamma (30–80 Hz). Additionally, distinct peaks are seen in the frequency spectrum in the alpha and beta bands (Figure 1).

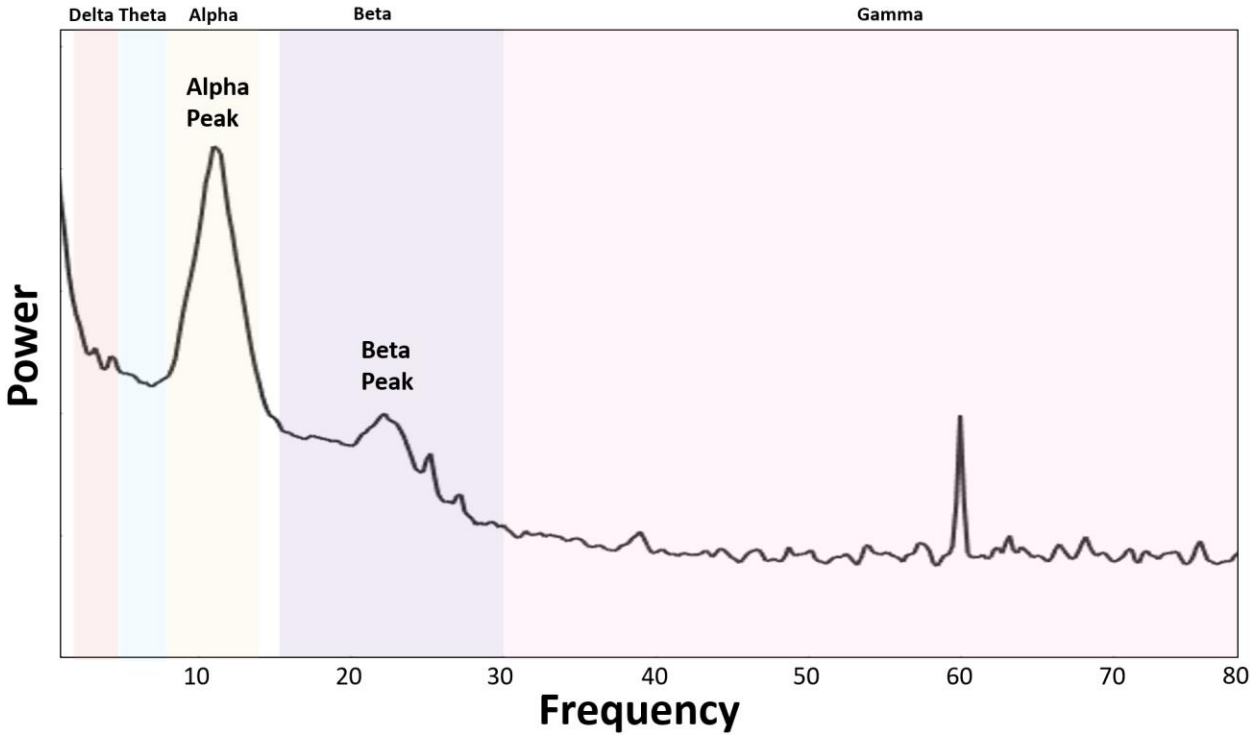

Figure 1: Example Power Spectrum Density of Resting Brain Activity. The average PSD across all sensors for a representative dataset is shown. The canonical frequency bands at which power was extracted are highlighted: delta (2–4 Hz), theta (4–8 Hz), alpha (8–12 Hz), beta (15–30 Hz), and gamma (30–80 Hz). Human resting state activity shows two distinct peaks of activity, one in the alpha band, and the other in the beta band. The frequency at which the maximum power is seen is defined to be the peak frequency. Note that the peak at 60 Hz represents noise from the line-in frequency.

Structural Processing Pipeline

Briefly, structural MRI data will undergo an automated tissue segmentation in order to quantify the amount of grey matter, white matter, and CSF. VBM and SBM analyses will also be utilized to generate spatially dependent measurements of brain structure, which will ultimately be utilized in our final statistical contrasts.

MRI Acquisition

Structural T1-weighted MRI images were acquired with a Philips Achieva 3T X-series scanner using an eight-channel head coil and a 3D fast field echo sequence with the following parameters: TR: 8.09 ms; TE: 3.7 ms; field of view: 24 cm; matrix: 256 × 256; slice thickness: 1 mm with no gap; in-plane resolution: 0.9375 × 0.9375 mm; sense factor: 1.5.

Voxel Based Morphometry

To study the regional distribution of grey matter, participants' high-resolution T1-weighted MRI data were processed using the standard voxel-based morphometry (VBM) pipeline in the computational anatomy toolbox (CAT12 v12.6)[117] within SPM12. Briefly, participants' high-resolution T1-weighted MRI data underwent noise reduction using a spatially-adaptive non-local means denoising filter [118] and a classical Markov Random Field approach.[119] An affine registration and a local intensity transformation were then applied to the bias corrected images. Finally, preprocessed images were segmented based on an adaptive maximum a posterior technique[120] and a partial volume estimation (PVE) with a simplified mixed model of a maximum of two tissue types.[121] Images were also normalized to MNI template space, and the resulting VBM images were smoothed using an 8mm FWHM Gaussian kernel. Total grey matter, white matter, and CSF volumes were extracted and normalized to total intracranial volume for further statistical analysis. VBM maps were also utilized in subsequent statistics.

Surface Based Morphometry

To examine the cortical thickness, T1-weighted MRI data were processed using additional surface-based morphometry calculations in the computational anatomy toolbox (CAT12 v12.6)[117] at a resolution of 1 mm^3. This method utilizes a projection-based thickness approach to estimate cortical thickness and reconstruct the central surface in one step.[122] Briefly, following the previous tissue segmentation, the white matter (WM) distance is estimated, and the local maxima are projected onto other gray matter voxels using a neighboring relationship described by the WM distance. This method accounts for partial volume correction, sulcal blurring, and sulcal asymmetries. Topological defects are corrected based on spherical harmonics,[123] and the cortical surface mesh was reparameterized into a common coordinate system via an algorithm that reduces area distortion.[124] Finally, the resulting maps were resampled and smoothed using a 15 mm FWHM Gaussian kernel. These maps of cortical thickness were ultimately utilized in subsequent statistical analysis.

Functional MRI Processing Pipeline

Functional MRI data will undergo standard preprocessing and denoising procedures, and then subsequent calculation of functional connectivity of previously established networks will be assessed. Ulitmately, estimates of within-network and between-network connectivity will be extracted for each participant to then undergo statistical analyses.

Scanning Parameters

Whole-brain blood oxygen level dependent (BOLD) data were acquired with a 3T Philips Achieva X-series scanner using an eight-channel head coil. A total of 480 functional volumes were taken with a T2* SENSE sequence (repetition time=2000 ms; echo time=35 ms; 78x78 matrix; 90o flip angle; 240 mm field of view). Whole-brain coverage was obtained with 33 axial slices

(thickness, 3.5 mm). Participants were instructed to rest with their eyes closed and were monitored throughout the scan. In the same session, a high-resolution T1-weighted anatomical scan was acquired to co-register with the SENSE dataset (parameters described in *Structural Processing* above).

Resting-state fMRI Preprocessing

The rs-fMRI data were preprocessed using SPM12 and the DPABI Toolbox.[125] Participants with excess head motion, defined as greater than 0.8 in frame-wise displacement[126] and/or greater than 2.5 mm of maximum motion, were excluded from the study. Preprocessing procedures included removal of the first 3 volumes, motion correction to the first volume with rigid-body alignment; co-registration between the functional scans and the anatomical T1-weighted scan; linear detrending; regression of motion parameters and their derivatives (24-parameter model),[127] and the scrubbing parameters,[126] as well as white matter (WM), cerebrospinal fluid (CSF) time series (using a component based noise reduction method, 5 principal components);[128] spatial normalization of the functional images into Montreal Neurological Institute (MNI) stereotaxic standard space; and spatial smoothing within the functional mask with a 6-mm at full-width at half-maximum Gaussian kernel; wavelet despiking;[129] Lastly, bandpass filtering was applied at [0.01-0.1] Hz.[130]

Extraction of Functional Connectivity Measures

We used the Yeo 7 network atlas,[115] a previously established functional brain atlas based on 1000 resting state fMRI scans, to partition the functional connectome into 7 replicated resting-state networks (RSNs)[131]: visual, somato-motor, dorsal attention (DAN), ventral attention (VAN), limbic, executive control, and default mode (DMN). In each participant, Fisher Z-transformed Pearson's correlation coefficients were computed to calculate functional connectivity within- and

between- networks. Within-network functional connectivity was computed as the average correlation of each voxel's BOLD signal time series with every other voxel within the network. Between-network functional connectivity was computed as the correlation between the average time-series of each pair of networks. One between-network functional connectivity metric was computed for each of the seven networks by averaging across all pairs that included the respective network. Each of the pairs was also later analyzed individually using functional connectivity matrix statistics.

To confirm and extend results with this seven network parcellation, we also calculated within- and between network functional connectivity using an independent 13 network parcellation.[132] This atlas notably contains a subcortical network, which is not included in the Yeo atlas. Thirteen network matrices underwent the same matrix statistics as the seven network matrices.

Resting State MEG Processing Pipeline

In brief, our MEG processing pipeline will involve data preprocessing, coregistration, and subsequent source analysis using dSPM. The frequency spectra of source-level data will then be analyzed via computation of power spectrum density, and extraction of power and peak frequency at canonical frequency bands (Figure 2). These metrics will be computed for whole-brain cortical surface maps, which will then undergo our statistical analyses. Estimates across broad regions of interest will also be extracted from these maps for further visualization and statistical analyses.

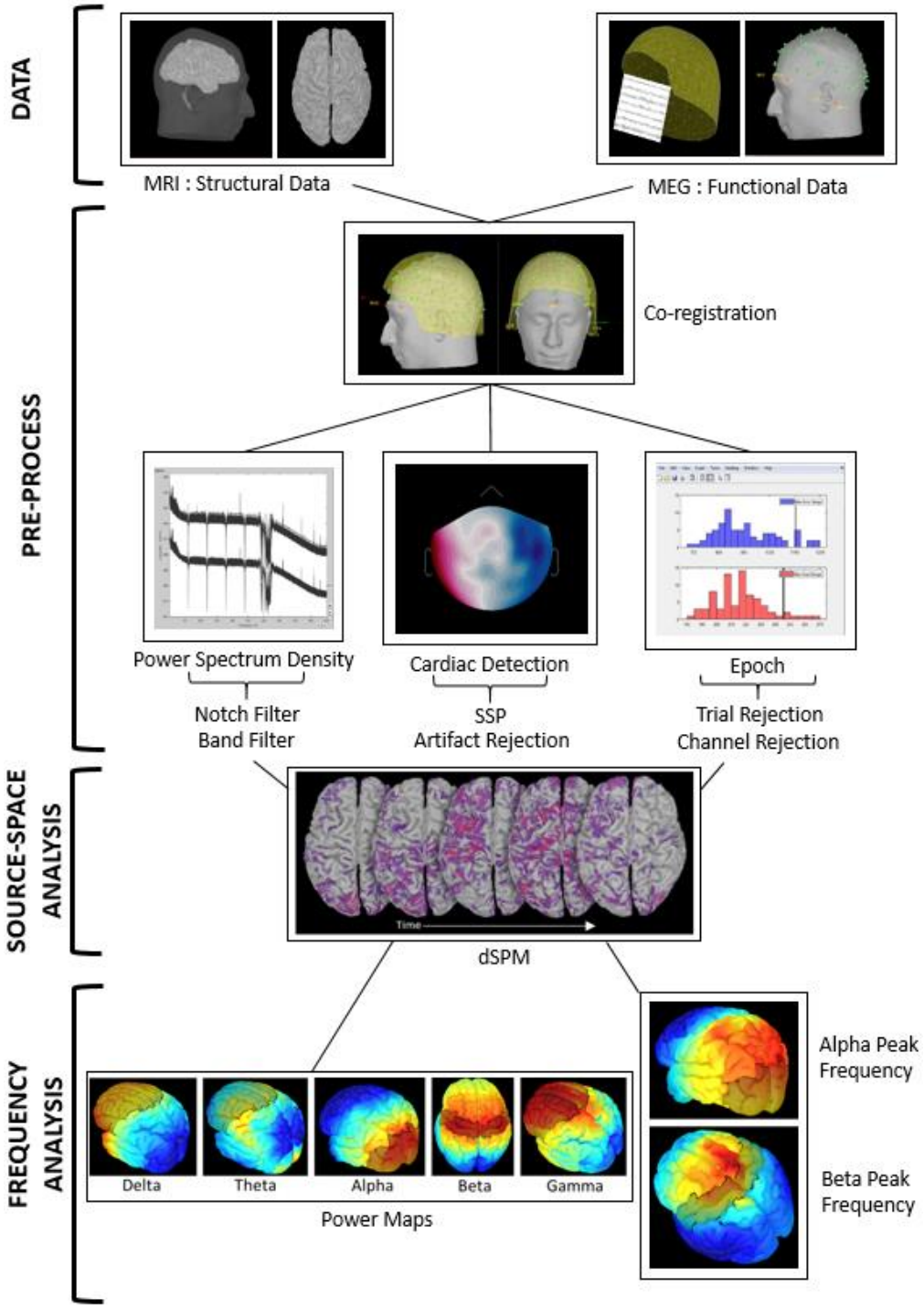

Figure 2: MEG Data Analysis Pipeline. Resting state MEG data underwent standard preprocessing procedures, including coregistration to sMRI data, filtering, artifact correction, and rejection of noisy segments of data by dividing the data into 4 second epochs and evaluating the distribution of amplitude and gradient estimates. Source-space analysis was then performed using a dSPM algorithm. Spectral analyses were then performed on these whole cortex level data to extract power at canonical frequency bands, and peak alpha and beta frequencies. Pre-defined ROIs were also utilized to extract these metrics for visualization and statistical analyses.

MEG Data Acquisition

All MEG recordings took place in a one-layer magnetically-shielded room with active shielding engaged for environmental noise compensation. A 306-sensor Elekta/MEGIN MEG system (Helsinki, Finland), equipped with 204 planar gradiometers and 102 magnetometers, was used to sample neuromagnetic responses continuously at 1 kHz with an acquisition bandwidth of 0.1 – 330 Hz. The same instrument was used across all recordings. Participants were seated in a custom-made nonmagnetic chair within a magnetically shielded room, with their heads positioned within the sensor array. Participants were instructed to rest with their eyes closed for 6 minutes, and were monitored by a real-time audio-video feed from inside the shielded room throughout MEG data acquisition.

Structural MRI Acquisition, Processing, and MEG-MRI Coregistration

Individual structural MRI data were obtained from a majority of participants. All T1-weighted sMRI data were acquired and segmented with the computational anatomy toolbox (CAT12 v12.6) [117] as described above. The resulting segmented files were then imported into Brainstorm for coregistration and source imaging.

Prior to MEG acquisition, four coils were attached to the participants' heads and localized, together with the three fiducial points and scalp surface, using a 3-D digitizer (Fastrak 3SF0002, Polhemus Navigator Sciences, Colchester, VT, USA). Once the participant was positioned for MEG recording, an electrical current with a unique frequency label (e.g., 322 Hz) was fed to each of the coils. This induced a measurable magnetic field and allowed each coil to be localized in reference to the sensors throughout the recording session. Since coil locations were also known in head coordinates, all MEG measurements could be transformed into a common coordinate system. With this coordinate system (including the scalp surface points), each participant's MEG data were

co-registered with the structural magnetic resonance images prior to source space analyses using Brainstorm supplemented with visual inspection. Notably, 11 participants did not have available T1 MRI data. For these participants, the MNI ICBM152 brain template [133] was utilized and warped to fit each participants' digitized headpoints.

MEG Data Pre-Processing

Each MEG dataset was individually corrected for head motion and subjected to noise reduction using the signal space separation method with a temporal extension (MaxFilter v2.2; correlation limit: 0.950; correlation window duration: 6 seconds).[134] MEG data processing then largely followed the same analysis pipeline outlined in Niso et al., 2019.[135] Noise-reduced MEG data underwent standard data preprocessing procedures using the Brainstorm software. A high pass filter of 0.3 Hz and notch filters at 60 Hz and at its harmonics were applied. Cardiac artifacts were identified in the raw MEG data and removed using an adaptive signal-space projection approach, which was subsequently accounted for during source reconstruction.[136,137] Data were then divided into four second epochs for detection and rejection of bad segments of data. Amplitude and gradient metrics for each epoch were computed, and epochs containing outlier values were rejected using an individualized fixed threshold method, supplemented with visual inspection. Briefly, in MEG, the raw signal amplitude is strongly affected by the distance between the brain and the MEG sensor array, as the magnetic field strength falls off sharply as the distance from the current source increases. To account for this source of variance across participants, as well as other sources of variance, we used an individually-determined threshold based on the signal distribution for both amplitude and gradient to reject artifacts.

MEG Source Imaging and Frequency Power Maps

As in Niso et al., 2019,[135] we computed minimum norm estimates normalized by a dynamic statistical parametric mapping (dSPM) algorithm for source imaging. To account for environmental noise, we utilized empty room data to compute a noise covariance matrix for source imaging [138]. The forward model was computed using an overlapping spheres head model [139] with 15000 cortical surface vertices. Finally, the imaging kernel of depth-weighted dSPM constrained to the individual cortical surface[140] was computed.

Using these source estimates, we then estimated the power of cortical activity in the canonical frequency bands: delta (2–4 Hz), theta (4–8 Hz), alpha (8–12 Hz), beta (15–30 Hz), and gamma (30–80 Hz). We used Welch's method for estimating power spectrum densities (PSD) per four second epoch across each MEG recording, with 1 second sliding Hamming windows overlapping at 50%. We then standardized the PSD values at each frequency bin to the total power across the frequency spectrum. For each participant, we then averaged PSD maps across epochs to obtain one set of six PSD maps (one per frequency band) per participant. Finally, we projected these maps onto the MNI ICBM152 brain template[133] and applied a 3mm full width half maximum (FWHM) smoothing kernel. Ultimately, it is these normalized source maps per frequency band that were used for further statistical analysis. Additionally, to further examine the data, broad ROIs were used to extract the average power in regions of the cortex typically associated with having the largest power in each frequency band (frontal delta, frontal theta, occipital alpha, central beta, and frontal gamma; Figure 2).

Peak Alpha and Beta Frequency Maps

Vertex-wise peak frequency maps were also computed for each participant. As before, Welch's method was used on source-level data to estimate power spectrum densities per four second epoch across each MEG recording, with 1 second sliding Hamming windows overlapping

at 50%, and then PSDs were normalized to total power across the frequency spectrum. The peak alpha frequency between 7-13 Hz and peak beta frequency between 15-30 Hz was then extracted at each vertex, creating whole cortex maps of peak alpha and beta frequencies. These two maps were then used for further statistical analysis. As with the power maps, average peak frequency across selected ROIs was also extracted (occipital alpha, central beta; Figure 2).

Epigenetic Age Advancement Processing

Epigenetic age advancement will also be utilized as an independent variable to determine the relationship between structural and functional metrics and age advancement. Calculation of epigenetic age advancement involved analysis of blood samples, which were collected from a subset of the full sample. Whole-blood samples were collected as closely as possible to their MRI scan date, and this time difference was used as a covariate of no interest in all analyses involving the two different types of measures. All of the methylation metrics, including the Horvath and Hannum models of DNA methylation age, were computed on the entire data set. The DNA sample collection, methylation analysis, and epigenetic age estimation followed the pipeline established in earlier work.[16]

Briefly, DNA was purified from whole-blood samples using BD Vacutainer EDTA collection tubes and DNeasy blood and tissue extraction kits (QIAGEN). Methylation analysis was performed using Infinium HumanMethylation450 BeadChip Kits (Illumina). Following hybridization, BeadChips were scanned using the Illumina HiScan System. All data were processed through the Minfi R processing pipeline.[141] Methylome data were downloaded from Hannum [17] and EPIC (GEO: GSE40279 and GSE51032)[142] and we processed these data together along with those from the current study. Beta values were extracted and quantile normalized using Minfi; cell counts were estimated using estimateCellComposition and resulting normalized beta values were adjusted for

cell types.[16,143] All data were then normalized using a modified BMIQ procedure provided by Horvath.[18] The gold standard was set to the median beta observed in the Hannum study.[17]

To compute epigenetic age, the "consensus model" of methylation age was used, which combines both the Horvath[18] and Hannum[17] methods of prediction and has been previously found to provide more predictive capacity than either model in isolation.[16] Upon calculating each participant's epigenetic age, we then subtracted each participant's consensus predicted biological age from their chronological age to obtain a measure of age disparity. This metric represents the participant-specific age advancement of biological age relative to chronological age.

Neuropsychological Testing

Participants completed a full neuropsychological battery to identify PWH who had HAND as described in Lew et al., 2018.[87] Briefly, this battery assessed multiple functional domains, including executive functioning (verbal fluency, semantic fluency, Stroop interference, and Trail Making Part B), attention (Symbol Search, Stroop word), speed of processing (Trail Making Part A, digit symbol, Stroop color), fine motor (grooved pegboard), verbal learning and memory (Hopkins Verbal Learning Test–Revised), and language (Wide Range Achievement Test 4 reading). Using published normative data, each participant's scores were converted to demographically-adjusted z scores, and composite scores for each domain were computed by averaging the z scores across the tests included in a specific domain. These composite scores were then used to identify participants with HAND according to the Frascati criteria.[144]

Outcome Variables

To summarize, processing of sMRI, fMRI, and MEG data will each result in discrete variables which will be utilized as dependent variables for subsequent statistical comparisons. From the structural analysis we will obtain total grey matter, white matter, and CSF volumes. We

will also have whole brain VBM and whole cortex SBM maps, which will also undergo statistical testing. From the resting state functional MRI analysis we will obtain average within network connectivity and average between network connectivity values for each of the atlas-defined resting state networks. Each between network connectivity pair will also be examined by performing statistics on functional connectivity matrices. Finally, from the resting state MEG analysis, we will have power estimations for each of the canonical frequency bands, as well as peak alpha and beta frequencies, at specific ROIs of the brain. Statistical testing will also be performed on whole cortex maps of frequency power at each band, and whole cortex maps of peak alpha and beta frequency. These neuroimaging metrics will be utilized as dependent variables in subsequent statistical analyses. Independent variables will include HIV serostatus and participant chronological age, and then separately, epigenetic age advancement, and HAND status.

Statistical Comparisons

Our aim is to understand the effects of HIV and aging on structural and functional neuroimaging metrics. With this in mind, we utilized multiple ANCOVA models to examine the independent and interactive effects of HIV and aging. The same statistical design was utilized across all three methods, giving a unified approach to our research question. Each neuroimaging metric was used as a dependent variable, while HIV status was used as a categorical independent variable, and participant age was used as a continuous independent variable. An additional model was then created by adding in the HIV by age interaction, focusing on the added significance of the interaction. For the fMRI connectivity matrices, Bonferroni correction was used to correct for multiple comparisons.

Whole brain and whole cortex statistical comparisons using SPM.

To determine the spatially-specific independent and interactive effects of HIV and aging, we ran ANCOVA models on the whole brain and whole cortex metrics. These statistical models were estimated using SPM12 and the CAT12 toolbox. HIV status was entered as a categorical factor, and chronological age was used as a covariate of interest, along with the interaction between HIV-status and age. In the VBM model, total intracranial volume was also used as a nuisance covariate, and an absolute threshold mask of 0.1 was used.

For structural data, correction for multiple comparisons involved a voxel-level FDR threshold of .05 and k threshold of 200 were used in both models. For MEG functional data, correction for multiple comparisons involved a vertex-level cutoff of $p<.001$ and cluster-level FWE correction at .05. Correction for multiple comparisons differed between the two due to the assumptions of each modality. Specifically, voxel data from sMRI data are sampled with a higher degree of independence from one another, therefore a voxel-level correction for multiple comparisons (allowing for voxel-level inference) may be appropriate to determine precisely which regions are displaying significant levels of atrophy. Source-level functional data from MEG on the other hand shows a high degree of non-independence from one spatial location to another. Therefore, a cluster-level correction (allowing for cluster-level inference) is a more appropriate method.[145,146]

Relationships Between Brain Structure and Biologically-Determined Age Advancement

To relate our neuroimaging metrics to molecularly-derived age, we utilized HIV infection, relative age advancement, and their interaction as independent variables in ANCOVAs to examine their effect on each metric. This analysis only used data from participants that had both complete methylation data and data for each neuroimaging modality. Specifiaclly, we ran ANCOVAs with each neuroimaging metric as dependent variables, examining the main effects of HIV and relative

age advancement, and the interaction between the two. We then examined whether there were region-specific effects of relative age advancement on brain structure by using the same ANCOVA model on our VBM and cortical thickness maps. We again probed for the main effects of HIV, relative age advancement, and their interaction, and as before, an FDR threshold of .05 and k threshold of 200 were used to correct for multiple comparisons.

Analysis of HIV-Associated Neurocognitive Disorder

To determine the impact of HAND, we performed post-hoc analyses repeating our statistical comparisons after splitting the PWH group by HAND. Specifically, we performed pairwise comparisons between uninfected controls, unimpaired PWH, and participants with HAND.

CHAPTER 4: Results & Discussion 1: Brain Structure

sMRI Results

Participants

Out of the 121 PWH and 133 uninfected controls recruited for this study, 110 PWH ($n_{age\ 22\text{-}39}$=32, $n_{age\ 40\text{-}59}$=62, $n_{age\ 60\text{-}72}$=16) and 122 controls ($n_{age\ 22\text{-}39}$=53, $n_{age\ 40\text{-}59}$=45, $n_{age\ 60\text{-}72}$=24) successfully completed the MRI protocol (Table 1) and had structural T1 MRI data that could be used for processing. All PWH were virally suppressed with a median current CD4 of 702 cells/µl (range: 102-2617) and a median CD4 nadir of 237 cells/µl (range: 3-586). Participant's body mass index (BMI) did not significantly differ between our HIV (M_{BMI}=28.62) and control (M_{BMI}=29.27) groups (p=.478) nor did BMI significantly correlate with age (p=.756).

Ninety-seven PWH and 87 controls completed a blood draw for epigenetic age estimation. Missing data were due to participants quitting the study, being lost to follow-up, or related issues. Notably, 12 participants who completed the blood draw did not successfully complete the MRI protocol, and three blood samples were inadequate for epigenetic age estimation. Ultimately this yielded a final sample of 86 PWH and 83 controls who had reliable data from both epigenetic age estimations and structural T1 MRI data. Subsequent MRI analyses included all 232 participants that completed MRI, and analyses examining only epigenetic data included all 181 participants that had completed methylation data. Analyses relating MRI to epigenetics only utilized participants that had data from both methods (n=169).

Table 1: Participant Demographics

	Sample with MRI Data		Subsample with MRI and Epigenetic Data	
	Uninfected Controls (n=122)	**PWH (n=110)**	**Uninfected Controls (n=83)**	**PWH (n=86)**
Chronological Age (years; mean/SD)	44.56 (15.33)	47.11 (12.29)	43.69 (14.68)	47.11 (12.15)
Sex (M/F; n/%)	65/57 (53.3/46.7%)	64/46 (58.2/41.8%)	43/40 (51.8/48.2%)	55/31 (64.0/36.0%)
Race (Caucasian/African American/Asian/Other: n/%)	82/33/5/2 (67.2/27.0/4.1/1.6%)	71/34/2/3 (64.5/30.9/1.8/2.7%)	57/21/4/1 (68.7/25.3/4.8/1.2%)	58/26/1/1 (67.4/30.2/1.2/1.2%)
Average Composite Neuropsychological Z-Score (mean/SD)	-0.12 (0.60)	-0.41 (0.64)	0.02 (0.50)	-0.43 (0.61)
HAND (n/%)	-	40 (36.4%)	-	34 (39.5%)
Time Since HIV Diagnosis (years; mean/stdv)	-	11.1 (7.32)	-	11.7 (7.43)
CD4 Nadir (median/range)	-	237 (3-586)	-	237 (3-585)
Current CD4 (median/range)	-	702 (102-2617)	-	743.5 (106-2617)

Note: HAND: HIV-Associated Neurocognitive Disorder

Independent Effects of HIV and Aging in Grey Matter Volume

To determine the best model fit we first ran hierarchical regressions of MRI volume on age, iteratively adding polynomial terms and assessing the significance of the change in R square. All volume data were normalized to each participant's total intracranial volume. The linear regression of grey matter volume on age was significant ($F(1,230)=240.02$; $p<.001$), and adding the age squared quadratic term did not show a significant improvement in model fit ($F(1,229)=0.04$; $p=.849$). The regression of white matter volume on age showed a significant linear effect ($F(1,230)=25.73$; $p<.001$), as well as a significant improvement with the addition of the quadratic term ($F(1,229)=32.44$; $p<.001$). Adding age cubed did not significantly improve the model ($F(1,228)=0.72$; $p=.397$). Similarly, the regression of CSF volume on age showed a significant linear effect ($F(1,230)=152.95$; $p<.001$), a significant improvement with the age squared term ($F(1,229)=11.98$; $p<.001$), and no significant improvement with the cubed term ($F(1,228)=1.70$; $p=.193$). Therefore, grey matter volume showed a linear trend with age, and white matter and CSF volumes showed a quadratic trend with age (Figure 3).

Next, using each tissue's respective model from the previous analysis, we assessed the main effect of HIV. This showed a main effect of HIV in grey matter volume (F(1,229)=10.31; p=.002) and CSF (F(1,228)=8.13; p=.005), with no significant effect in white matter volume (F(1,228)=2.14; p=.145). Finally, we added the interactive term(s) of group by age (and group by age squared for white matter and CSF) in one block and examined the significance in R squared change. There was no significant interactive effect for grey matter volume (F(1,228)=0.11; p=.737), nor CSF (F(2,226)=2.08; p=.127), however there was a trending interactive effect for white matter volume (F(2,226)=2.71; p=.069). These statistics are summarized in Table 2.

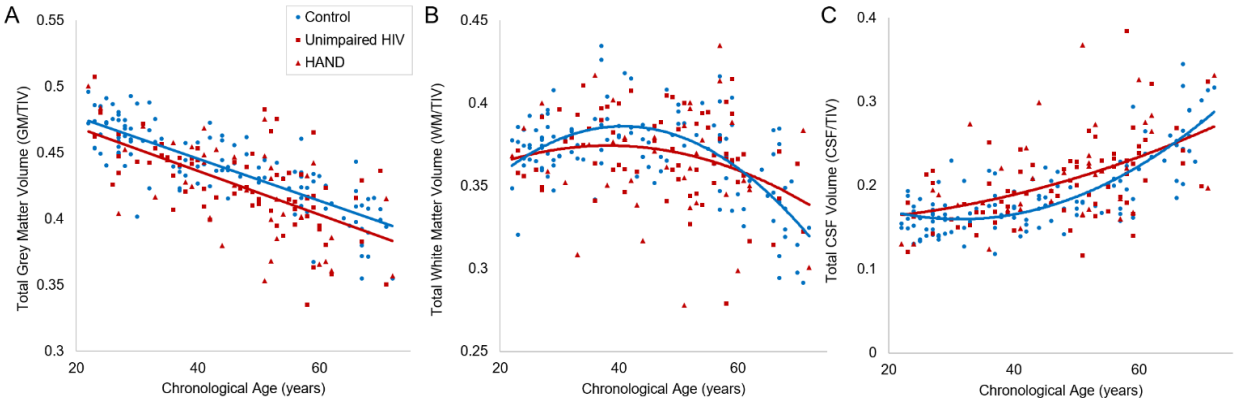

Figure 3: Tissue volumes by HIV status and age. Total grey matter (A), white matter (B) and CSF (C) volumes were calculated from T1 MRIs and normalized to total intracranial volume. Hierarchical regressions with chronological age were used to determine the relationships between each tissue volume and age, and then the main effect of HIV, and interaction effect of HIV by age were tested. PWH specifically displayed significantly less grey matter volume relative to uninfected controls, independent of age. No interaction effects of HIV by age were found. TIV=Total intracranial volume.

In summary, only total grey matter showed a main effect of HIV, and the trajectory of the linear decrease in grey matter volume with age did not significantly differ from controls.

Independent Effects of HIV and Aging in Cortical Thickness

Cortical thickness surface maps were used to test the independent effects of HIV and aging, as well as the HIV by age interaction. After multiple comparisons correction, significant widespread reductions in cortical thickness were found to be associated with HIV infection,

independent of age (Figure 4A). The main effect of age showed an expected reduction in cortical thickness with increasing age across the cortical mantle (Figure 4B). No significant clusters displaying an HIV by age interaction survived multiple comparisons correction.

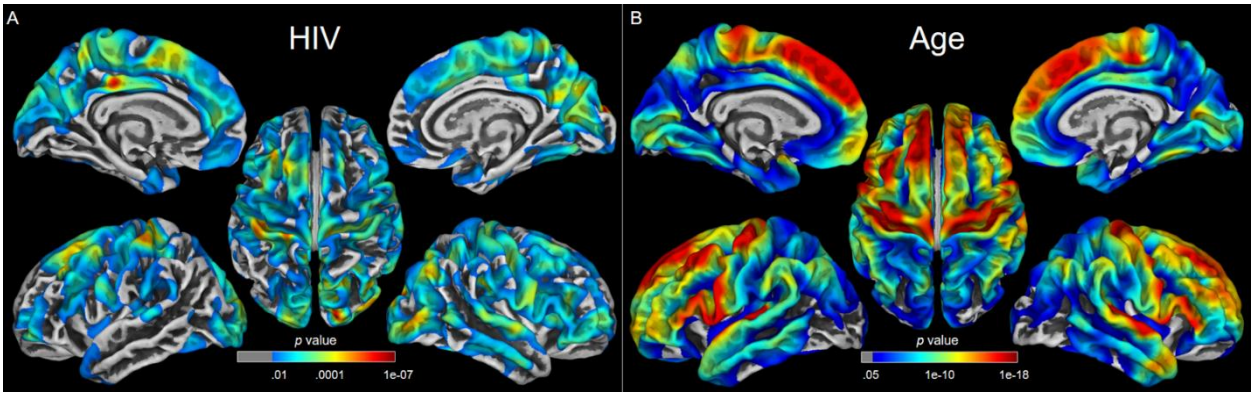

Figure 4: Statistical parametric maps of cortical thickness on HIV and Aging. Surface based morphometry was used to estimate cortical thickness from T1 MRIs and the independent and interactive effects of HIV and age were estimated. PWH displayed widespread reduced cortical thickness in comparison to controls, independent of age (A). The model also showed an expected pattern of reduction in cortical thickness with age (22-72 years; B). No HIV by age interaction was found. Color bars display p-values scaled by -log(p), and corrected with a .05 FDR and k=200 threshold.

Independent Effects of HIV and Aging in VBM

Voxel based morphometry maps were used to test for the independent effects of HIV and age, as well as the interaction between the two. As expected, the independent effect of age showed widespread cortical and subcortical reductions in grey matter with increasing age (Figure 5A). The independent effect of HIV showed a collection of subcortical and cortical significant clusters that survived multiple comparisons correction (Figure 5B).

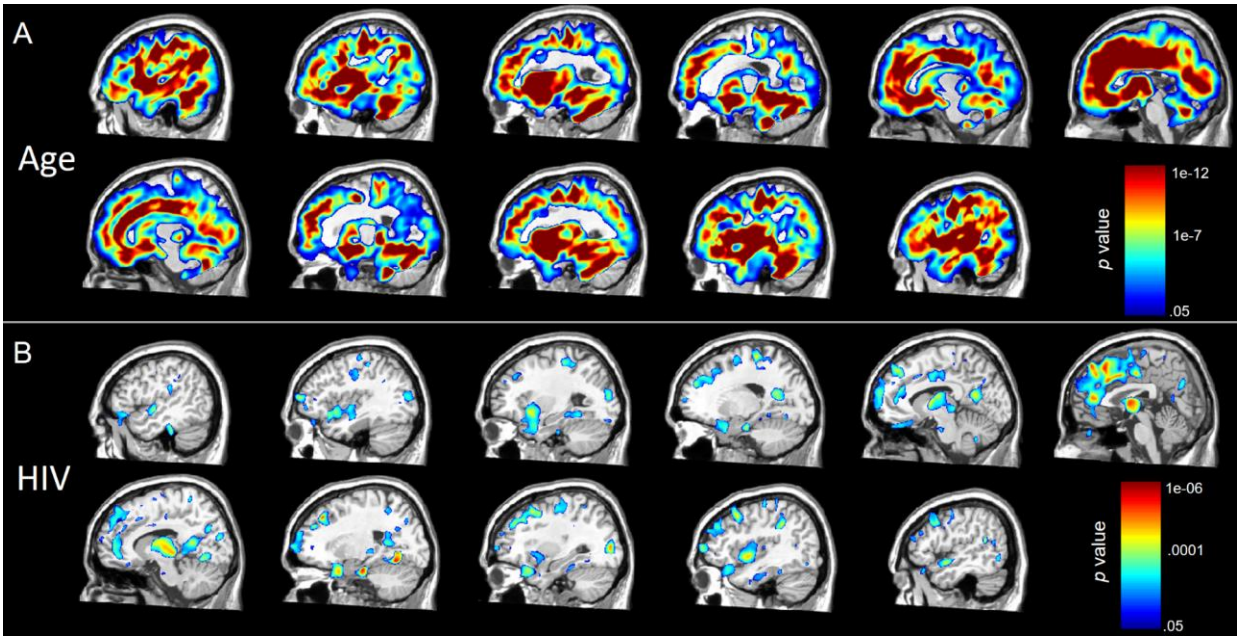

Figure 5: Statistical parametric maps of VBM on HIV and aging. Voxel based morphometry was computed from T1 MRIs and the independent and interactive effects of HIV and age were tested. (A) VBM maps showed widespread reductions in grey matter with increasing age. (B) PWH displayed significant reductions in grey matter in comparison to controls across a collection of brain regions, including the cingulate cortex, bilateral thalamus, and hippocampus independent of age. No HIV by age interaction was found. Color bars display p-values scaled by -log(p), and corrected with a .05 FDR and k=200 threshold.

HIV-Specific Relationship between Grey Matter Volume and Advanced Aging

Epigenetic age was calculated per participant, and each participant's relative age advancement was determined by subtracting consensus predicted epigenetic age from their age at blood draw. Examining group differences in epigenetic age advancement alone, we conducted an independent samples Mann-Whitney U test, due to the presence of several outliers (>3 standard deviations from the group mean). A two tailed Mann-Whitney U test showed a non-significant, but trending, difference between uninfected controls and PWH (U = 4757; p = .056; effect size r = .142). This comparison utilized all participants that had epigenetic data, irrespective of whether they had MRI data.

ANCOVA examining the relationship between normalized total grey matter volume and relative age advancement by HIV status revealed significant main effects of HIV and age

advancement on total grey matter volume such that both greater molecular age advancement (F(1,165)=7.59; p=.007, η^2=.044) and HIV infection (F(1,165)=11.47; p=.001, η^2=.065) were independently related to reductions in total grey matter volume. Additionally, there was a significant HIV by age advancement interaction such that PWH showed a stronger relationship between reduced grey matter and relative age advancement when compared to controls (F(1,165)=4.18; p=.043, η^2=.025). This effect remained significant after covarying for BMI (F(1,164)=4.25; p=.041). To probe this interaction, we then performed simple effects testing on controls and PWH separately. This showed that the relationship between age advancement and total grey matter volume was significant in PWH (r(84)= -.346; p=.001), and non-significant in controls (r(81)= -.057; p=.611). Ultimately, this shows that specifically for PWH, the greater biological age advancement a participant displayed, the smaller their total grey matter volume (Figure 6).

ANCOVAs examining the relationship between white matter and CSF volumes with relative age advancement by HIV status both failed to show a significant main effect of relative age advancement, and failed to show an interactive HIV by relative age advancement effect. As in earlier models examining chronological age, the main effect of HIV on CSF volume did remain significant (F(1,165)=10.04; p=.002, η^2=.057) and the main effect of HIV on white matter volume remained non-significant. These results are summarized in Table 2.

Table 2: Total Tissue Volume Statistics

Hierarchical Regression

	Age	HIV	HIV x Age
Grey Matter	linear: F(1,230)=240.02; p <.001	F(1,229)=10.31; p = .002	F(1,228)=0.11; p = .737
White Matter	quadratic: F(1,229)=32.44; p<.001	F(1,228)=2.14; p = .145	F(2,226)=2.71; p = .069
CSF	quadratic: F(1,229)=11.98; p =.001	F(1,228)=8.13; p = .005	F(2,226)=2.08; p = .127

ANCOVA

	Age Advancement	HIV	HIV x Age Advancement
Grey Matter	F(1,165)=7.59; p = .007	F(1,165)=11.47; p = .001	F(1,165)=4.18; p = .043
White Matter	F(1,165)=0.05; p = .831	F(1,165)=2.79; p = .097	F(1,165)<0.01; p = .961
CSF	F(1,165)=3.84; p = .052	F(1,165)=10.04; p = .002	F(1,165)=1.63; p = .204

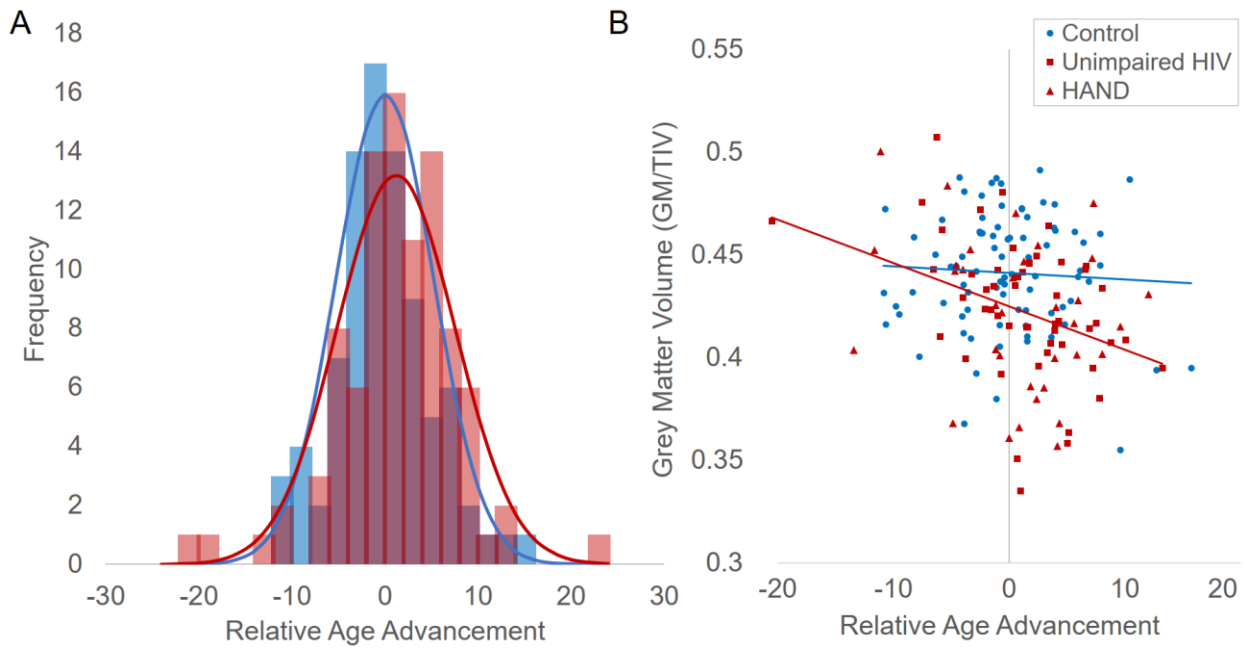

Figure 6: HIV-related age advancement is related to reduced grey matter volume. When comparing chronological age to epigenetic age, PWH showed a greater relative age advancement compared to uninfected controls (A). When examining the relationship between participants' relative age advancement and total grey matter volume, a significant HIV by age advancement interaction was found such that the greater advanced age seen in PWH was related to reduced total grey matter volume, while controls showed no relationship (B). GM/TIV = Total grey matter volume/ total intracranial volume.

In regard to local effects, statistical parametric mapping of both VBM and cortical thickness maps examining HIV, relative age advancement, and their interaction failed to display any region-specific main effect of relative age advancement, nor an interactive effect of HIV by relative age advancement after correcting for multiple comparisons. The main effects of HIV still remained and had similar topographies to previous models using chronological age (Figures 2 & 3).

In summary, only total grey matter volume showed a relationship with epigenetic age advancement, such that greater age advancement was associated with smaller grey matter volume, specifically in PWH. Whole brain statistics indicated that this pattern did not appear to be localized to a specific region.

Pairwise Comparisons by HAND Status

Post-hoc analyses were executed to identify whether effects were driven by participants with HAND. Total brain volume split by HAND showed that both participants with HAND, and unimpaired PWH had significantly less total grey matter volume in comparison to controls (HAND: $F(1,159)=9.57$; $p=.002$; Unimpaired PWH: $F(1,189)=6.84$; $p=.010$). Similarly, both participants with HAND and unimpaired PWH also had significantly greater total CSF volume in comparison to controls (HAND: $F(1,158)=9.54$; $p=.002$; Unimpaired PWH: $F(1,188)=5.50$; $p=.020$). However, neither HIV group showed significant differences from controls in total white matter volume (HAND: $F(1,158)=3.35$; $p=.069$; Unimpaired PWH: $F(1,188)=1.10$; $p=.296$). When comparing participants with HAND to unimpaired PWH, no significant differences were found in total grey matter ($F(1,107)=0.61$; $p=.436$), white matter ($F(1,106)=0.81$; $p=.369$), or CSF volume ($F(1,106)=0.93$; $p=.336$). Finally, the age-by-group interactive term remained non-significant for all group comparisons in all tissue types (all $p > .05$).

After splitting the PWH by HAND status, whole-brain cortical thickness ANCOVAs also showed no significant differences between unimpaired PWH and participants with HAND. Comparing controls to the two PWH groups separately (controls vs unimpaired HIV, and controls vs HAND) showed similar significant differences to the original model (Figure 7A and 7B). Notably, the control versus HAND comparison showed less significant clusters, which may be a reflection of decreased power due to the smaller number of HAND participants. To further investigate this, we calculated the effect size *r* for each of these comparisons (Figure 7C and 7D). This showed that the effect sizes of both comparisons were of similar pattern and magnitude, confirming that the differences in significance were likely due to differences in statistical power.

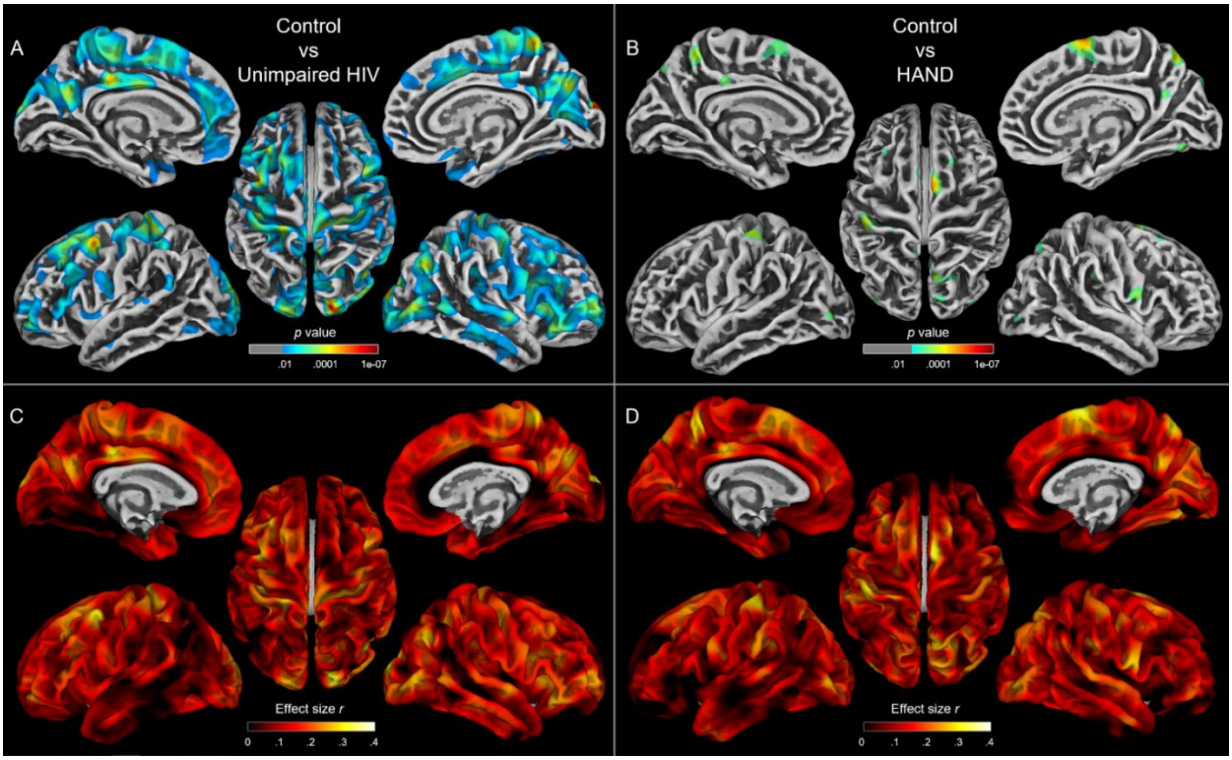

Figure 7: Pairwise comparisons by HAND status on cortical thickness. (A) When comparing only unimpaired PWH to uninfected controls, widespread areas showed reductions of cortical thickness related to HIV above and beyond age. (B) When comparing participants with HAND to uninfected controls, fewer regions showed significant reductions in cortical thickness after correction, potentially due to a reduction in statistical power. (C&D) To circumvent power concerns, we computed the effect sizes of each comparison, which revealed a relatively similar pattern and magnitude for the control vs unimpaired PWH (C) and control vs HAND (D) comparisons. No significant clusters were found comparing unimpaired HIV participants to participants with HAND. Color bars display p-values scaled by -log(p), and corrected with a .05 FDR and k=200 threshold. Color bars for the bottom panel display effect size (r-values).

Whole-brain VBM ANCOVAs also showed no significant differences between unimpaired PWH and participants with HAND. However, when comparing controls to the two PWH groups separately, the controls vs HAND comparison had predominantly more regions displaying significantly reduced grey matter compared to the controls vs unimpaired HIV comparison, particularly in the bilateral thalamus and bilateral hippocampus (Figure 8A and 8B). Unlike the cortical thickness pairwise comparisons, this is despite the decreased power in the HAND vs control contrast relative to the unimpaired HIV vs control contrast. Further investigating the effect sizes of these comparisons shows that the control vs HAND comparison had relatively large effect sizes in the bilateral thalamus and bilateral hippocampus, while the control vs unimpaired PWH comparison had relatively small effect sizes in these regions.

When examining relative age advancement split by HAND, there were no significant pairwise effects (*p*'s>.05). Examining the interaction between HIV status and relative age advancement on grey matter volume broken up by group revealed a significant HIV by relative age advancement interaction when using the unimpaired HIV group only ($F(1,131)=5.42$; $p=.021$). However when using the HAND group only, there is no significant interaction ($F(1,113)=1.19$; $p=.277$). Thus, the interaction in our main model does not appear to be by participants with HAND.

In summary, participants with HAND appeared to drive grey matter differences in the thalamus and hippocampus, but did not appear to drive the broad relationship between HIV and reduced total grey matter, nor the relationship between age advancement and reduced grey matter.

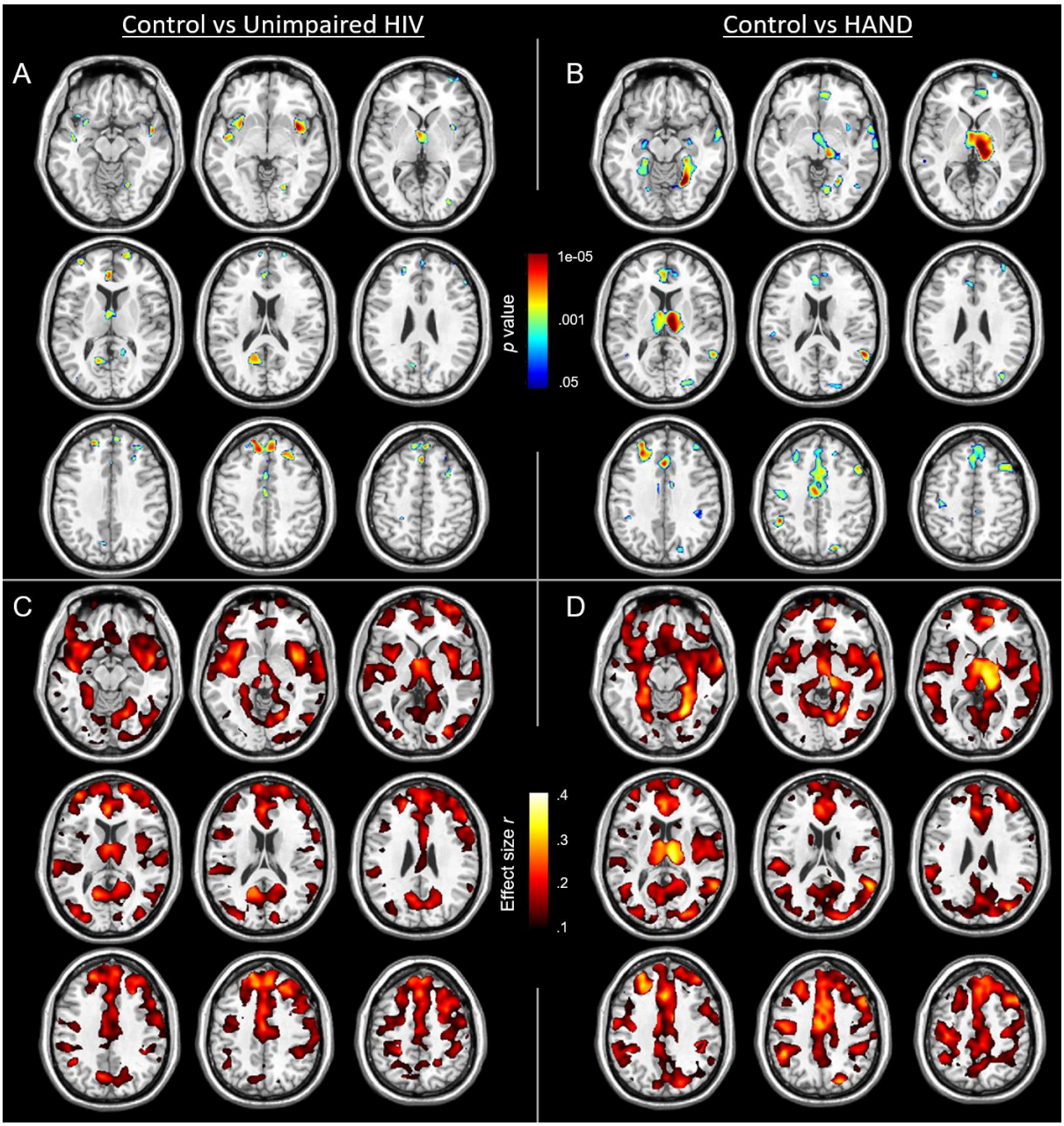

Figure 8: Pairwise comparisons by HAND status on VBM maps. (A) The control versus unimpaired HIV comparison had relatively few clusters showing significant group differences above and beyond the effect of age. (B) By comparison, the control versus HAND comparison revealed many significant clusters independent of age, most notably in the bilateral thalamus, and bilateral hippocampus, despite the reduced power of this contrast. (C&D) Examining the effect sizes of each pairwise comparison revealed that these regions had a relatively large effect size in the control vs HAND comparison (D), and a small effect size in the control vs unimpaired PWH comparison (C). No significant clusters survived multiple comparisons correction when comparing unimpaired HIV participants to participants with HAND. Color bars for the top panel display p-values scaled by -log(p), and corrected with a .05 FDR and k=200 threshold. Color bars for the bottom panel display effect size (r-values).

sMRI Discussion

This study used morphometric analyses of structural MRIs and epigenetic biomarkers of advanced aging to study the differential impact of aging on brain structure in a large sample of PWH. We found independent effects of HIV and aging on total grey matter volume, and widespread reductions in cortical thickness, and local grey matter content as identified by voxel based morphometry. Further, when using the epigenetic clock to calculate relative age advancement, we found that reduced total grey matter volume is related to increased age advancement. This relationship was specific to the HIV group, suggesting that HIV infection is the process that underlies this relationship. Finally, when taking cognitive status into account, we identified HAND-related grey matter reductions in the thalamus and hippocampus, and find that our earlier relationships with epigenetic age did not appear to be driven by those with HAND.

When examining total tissue volumes, grey matter decreased linearly throughout adulthood, white matter volume appeared to peak at middle age, and CSF volume sharply increased in older adulthood. These relationships have been established in previous literature [40,147], which provides an important foundation for our subsequent comparisons. We then found that PWH had reduced total grey matter volume irrespective of age. This finding is consistent with a long list of studies [67,148,149], including a recent meta-analysis [150], and may be reflective of neuronal loss due to HIV [151], although other health factors may also be at play [44,47,48]. Our study adds to this literature, specifically with a virally-suppressed sample spanning almost the full extent of adulthood, and extends previous findings by relating such grey matter loss to epigenetic aging. Interestingly, the grey matter loss identified in our sample did not appear to be driven by participants with HAND. We suspect this may be due to the small number of HAND participants, particularly the predominant number of HAND participants with asymptomatic neurocognitive impairment (the mildest form). Indeed, recent studies have suggested that HAND prevalence may

be overestimated,[152,153] and our lack of findings with HAND may be reflective of this. On the other hand, these data clearly show that grey matter reductions are present in PWH, even without clear signs of cognitive impairment. Such atrophy may be directly related to HIV infection, or may also be associated with health factors not controlled for in this study.

Our surface based morphometry results showed a widespread main effect of HIV in cortical thickness above and beyond age. Given the amount of cortex displaying this reduction in cortical thickness, our data suggest HIV-related reductions in cortical thickness do not follow a specific regional pattern, but rather affect the cortical mantle relatively globally. In comparison, our main effect of age also showed a global reduction in cortical thickness, but also displayed an especially strong effect in the frontal cortex, which has been shown in previous studies of normative aging [154]. Examining the effect of HAND showed similar effect sizes for the control versus unimpaired and control versus HAND comparisons, suggesting that our HIV-related reductions in cortical thickness were also not driven by participants with HAND. Therefore, expanding upon our total grey matter findings, this may indicate that cortical thinning can occur without HIV-related cognitive impairment.

Similarly, our voxel based morphometry results also showed a collection of regions with reduced grey matter related to HIV infection above and beyond age. Notably however, there was a particularly strong difference in the cingulate cortex, bilateral thalamus, and bilateral hippocampus. Upon probing the effect of HAND, significant differences in the thalamus and hippocampus were not present and had low effect sizes in the control versus unimpaired HIV comparison, but were present with relatively large effect sizes in the control versus HAND comparison, despite reduced power in the HAND comparison. Therefore, we believe these HIV-related reductions in grey matter are driven by those with cognitive impairment. This is a particularly interesting finding given other studies examining the relationship between cognitive

status and brain structure in PWH [155–157]. Specifically, a recent longitudinal study found that thalamus volume is decreased in PWH specifically during the period of time before patients begin cART therapy [158]. Therefore, thalamic volume may be affected during primary HIV infection, and the degree to which may be an indicator of future cognitive impairment. Further, the specificity of both thalamus and hippocampal volume decreases relating to cognitive impairment has been seen in a previous study examining PWH and alcohol use disorder [159]. Relating brain regions from a whole brain parcellation to neuropsychological performance, they found that volumes of both the thalamus and the hippocampus were each unique independent predictors of explicit memory scores. Our findings therefore replicate and extend this finding in a sample of cognitively impaired PWH without alcohol use disorder.

In all of these measures (total grey matter volume, cortical thickness, and VBM), we did not find any HIV by age interactions. This may relate to the debate on whether HIV infection leads to premature/accentuated versus accelerated aging, which largely focuses on whether HIV related aging occurs as a single "hit" at the time of infection (premature/accentuated), or whether continued HIV pathology accumulates over time and progressively advances pathological aging (accelerated) [9,67]. Our lack of a significant HIV by age interaction may imply that, while HIV-related reductions in grey matter reflect age-related changes, the trajectory of these changes with increasing age does not differ in PWH. In other words, given these group-level data, grey matter changes do not appear to be progressively worsening with age in PWH with viral suppression, but rather an accentuated aging mechanism (as indicated by the main effect of HIV) may be at play. This is in agreement with recent longitudinal studies showing decreased grey matter volume in PWH at baseline in comparison to uninfected controls, but with a relatively normal trajectory of change in brain structure over the two year follow-up, ultimately suggesting a lack of evidence for accelerated aging [67,160]. However, to definitively make such a distinction between accentuated

and accelerated aging, data derived from a longitudinal study would be needed. In this study, we use the term advancement to encompass both terms.

When combining the epigenetic data with measures of brain structure, we identified an HIV by age advancement interaction, such that, specifically for PWH, the greater biological age advancement a participant displayed, the smaller their total grey matter volume. The lack of such an association between relative age advancement and grey matter volume in uninfected participants further points towards HIV infection being the underlying link between age advancement and grey matter reductions. We therefore propose that grey matter changes related to HIV are indeed associated with age advancement at a molecular level. This is important because epigenetic aging is a peripheral biomarker used to quantify individual-specific levels of age advancement, beyond their chronological age. Importantly, DNA methylation age of brain tissue has been shown to be highly concordant with that of peripheral blood [18,161]. Brain-related age advancement had largely been studied using only chronological age, and biological age advancement has been showed to be associated with age-related mortality [19]. Therefore, our study not only illuminates the nature of HIV-related brain atrophy, but also further validates epigenetic advanced aging as a relevant biomarker in HIV. Mechanistically, this relationship may also suggest that epigenetic change could be a primary pathway by which grey matter atrophy occurs and/or persists in PWH. That is, viral reservoirs in the CNS and throughout the body may lead to inflammation, cellular damage, and ultimately epigenetic change that reflects advanced aging, and this may drive brain atrophy related to HIV. However, further study is needed to examine such causality. With regard to HAND, this relationship persisted even in those without HAND. Impairment may therefore be more closely related to atrophy in specific regions, or may be more tied to neural function rather than structure more broadly.

While these findings replicate previous grey matter and epigenetic changes that occur with HIV infection, the link between these two metrics is highly novel and needs to be replicated in other large-cohort studies of HIV. Further, this study's limitations include the fact that PWH were specifically recruited because they had well-managed HIV-infection. That is, all PWH were receiving effective combination antiretroviral medications, had undetectable plasma levels of HIV, and had no other substantial neurologic/psychiatric comorbidities including substance use disorders. Therefore, these data may not generalize well to a broader population of PWH that may have a variety of other complications. On the other hand, we did not examine common health comorbidities such as obesity, hypertension, or diabetes, nor did this study assess the effects of socioeconomic factors or health habits. Further study is needed to examine the impact of these common other health factors on our findings.

In conclusion, our study found broad decreases in grey matter volumes and cortical thickness, independently related to HIV and aging. Biomarkers of epigenetic age advancement revealed that PWH with increased age advancement had an associated decrease in grey matter volume, and this relationship was not seen in uninfected controls. We also identified age-independent HAND-related reductions in grey matter, specifically in the thalamus and hippocampus. These findings ultimately link molecular epigenetic age advancement to large scale aberrations in brain structure in PWH, which provides additional evidence supporting the epigenetic clock as a relevant biomarker for HIV-related age advancement, and may also begin to reveal the underlying mechanisms of advanced aging in the HIV-infected brain.

CHAPTER 5: Results & Discussion 2: Functional Networks

fMRI Results

Participants

Out of the 121 PWH and 133 uninfected controls recruited for this study, 105 PWH and 116 controls successfully completed the sMRI and fMRI protocols. After exclusions for excess head motion, 86 PWH and 99 uninfected controls had both structural and functional MRI data that could be used for further processing (Table 3). All PWH were virally suppressed with a median current CD4 of 701.5 cells/µl (range: 102-2617) and a median CD4 nadir of 234 cells/µl (range: 3-586).

Table 3: fMRI Participant Demographics

	Sample with MRI Data		**Subsample with MRI and Epigenetic Data**	
	Uninfected Controls (n=99)	**PWH (n=86)**	**Uninfected Controls (n=67)**	**PWH (n=70)**
Chronological Age (years; mean/SD)	45.02 (15.41)	48.09 (12.77)	43.83 (14.66)	47.66 (12.45)
Sex (M/F; n/%)	55/44 (55.5/44.4%)	53/33 (61.6/38.4%)	36/31 (53.7/46.3%)	47/23 (67.1/32.9%)
Race (Caucasian, African American, Asian, Other: n/%)	70/22/5/2 (70.1/22.2/5.1/1.0%)	55/26/2/3 (64.0/30.2/2.3/3.4%)	49/13/4/1 (73.1/19.4/6.0/1.5%)	47/21/1/1 (67.1/30.0/1.4/1.4%)
Average Composite Neuropsychological Z-Score (mean/SD)	-0.08 (0.61)	-0.41 (0.57)	0.06 (0.50)	-0.43 (0.54)
HAND (n/%)	-	31 (36.0%)	-	27 (38.6%)
Time Since HIV Diagnosis (years; mean/SD)	-	11.29 (7.34)	-	11.33 (7.47)
CD4 Nadir (median/range)	-	234 (3-586)	-	234 (3-585)
Current CD4 (median/range)	-	701.5 (102-2617)	-	726.5 (106-2617)

Note; HAND: HIV-Associated Neurocognitive Disorder

Ninety-seven PWH and 87 controls completed a blood draw for epigenetic age estimation. Missing data were due to participants quitting the study, being lost to follow-up, or related issues. Notably, 12 participants who completed the blood draw did not successfully complete the MRI

protocol, and three blood samples were inadequate for epigenetic age estimation. Ultimately this yielded a final sample of 70 PWH and 67 controls who had reliable data from both epigenetic age estimations and MRI data. Subsequent fMRI analyses included all 185 participants that completed MRI, and analyses relating fMRI to epigenetics only utilized participants that had data from both methods (n=137).

HIV by Age Effect in Ventral Attention Network Within-Network Connectivity

Within-network connectivity was estimated for seven established functional networks, and ANCOVAs were used to examine for the main effects of age and HIV. Across all seven networks, only the visual network showed a significant main effect of age ($F(1,182)=9.25$; $p=.003$, $\eta^2=.047$). None of the other six networks showed a significant main effect of age. Additionally, no main effects of HIV were identified in any of the seven within-network functional connectivity metrics (all $p>.05$; Figure 9).

However, adding in the HIV by age interaction to the models showed that within-network connectivity of the ventral attention network had a significant HIV by age interaction such that PWH showed a greater decrease in connectivity with age relative to controls ($F(1,181)=4.70$, $p=.031$, $\eta^2=.025$). None of the other within-network models displayed a significant HIV by age interaction (all $p>.05$; Table 4).

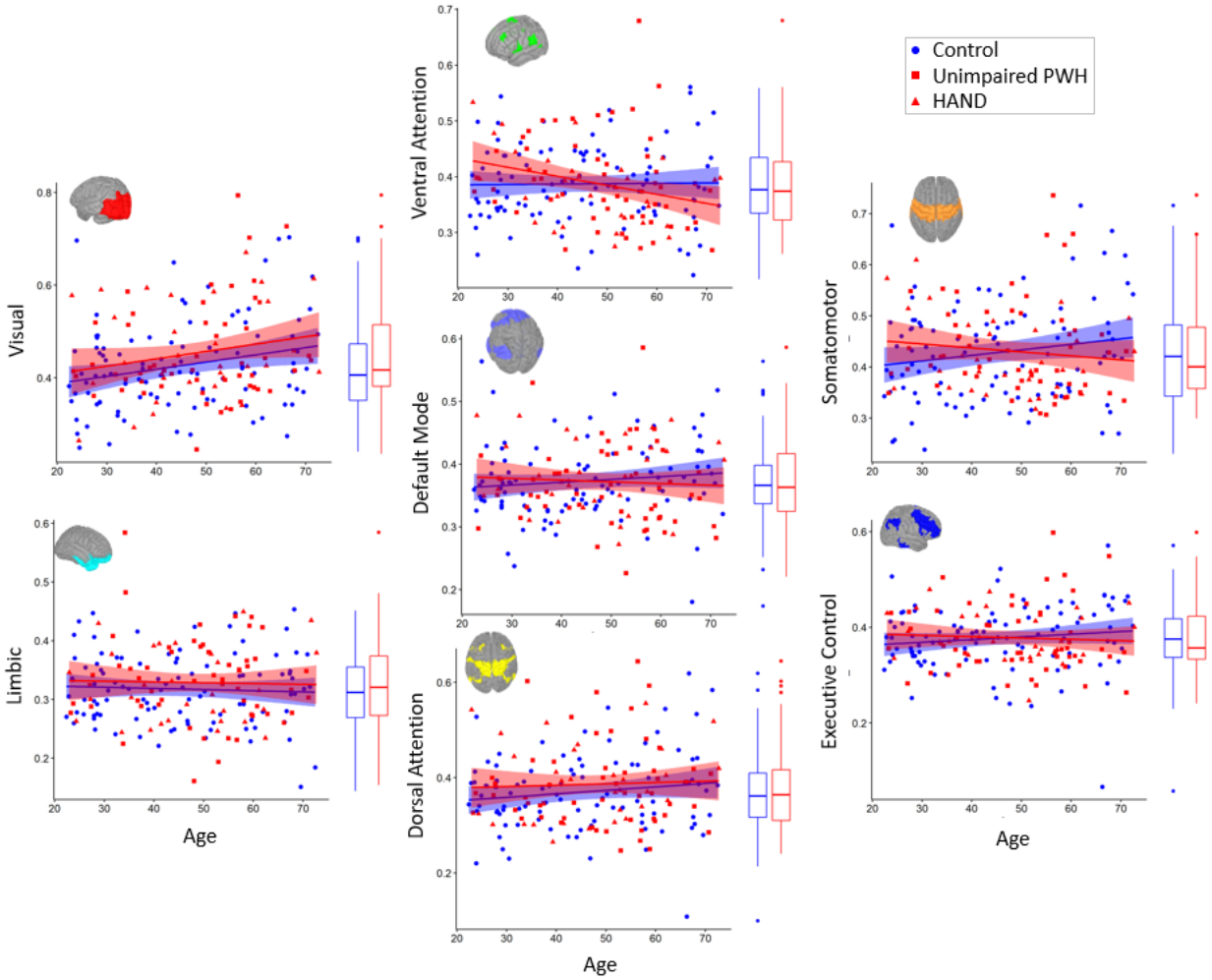

Figure 9: Within-Network Functional Connectivity by Age and HIV. The average correlation within each network was calculated and z transformed. ANCOVAs testing the independent effects of HIV and age showed no significant main effects of HIV, and a significant main effect of age only in the visual network. Scatter plots display z values of each within-network functional connectivity metric by age, with uninfected controls in blue and PWH in red. HAND status is differentiated by shape for display purposes. Linear fits for each group are displayed with 95% confidence intervals. Boxplots displaying group differences are added to the right of each plot, and visual representations of each network are inset.

Widespread Independent Effects of Aging and HIV in Between-Network Connectivity

The functional connectivity between each of the seven networks was estimated and the average pairwise correlation was computed and z transformed for each network. This resulted in seven between network functional connectivity metrics (one for each network). Significant main effects of age were identified in all seven between-network functional connectivity metrics (visual: $F(1,182)=15.84$, $p<.001$, $\eta^2=.079$; somato-motor: $F(1,182)=23.63$, $p<.001$, $\eta^2=.111$; dorsal

attention (DAN): $F(1,182)=16.51$, $p<.001$, $\eta^2=.080$; ventral attention (VAN): $F(1,182)=18.18$, $p<.001$, $\eta^2=.087$; limbic: $F(1,182)=16.18$, $p<.001$, $\eta^2=.077$; executive control $F(1,182)=17.57$, $p<.001$, $\eta^2=.050$; and default mode: $F(1,182)=20.79$, $p<.001$, $\eta^2=.097$; Table 2). All of these effects showed consistent increases in between-network functional connectivity with increasing age.

With regard to HIV, many of the between-network functional connectivity metrics also showed a significant independent main effect of HIV status. Specifically, the limbic ($F(1,182)=8.50$, $p=.004$, $\eta^2=.054$), executive control ($F(1,182)=7.70$, $p=.006$, $\eta^2=.084$), and default mode ($F(1,182)=8.36$, $p=.004$, $\eta^2=.054$) networks all showed significant effects of HIV at *p<.01* such that PWH had increased between-network functional connectivity compared to controls, above and beyond the effect of age. Additionally, the ventral attention ($F(1,182)=5.40$, $p=.021$, $\eta^2=.038$), dorsal attention ($F(1,182)=4.52$, $p=.035$, $\eta^2=.032$), and somato-motor ($F(1,182)=4.14$, $p=.043$, $\eta^2=.031$) networks showed significant main effects of HIV at $p<.05$ (Figure 10). All of these effects showed an increase in between-network functional connectivity in PWH relative to controls, above and beyond the effect of age. Adding in the HIV by age interaction to the models showed no interaction effects in any of the between-network connectivity metrics. Importantly, we also performed a quality assurance check to ensure our results were not due to residual motion artifacts in the data by adding in mean framewise displacement as a covariate. Effects of group remained significant for the limbic, executive control, and DMN between network functional connectivity metrics (all $p<.05$).

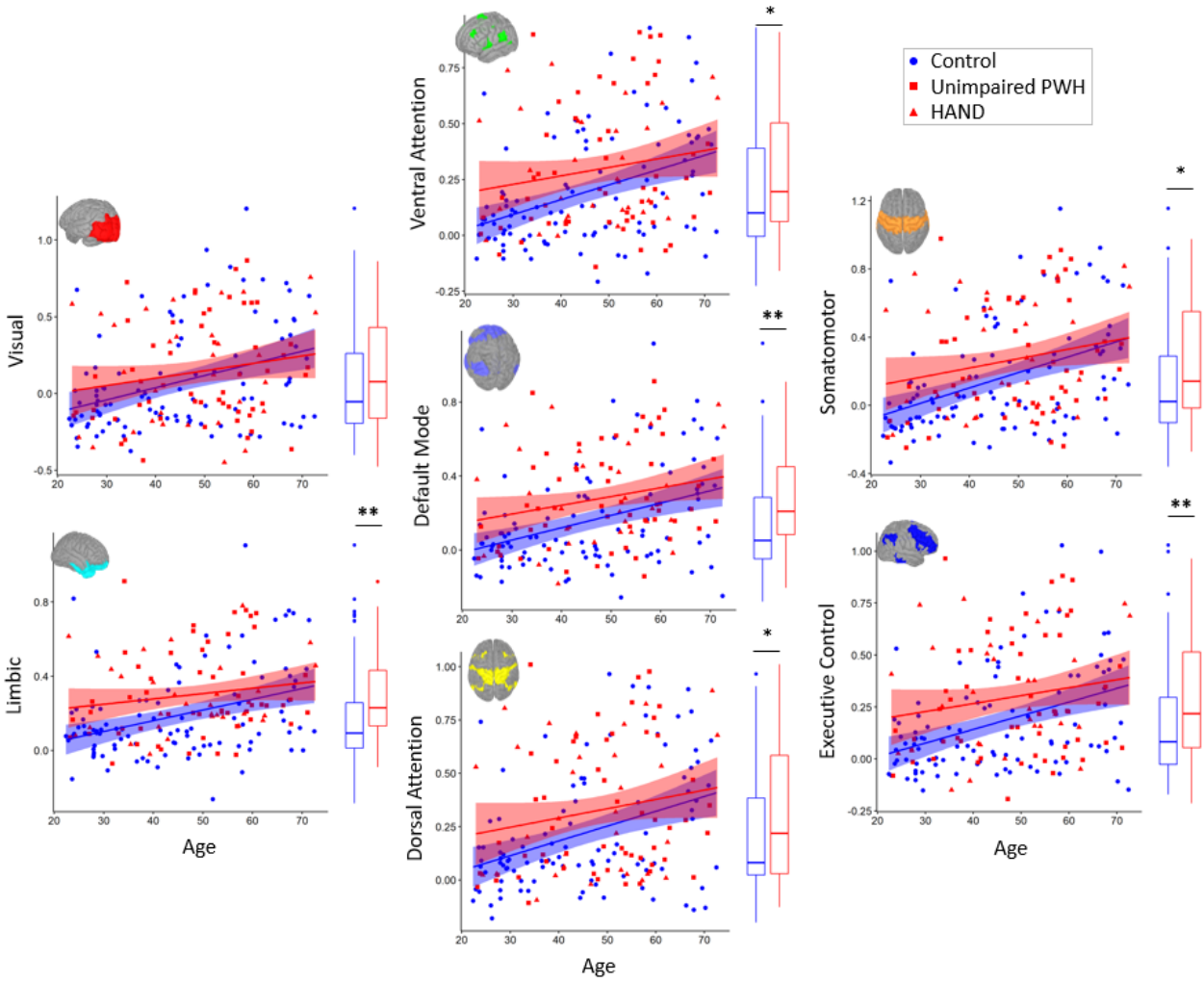

*Figure 10: Between-Network Functional Connectivity by Age and HIV. The correlation between each network was calculated, z transformed, and then averaged for each network. ANCOVAs testing the independent effects of HIV and age showed significant main effects of age in every network. Significant main effects of HIV were identified in all networks except in functional connectivity with the visual network. Scatter plots display z values of each between-network functional connectivity metric by age, with uninfected controls in blue and PWH in red. HAND status is differentiated by shape for display purposes. Linear fits for each group are displayed with 95% confidence intervals. Boxplots displaying group differences are added to the right of each plot, and visual representations of each network are inset. * p<.05, **p<.01.*

Table 4: Average Network Statistics

Within-Network Functional Connectivity									
	Age			**HIV**			**HIV x Age**		
	F (1,182)	*p*	η^2	*F (1,182)*	*p*	η^2	*F (1,181)*	*p*	η^2
Visual	9.25	.003*	.047	2.38	.125	.018	0.00	.972	.000
Somato-motor	0.63	.429	.003	0.01	.906	.000	3.43	.066	.019
DAN	1.68	.197	.009	1.42	.234	.010	0.25	.620	.001
VAN	2.18	.141	.012	0.05	.831	.000	4.70	.031*	.025
Limbic	0.27	.606	.001	1.37	.243	.007	0.01	.926	.000
Executive	0.51	.478	.003	0.00	.978	.000	1.35	.248	.007
DMN	0.32	.575	.002	0.03	.852	.000	1.20	.276	.007
Between-Network Functional Connectivity									
	Age			**HIV**			**HIV x Age**		
	F (1,182)	*p*	η^2	*F (1,182)*	*p*	η^2	*F (1,181)*	*p*	η^2
Visual	15.84	<.001*	.079	0.70	.405	.008	0.78	.380	.004
Somato-motor	23.63	<.001*	.111	4.14	.043*	.031	1.18	.279	.006
DAN	16.51	<.001*	.080	4.52	.035*	.032	0.72	.397	.004
VAN	18.18	<.001*	.087	5.40	.021*	.038	1.11	.293	.005
Limbic	16.18	<.001*	.077	8.50	.004*	.054	1.46	.228	.007
Executive	17.57	<.001*	.050	7.70	.006*	.084	1.01	.316	.005
DMN	20.79	<.001*	.097	8.36	.004*	.054	0.51	.475	.002

Note: DAN: Dorsal Attention Network; VAN: Ventral Attention Network; DMN: Default Mode Network; * $p<.05$; note that the HIV and Age columns represent the significance of the main effects without the interaction term, and the HIV x Age significance is derived in from an additional model after adding in the interaction.

Increased Functional Connectivity with Ventral Attention Network Driven by HAND

To examine whether our effects of HIV were driven by participants with HAND, we split the HIV group by HAND status and performed comparisons between controls, unimpaired PWH, and PWH with HAND. Ultimately, no significant differences were identified between unimpaired

PWH and those with HAND. Significant differences between controls and unimpaired PWH remained in limbic, executive, and DMN between-network functional connectivity metrics (all p<.05), above and beyond the effects of age. Similarly, significant differences between controls and PWH with HAND were present in VAN, limbic, executive, and DMN between-network functional connectivity metrics (all p<.05), above and beyond the effects of age (Figure 11).

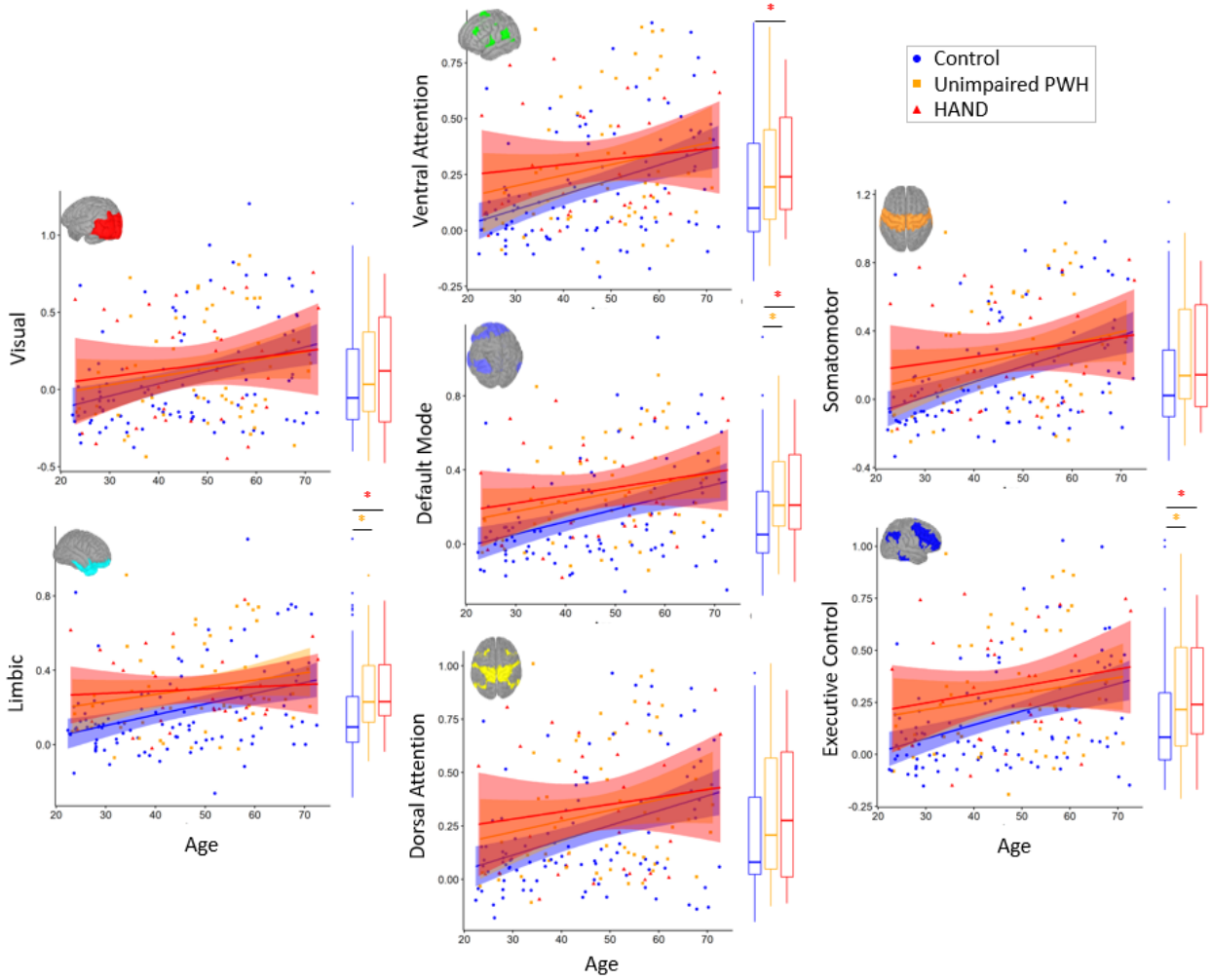

*Figure 11: Between-Network Functional Connectivity Split by HAND. The correlation between each network was calculated, z transformed, and then averaged for each network. ANCOVAs testing the independent effects of HIV and age showed significant main effects of age in every network. Significant main effects of HIV were identified in limbic, default mode, and executive control networks. Scatter plots display z values of each between-network functional connectivity metric by age, with uninfected controls in blue and PWH in red. HAND status is differentiated by shape for display purposes. Linear fits for each group are displayed with 95% confidence intervals. Boxplots displaying group differences are added to the right of each plot, and visual representations of each network are inset. * p<.05.*

No Interactions of HIV with Epigenetic Age Advancement

To examine whether these between-network functional connectivity metrics related to epigenetic age advancement, we performed ANCOVAs aiming to identify HIV by Age Advancement interactions. Ultimately, none of the seven between-network metrics displayed a significant HIV by Age Advancement interaction (Appendix A).

Pairwise Examination of Between-Network Functional Connectivity

To further probe the effects of HIV and age in between-network connectivity, we performed additional statistics on the connectivity matrices. Group averaged connectivity matrices show that PWH have broadly larger between-network connectivity values than in comparison to controls (Figure 12). Subtracting the two matrices highlights that such was the case for nearly every pair of networks, and similarly, performing a correlation with age on these networks shows that every pair of networks showed a positive correlation with age (Figure 13).

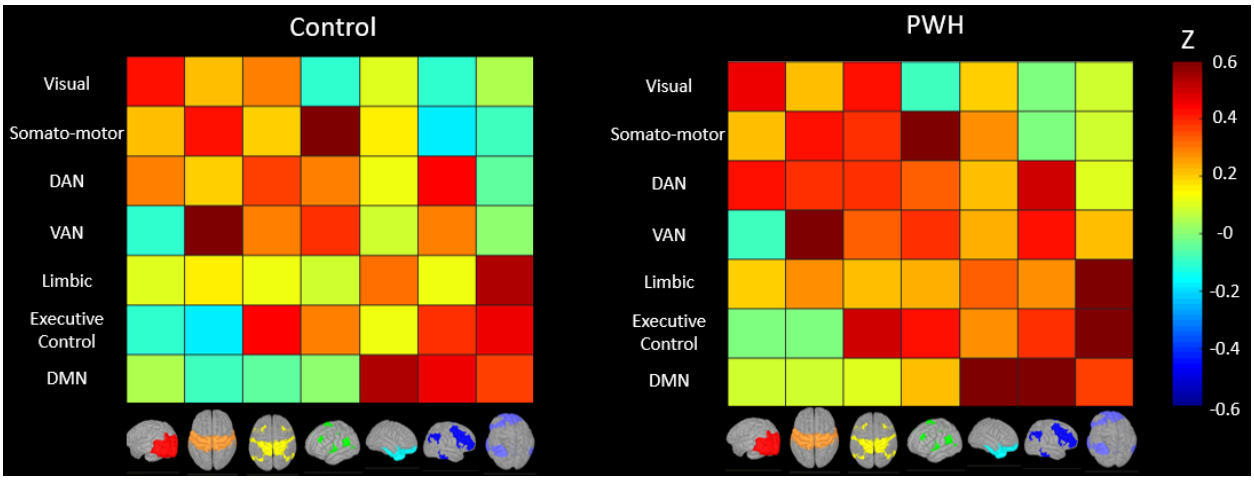

Figure 12: Group Averaged Pairwise Functional Connectivity. Between- and within- (diagonal) network connectivity matrices. Matrices are symmetric with labels on the left, and visual representations of each network displayed on the bottom. Color bar to the right applies to both matrices and represents Z values, with warm colors representing positive functional connectivity and cool colors representing negative functional connectivity.

We then tested for the main effects of HIV and age on these connectivity matrices. After bonferroni correction for multiple comparisons, the main effect of HIV was significant in VAN-

Limbic, VAN-DMN, Limbic-Executive, and Executive-DMN pairs. Therefore, PWH broadly showed the largest increases in between-network connectivity between the VAN, Limbic, Executive, and DMN networks. The main effect of age on the other hand showed widespread significant effects, suggesting that the increase in between-network connectivity with age is not driven by a particular set of networks (Figure 13).

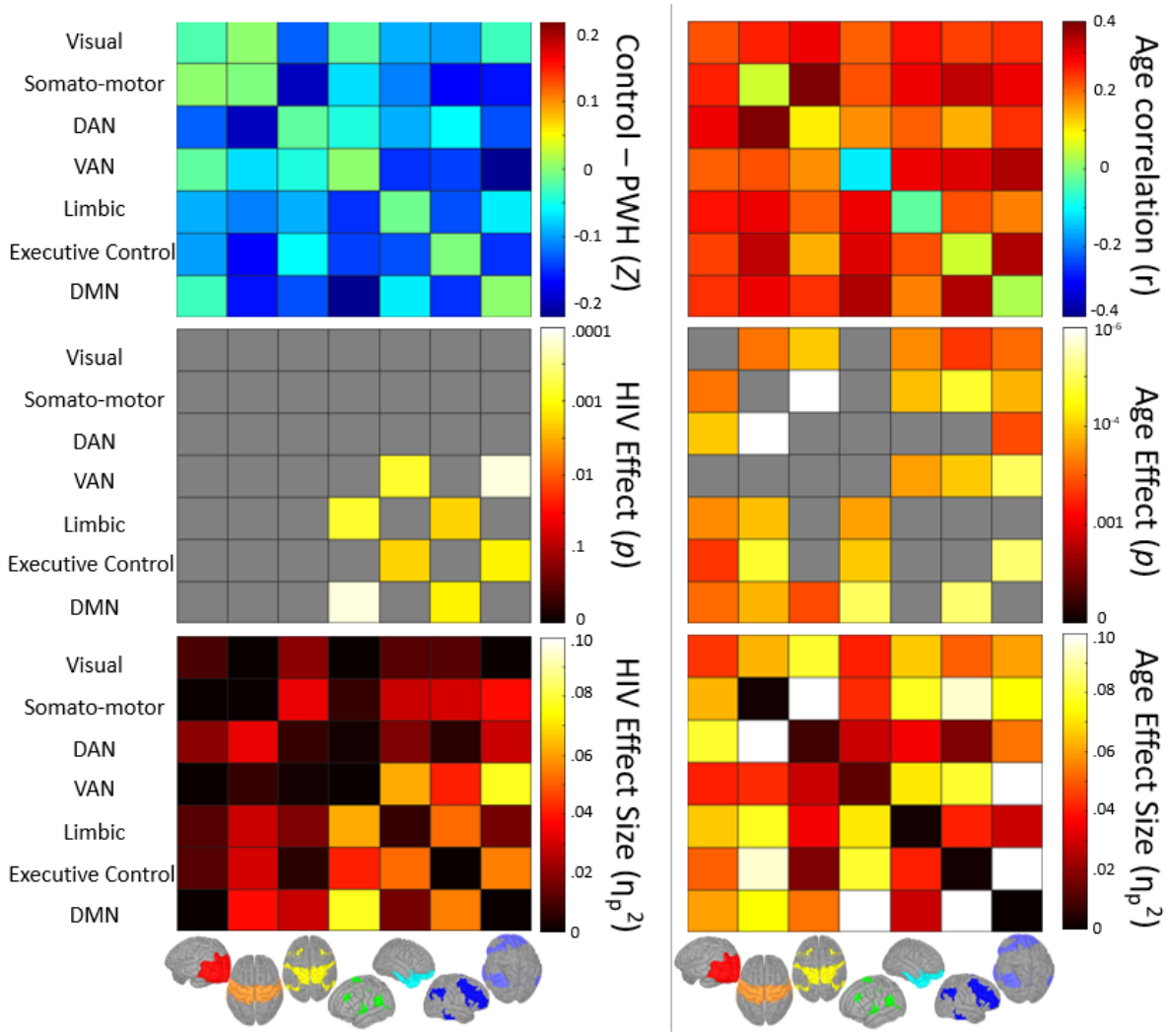

Figure 13: Pairwise Functional Connectivity Statistics: Effects of Age and HIV. Matrix statistics performed on between- and within- (diagonal) network connectivity matrices allowed pairwise between-network connectivity to be examined. Top left: Subtraction matrix with hot colors representing controls>PWH and cool colors representing controls<PWH. Top right: Simple age correlation matrix with hot colors representing increasing connectivity with age and cool colors representing decreasing connectivity with age. Middle: Significance matrices for the main effects of HIV (left) and age (right) displaying p values on a log scale and thresholded using a bonferroni correction. Bottom: Effect size matrices for the main effects of HIV (left) and age (right) displaying η_p^2 values. Matrices are symmetric with labels on the left, and visual representations of each network displayed on the bottom.

Replication and Extension of HIV and Age Effects Using a 13 Network Parcellation

We then aimed to replicate and extend these effects in between-network connectivity by using a 13 network parcellation. Notably, this atlas includes a subcortical network, which was not present in the seven network atlas, and includes subdivisions of the seven networks. Statistics on these matrices showed the same patterns of increased between-network functional connectivity with age, and with HIV infection, displayed by the subtraction and age correlation matrices (Figure 6). One notable difference however, was a single pair (Anterior DMN-Posterior DMN) which showed a large decrease in between-network functional connectivity with age.

Testing for the main effects of HIV and age on these connectivity matrices showed a similar numerous amount of pairs displaying an age effect. The effect of HIV however displayed more sparse significance due to a larger Bonferroni correction for multiple comparisons. Interestingly however, the pairs that did survive correction were an increase in Subcortical-Medial Temporal and Subcortical-Anterior DMN connectivity in PWH relative to controls, and a decrease in Anterior DMN-Posterior DMN in PWHrelative to controls (Figure 14). Comparing partial eta squared effect size matrices display the larger effect size of aging compared to the effect of group, as well as the similar effect sizes between the seven and 13 network parcellations.

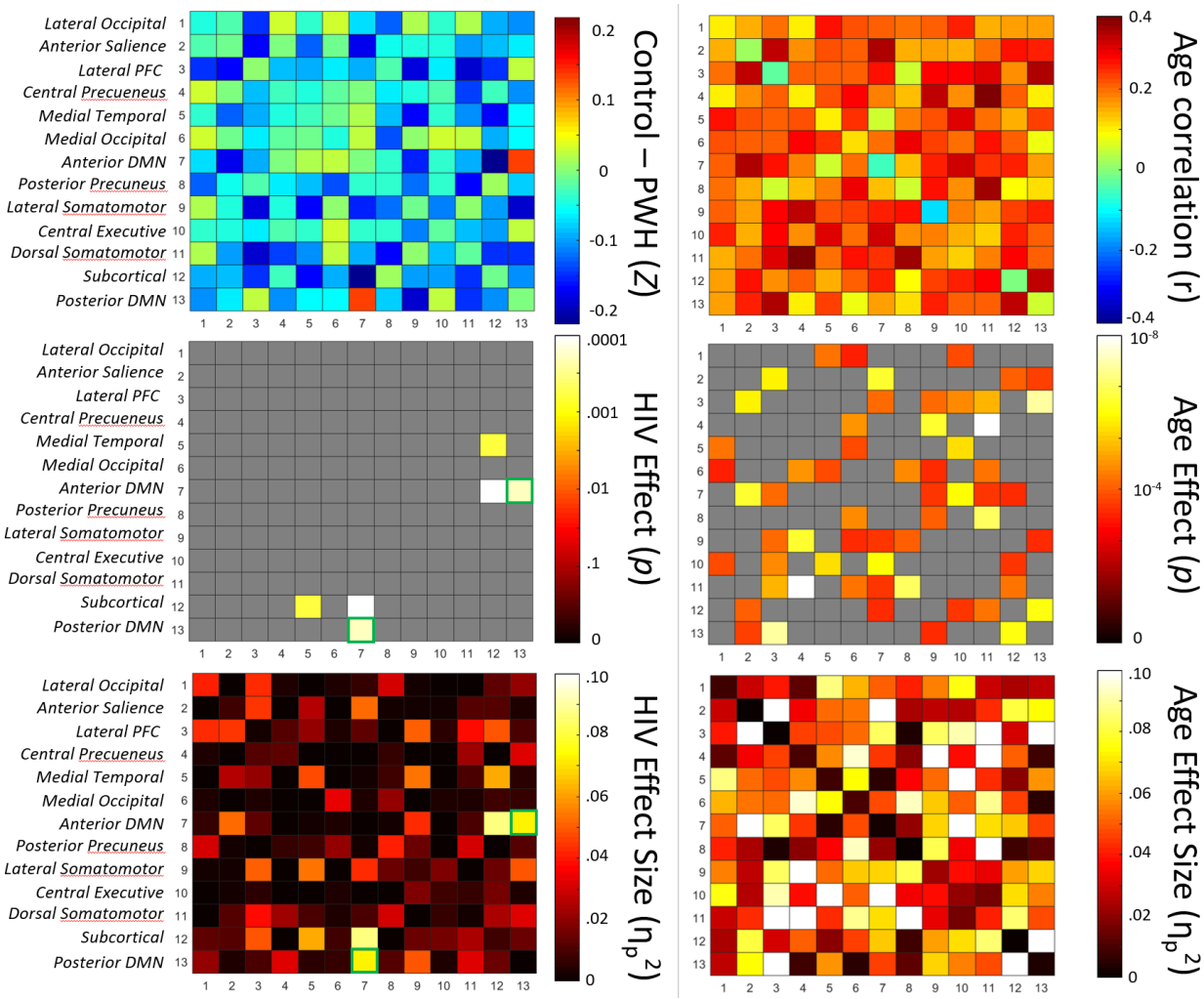

Figure 14: Pairwise Functional Connectivity Statistics: 13 Network Atlas. Matrix statistics performed on between- and within- (diagonal) network connectivity for the Doucet 13-network atlas. Top left: Subtraction matrix with hot colors representing controls>PWH and cool colors representing controls<PWH. Top right: Simple age correlation matrix with hot colors representing increasing connectivity with age and cool colors representing decreasing connectivity with age. Middle: Significance matrices for the main effects of HIV (left) and age (right) displaying p values on a log scale and thresholded using a bonferroni correction. Effects for controls>PWH are labeled with green borders. Bottom: Effect size matrices for the main effects of HIV (left) and age (right) displaying η_p^2 *values.*

fMRI Discussion

Our study examined a large sample of PWH and uninfected controls spanning age 22-72 and identified independent effects of age and HIV in between-network connectivity. Age related increases in between network connectivity were widespread, while PWH displayed further increases above and beyond aging, specifically between default mode, executive control, and limbic networks. Utilization of a further parcellated atlas which also included subcortical regions

allowed us to identify robust HIV-related increases in functional connectivity between subcortical-medial temporal regions, and subcortical-anterior DMN areas. Additionally, PWH displayed a specific and strong decrease in anterior DMN-posterior DMN connectivity compared to controls. These findings broadly support the framework that HIV infection leads to alterations in functional connectivity that are highly similar to the aging phenotype. Below we discuss these findings in the context of previous literature.

One of our main findings was that HIV infection was related to widespread increases in between-network functional connectivity. At first this may seem contradictory to previous studies such as Thomas et al.[64], who showed decreased magnitude of between-network connectivity in multiple pairs of networks in PWH compared to controls. However, we believe our results are consistent with their findings, and the discrepancy is simply due to differences in processing and presentation of results. That is, they indeed found more positive between-network connectivity in PWH, which was presented as a reduction in magnitude due to these networks being anti-correlated. These more negative correlations are simply due to their utilization of global signal regression, which creates more negative correlations in the data.[162,163] Therefore, our findings are indeed consistent with previous network level investigations of HIV. Importantly, our results expand upon these by integrating with an aging framework. Increased between-network connectivity was also seen with increasing age, which a well-established pattern of aging,[73] and overall suggests that PWH display a connectivity profile that resembles an advancement in age.

Our post-hoc analyses of HAND status showed that altered functional connectivity with the ventral attention network was seen more prominently in PWH with HAND. This may indicate that this network is particularly sensitive to cognitive impairment. Supporting this, previous studies have also found HAND related differences in the salience network,[164] and therefore this network may be a promising indicator of HAND. Broadly however, many of the deficits in

functional connectivity were largely present in both PWH with and without cognitive impairment. Previous studies have also identified the presence of functional deficits related to HIV in the absence of HAND, with one study specifically noting no difference in resting state functional connectivity by HAND status. [165] This ultimately suggests that a reorganization of brain networks occurs irrespective of neuropsychological changes. At the same time, our sample of PWH with HAND may not represent a severe enough sample to detect further exacerbations of functional connectivity. That is, the majority of our participants with HAND were of the mildest category (asymptomatic neurocognitive impairment). This could have led our HAND group to be similar to the unimpaired group. Further study is needed to examine the more severe presentations of HAND.

Upon utilizing a more subdivided 13 network atlas, we further identified robust increases in subcortical-medial temporal and subcortical-anterior DMN connectivity in PWH relative to controls, and a decrease in anterior DMN-posterior DMN in PWH relative to controls. These more regionally specific effects could not have been identified with the seven network atlas, and are highly consistent with previous fMRI studies of HIV. Alterations in cortico-striatal connectivity have been consistently linked to HIV in both task based and resting state fMRI studies.[63,65,66] Similarly, decreases in DMN functional connectivity have been reported in multiple resting-state studies of PWH.[64,67] Here we replicate and expand upon these studies by showing that these changes are present independent of aging. Taken together with our previous results, this suggests a decrease in modularity related to HIV infection, where PWH have decreased connectivity in the DMN, and increased connectivity between DMN and other networks. Indeed previous studies have shown this decrease in modularity related to HIV,[76] and our data further work should utilize such graph metrics in the study of HIV.

In this dataset, we did not identify significant decreases in within-network functional connectivity with age. While previous lifespan studies have shown decreasing within-network functional connectivity with aging, this may simply be due to the age range of our participants. That is, the steepest decline in within-network functional connectivity appears to occur after age 60+. Our sample ranged in age up to age 72, and studies identifying decreasing within-network functional connectivity show the largest effects in those approaching 80 years old.[72,166] In contrast, between network functional connectivity appears to display a sharper increase beginning at a younger age,[72] which is consistent with our findings. Therefore, within-network changes with age may be specific to older age, and further studies may need to include older adults to study how such trends change with HIV infection. Notably, we did identify a significant HIV by age interaction in the ventral attention network such that PWH showed a greater decrease in functional connectivity compared to controls. Therefore, the age-related pattern of decreased within network connectivity may have been seen in our PWH, albeit specific to one network. Interestingly, this is the same network that showed HAND specific changes in between-network connectivity. Therefore the ventral attention network may be altered more readily with HIV infection, and further studies might examine this network more specifically.

In regards to the between-network connectivity metrics, we did not identify any significant HIV by age interaction. This is in agreement with multiple studies showing that the effects of age and HIV on brain function are independent.[66,69,70] Importantly however, this does not mean that the changes seen with HIV do not fit into an aging framework. A significant HIV by age interaction would show that the trajectory of aging is differing with HIV infection. Instead, our data show that the trajectory remains the same, but there is an added insult related to HIV infection that is in the same direction as age related degradation. Thus, HIV-related alterations in functional connectivity may be seen as an advancement in aging. This model is consistent with

multiple studies suggesting HIV infection causes a “hit” to biological systems, advancing the aging process.[9]

However, we did not find a specific association of functional connectivity to HIV-related epigenetic advanced aging. This suggests a disconnect between epigenetic markers of age advancement from functional reorganization of the brain. Reorganization of functional networks is certainly a more dynamic process, and has been shown to be independent of age related structural changes.[167] Therefore, while our structural results indicate a relation in grey matter loss to HIV related epigenetic aging, our functional network results may be more independent of these metrics due to the more indirect nature of functional organization. Further study is therefore needed to examine the complexities that may lie between functional connectivity and peripheral epigenetic markers of aging.

The study has a number of limitations that must be considered. Firstly, as mentioned previously, our sample of PWH had very well-managed HIV-infection in the form of effective combination antiretroviral medications and undetectable viral loads. Further study is needed to examine the impact of common other health factors on our findings. Additionally, as stated before, future studies should examine older adults (beyond age 72) and PWH with more severe diagnoses of HAND. This study also focused on the between and within network functional connectivity of pre-defined networks, and future studies should examine graph theory metrics given our interpretation of decreased modularity in PWH.

In conclusion, HIV infection may be related to a reorganization of functional connectivity in a manner similar to aging. Specifically, both HIV infection and aging are associated with independent increases in between-network functional connectivity. The effect of HIV was driven by increases in connectivity between default mode, executive control, and limbic networks.

Additionally, VAN may be related to cognitive dysfunction in HIV, as the functional connectivity with the VAN was found to be altered specifically in PWH with HAND. Effects of other networks were present in PWH with and without HAND, suggesting such reorganization occurs despite lack of cognitive impairment. Finally, PWH also showed increases in subcortical-DMN functional connectivity, and decreases in anterior DMN-posterior DMN.

CHAPTER 5 – Results & Discussion 3: Resting Oscillatory Activity

MEG Results

Participants

Out of the 121 PWH and 133 uninfected controls recruited for this study, 115 PWH and 126 controls successfully completed the MEG protocol (Table 5). All of these participants completed a structural T1 scan except for 11 participants, for whom warped template brains were used. All PWH were virally suppressed with a median current CD4 of 702 cells/µl (range: 102-2617) and a median CD4 nadir of 237 cells/µl (range: 3-586).

Table 5: MEG Participant Demographics

	Sample with MEG Data		**Subsample with MEG and Epigenetic Data**	
	Uninfected Controls (n=126)	**PWH (n=115)**	**Uninfected Controls (n=85)**	**PWH (n=90)**
Chronological Age (years; mean/SD)	45.23 (15.37)	47.63 (12.22)	43.80 (14.60)	47.60 (12.14)
Sex (M/F; n/%)	71/55 (56.3/43.7%)	66/49 (57.4/42.6%)	45/40 (52.9/47.1%)	57/33
Race (Caucasian, African American, Asian, Other: n/%)	86/32/5/3 (68.2/25.3/4.0/2.3%)	72/38/2/3 (62.6/33.0/1.7/2.6%)	58/21/4/2 (68.2/24.7/4.7/2.4%)	59/29/1/1 (65.6/32.2/1.1/1.1%)
Average Composite Neuropsychological Z-Score (mean/SD)	-0.11 (0.61)	-0.39 (0.65)	0.01 (0.52)	-0.42 (0.62)
HAND (n/%)	-	41 (35.6%)	-	35 38.9%
Time Since HIV Diagnosis (years; mean/SD)	-	11.25 (7.25)	-	11.33 (7.47)
CD4 Nadir (median/range)	-	237 (3-586)	-	234 (3-585)
Current CD4 (median/range)	-	702 (102-2617)	-	726.5 (106-2617)

Note; HAND: HIV-Associated Neurocognitive Disorder

Ninety-seven PWH and 87 controls completed a blood draw for epigenetic age estimation. Missing data were due to participants quitting the study, being lost to follow-up, or related issues. Notably, 6 participants who completed the blood draw did not successfully complete the MEG

protocol, and three blood samples were inadequate for epigenetic age estimation. Ultimately this yielded a final sample of 90 PWH and 85 controls who had reliable data from both epigenetic age estimations and MEG data. Subsequent MEG analyses included all 241 participants that completed MRI, and analyses relating fMRI to epigenetics only utilized participants that had data from both methods (n=175).

Significant Age Effects in Delta and Beta Power

Statistical parametric mapping identified significant main effects of age in the delta and beta bands (Figure 15). After correction for multiple comparisons, delta power was shown to significantly decrease with age in the left posterior temporal cortex. Beta power on the other hand showed a significant increase in power with increasing age in the somato-motor cortices. Both of these effects represent the effect of age after statistically controlling for the effect of HIV. Analysis of predefined regions of interest identified similar effects to the whole brain statistics. That is, average somato-motor (central) beta activity showed a robust significant main effect of age ($F(1,238)=41.78$; $p<.001$; $\eta^2 =.149$), and average frontal delta showed a significant main effect of age ($F(1,238)=4.41$; $p=.037$; $\eta^2 =.018$).

No significant clusters were identified after multiple comparison correction in the theta, alpha, or gamma bands. Similarly, no significant main effects of age were identified using frontal theta, occipital alpha, or frontal gamma regions of interest (all $p>.05$; Table 6).

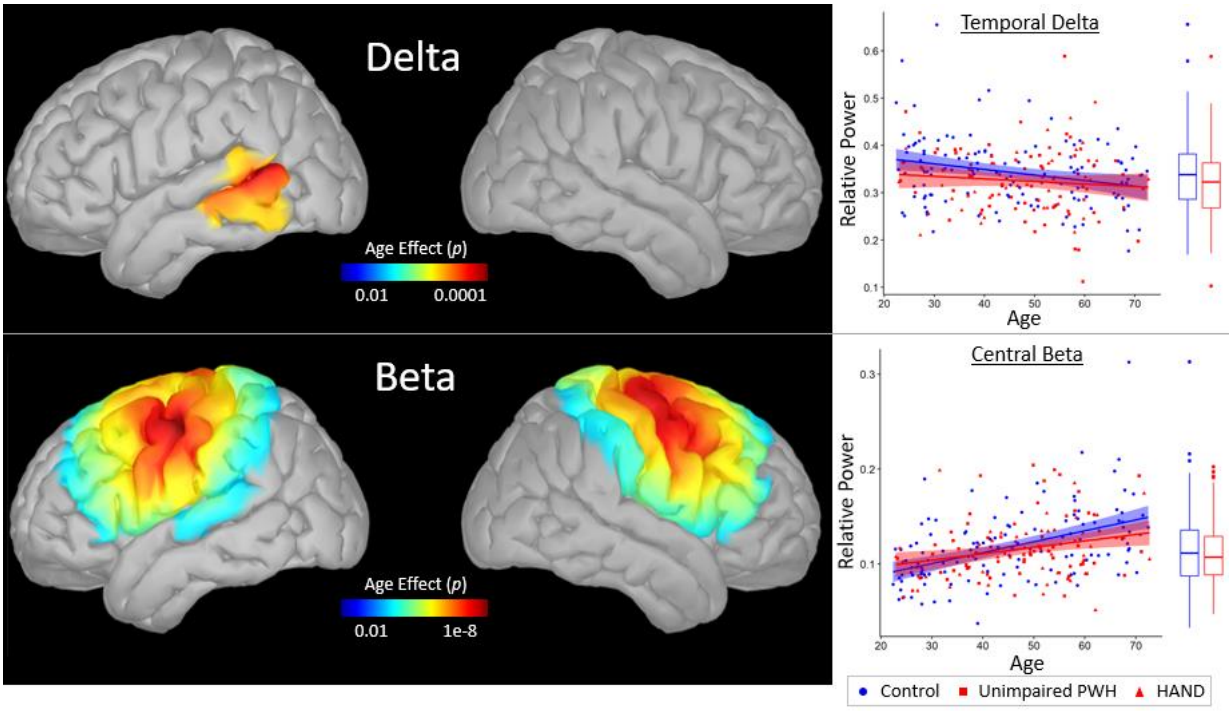

Figure 15: Age Effects in Frequency Power. Statistical parametric maps displaying the main effect of age in delta (top) and beta (bottom) bands. After correction for multiple comparisons, a cluster in the posterior left temporal cortex showed a significant decrease in delta power with age. Maps of beta power showed a significant cluster encompassing the somato-motor cortices, showing a significant increase in power with age. Color bars show uncorrected p values, thresholded by p<.001 and FWE .05 cluster correction. These effects are shown in scatter plots to the left, displaying power values at the temporal cortices for delta (top), and somato-motor cortices for beta (bottom), by age, with uninfected controls in blue and PWH in red. HAND status is differentiated by shape for display purposes. Linear fits for each group are displayed with 95% confidence intervals. Boxplots displaying group differences are added to the right of each plot.

No Effects of HIV in Resting State Oscillatory Power

For estimates of oscillatory power, all whole brain statistical parametric maps showed no clusters displaying significant effects of HIV. Group averaged maps showed qualitatively similar magnitude and topography of power in all frequency bands (Figures 16 and 17). Similarly, average values from predetermined regions of interest also showed no significant effects of HIV for all frequency bands (all p>.05; Table 6).

Interestingly, there was a significant HIV by age interaction in frontal gamma (F(1,237)=4.29; p=.039; η^2 =.018). However, no significant HIV by age interaction was identified in

the gamma whole cortical SPM contrasts. This was also the case for all other frequency bands, as no other HIV by age interaction was found to be significant.

Table 6: Oscillatory Activity Statistics

Power												
	Age				**HIV**				**HIV x Age**			
	F (1,238)	*p*	η^2	*BF*	*F (1,238)*	*p*	η^2	*BF*	*F (1,237)*	*p*	η^2	*BF*
Frontal Delta	4.41	.037*	.018	1.39	3.00	.084	.015	0.69	3.25	.073	.013	0.87
Frontal Theta	0.10	.751	.000	0.14	2.99	.085	.012	0.56	0.85	.358	.004	0.32
Occipital Alpha	0.26	.612	.001	0.16	0.01	.935	.000	0.14	0.02	.873	.000	0.20
Central Beta	41.78	<.001*	.149	1e7	1.08	.301	.001	0.23	2.28	.133	.008	0.45
Frontal Gamma	0.52	.471	.002	0.18	0.01	.937	.000	0.14	4.29	.039*	.018	1.62
Peak Frequency												
	Age				**HIV**				**HIV x Age**			
	F (1,238)	*p*	η^2	*BF*	*F (1,238)*	*p*	η^2	*BF*	*F (1,237)*	*p*	η^2	*BF*
Occipital Alpha	8.98	.003*	.036	11.37	0.75	.387	.005	0.20	0.09	.755	.000	0.20
Central Beta	1.36	.244	.006	0.26	0.43	.511	.001	0.17	1.24	.266	.005	0.36

Note: BF: Inclusion Bayes Factor. *p<.05; note that the HIV and Age columns represent the significance of the main effects without the interaction term, and the HIV x Age significance is derived in from an additional model after adding in the interaction.

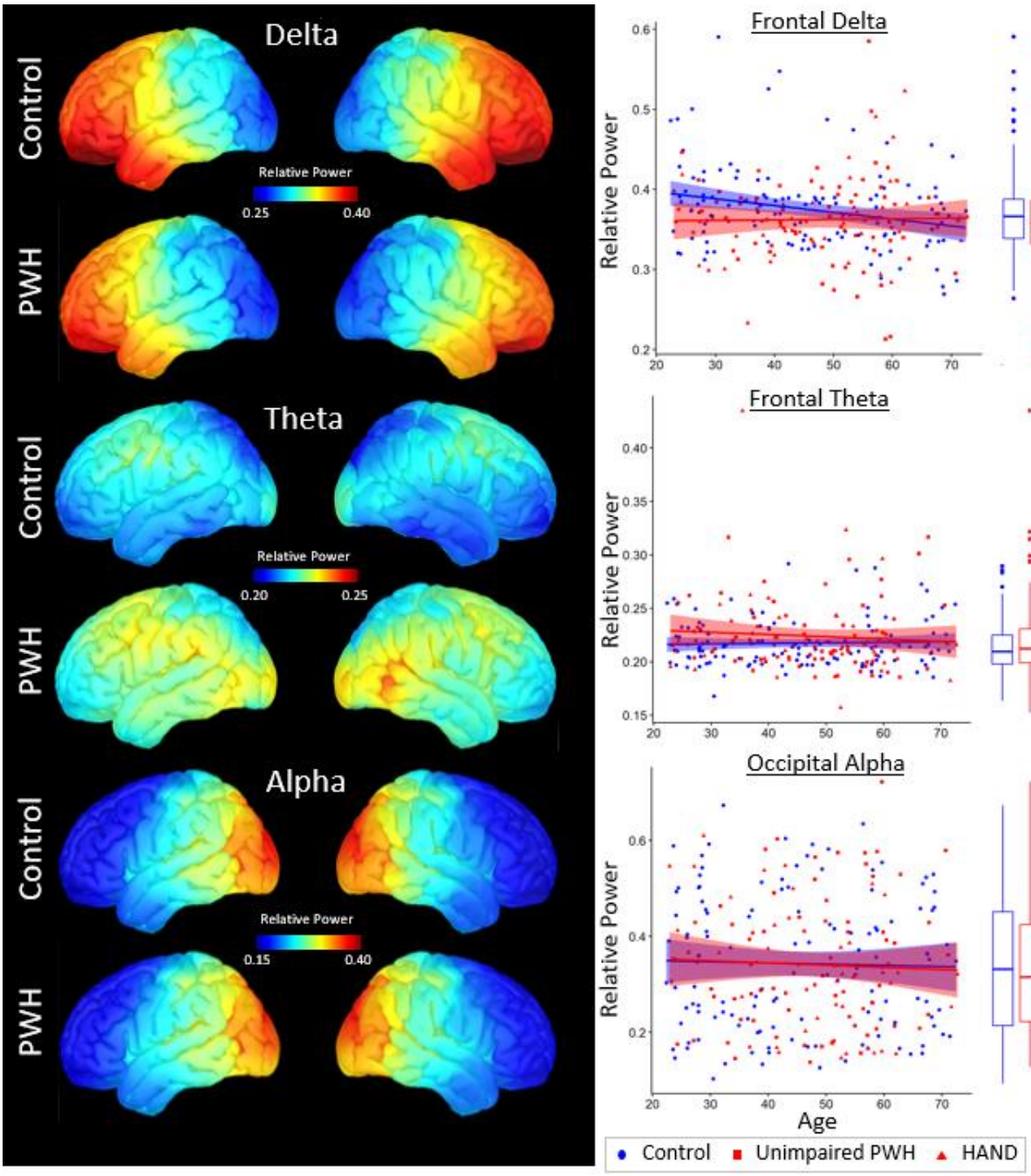

Figure 16: Delta, Theta, and Alpha Oscillatory Power by Age and HIV Status. Average power maps for uninfected controls are displayed above average maps for PWH. Color bars show relative power values, scaled for each band. Delta (top), theta (middle), and alpha (bottom) bands showed no significant differences between uninfected controls and PWH. Extracted power across pre-defined regions of interest are shown in scatter plots to the left, displaying power values at the frontal delta (top), frontal theta (middle), and occipital alpha (bottom) by age, with uninfected controls in blue and PWH in red. HAND status is differentiated by shape for display purposes. Linear fits for each group are displayed with 95% confidence intervals. Boxplots displaying group differences are added to the right of each plot, ultimately displaying a lack of group differences.

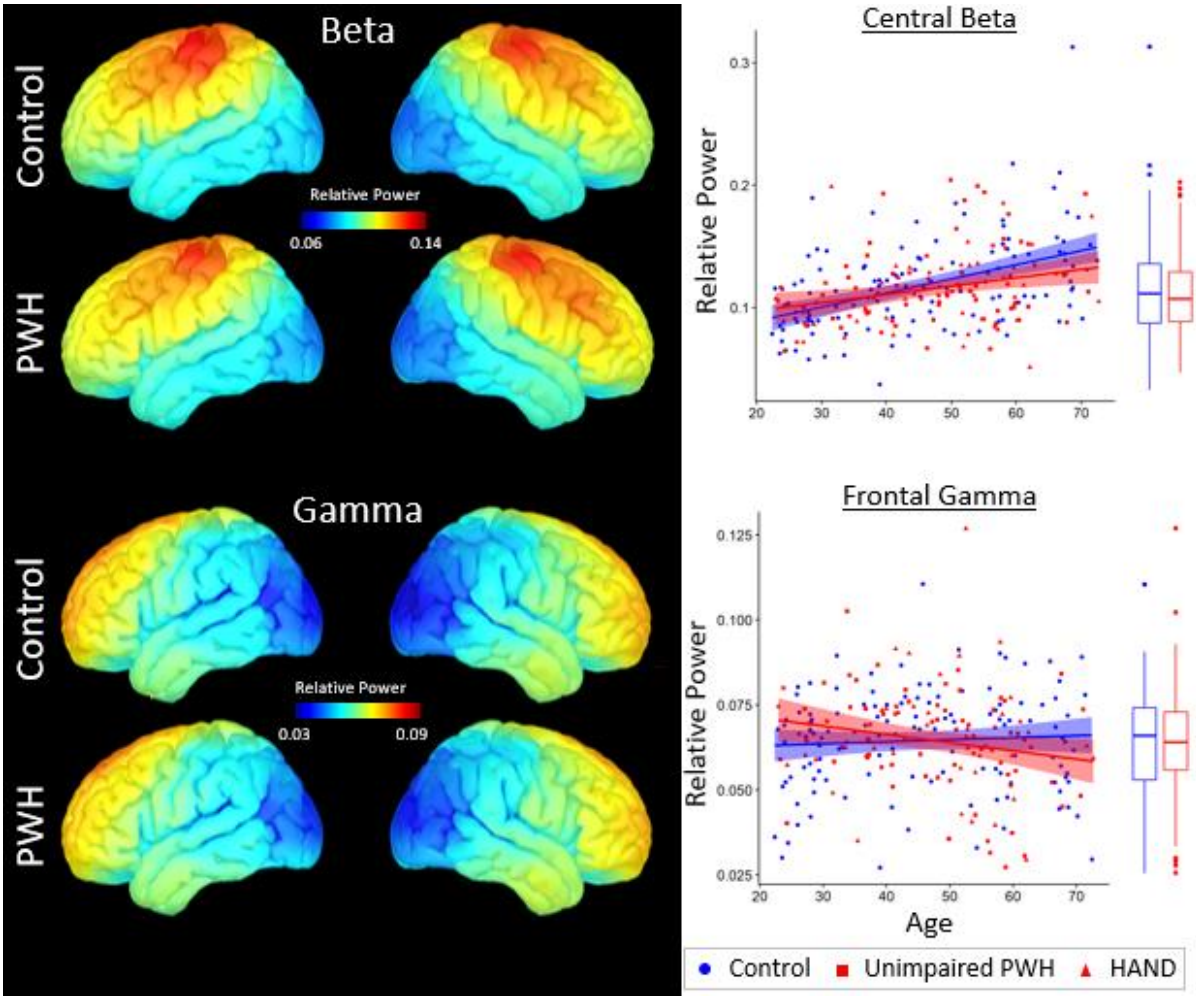

Figure 17: Beta and Gamma Oscillatory Power by Age and HIV Status. Average power maps for uninfected controls are displayed above average maps for PWH. Color bars show relative power values, scaled for each band. Beta (top), and gamma (bottom) bands showed no significant differences between uninfected controls and PWH. Extracted power across pre-defined regions of interest are shown in scatter plots to the left, displaying power values at the somato-motor beta (top), and frontal gamma (bottom) by age, with uninfected controls in blue and PWH in red. HAND status is differentiated by shape for display purposes. Linear fits for each group are displayed with 95% confidence intervals. Boxplots displaying group differences are added to the right of each plot, ultimately displaying a lack of group differences.

Decreasing Occipital Peak Alpha Frequency with Age

Examining peak frequency, statistical parametric mapping identified significant main effects of age in alpha peak frequency (Figure 18). After correction for multiple comparisons, a cluster in the posterior occipital lobe showed a significant decrease in peak alpha frequency with age. Analysis of average occipital peak alpha frequency identified a similar effect ($F(1,238)=8.98.$; $p=.003$; $\eta^2 =.036$).

No significant clusters were identified for beta peak frequency. Similarly, average somato-motor beta peak frequency did not show a main effect of age (Table 6).

No Effects of HIV in Peak Alpha and Beta Frequency

Similar to the power maps, whole brain statistical parametric maps on peak frequency also showed no clusters displaying significant effects of HIV. Group averaged maps showed qualitatively similar magnitude and topography of power in all frequency bands (Figure 18). Average values from predetermined regions of interest also showed no significant effects of HIV for occipital alpha peak frequency, nor somato-motor beta peak frequency (all $p>.05$; Table 6). No significant HIV by age interactions were identified in both whole cortex and region of interest peak frequency analyses.

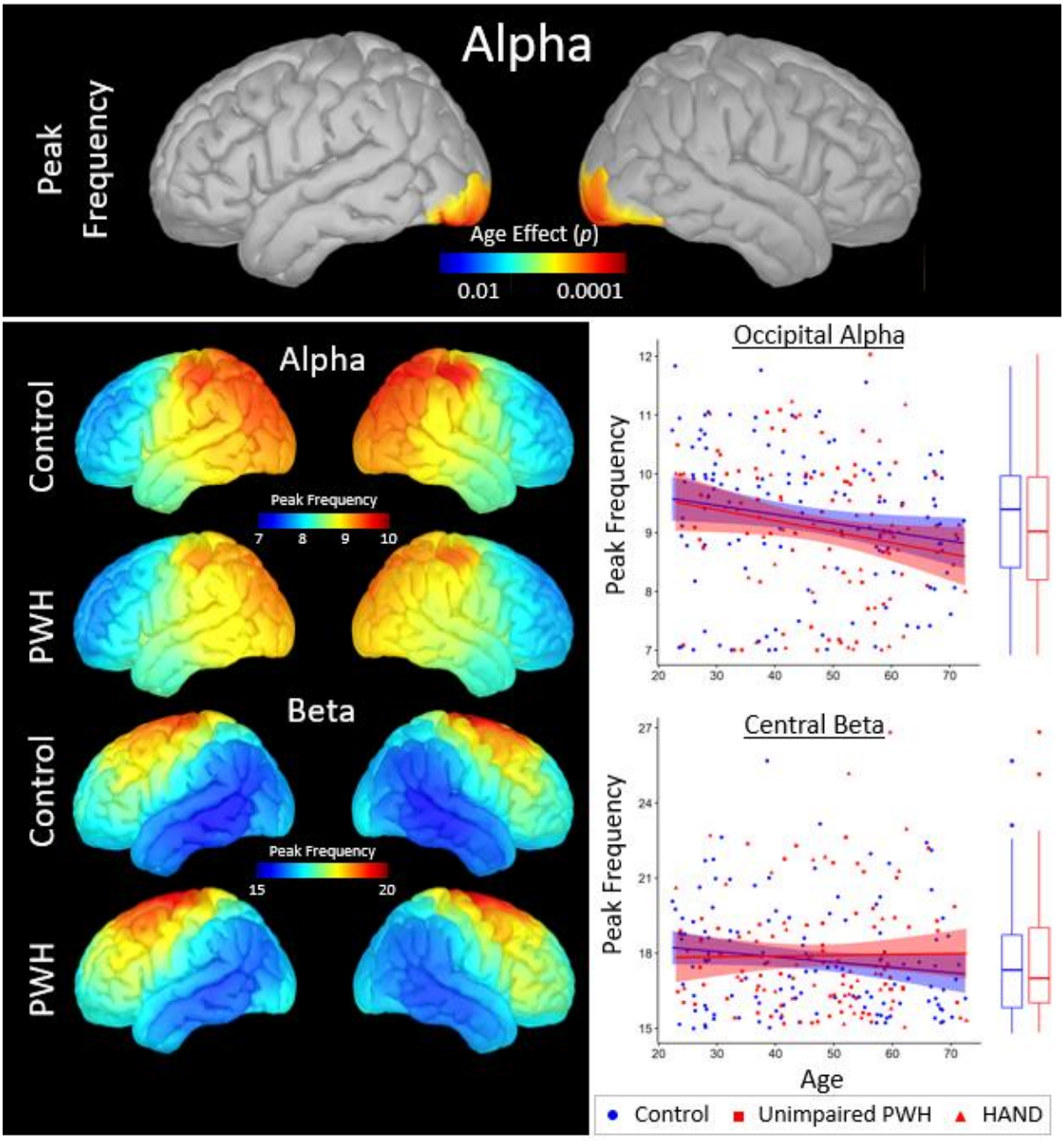

Figure 18: Alpha and Beta Peak Frequency by Age and HIV. Top: Statistical parametric maps displaying the main effect of age in alpha peak frequency. After correction for multiple comparisons, a cluster in the posterior occipital cortex showed a significant decrease in alpha peak frequency with age. Color bars show uncorrected p values, thresholded by p<.001 and FWE .05 cluster correction. Bottom panel: Average peak frequency maps for uninfected controls are displayed above average maps for PWH. Color bars show relative power values, scaled for each band. alpha (top), and beta (bottom) bands showed no significant differences between uninfected controls and PWH. Extracted power across pre-defined regions of interest are shown in scatter plots to the left, displaying peak frequency values at occipital alpha (top), and somato-motor beta (bottom) by age, with uninfected controls in blue and PWH in red. HAND status is differentiated by shape for display purposes. Linear fits for each group are displayed with 95% confidence intervals. Boxplots displaying group differences are added to the right of each plot, ultimately displaying a lack of group differences.

Post-Hoc Bayesian Analysis

To further explore our null findings, we calculated post-hoc inclusion Bayes factors for the age and HIV terms. Inclusion Bayes factors can be interpreted as the evidence for (or against) including a predictor in a model, thereby quantifying support for or against a null hypothesis.[168] Inclusion Bayes factors were computed by comparing only matched models (ie, excluding models with higher order interaction terms).

Examining age effects, frontal theta power, occipital alpha power, frontal gamma power, and somato-motor beta peak frequency all showed substantial (BF: 0.1 - 0.3)[169] support against inclusion of age in the model, suggesting evidence that age is not related to these metrics. Conversely, somato-motor beta power showed decisive (BF: >100) evidence, occipital alpha peak frequency showed strong (BF: 10-30) evidence, and frontal delta showed anecdotal evidence (BF: 1 - 3) for inclusion of age in the model.

For the effect of HIV, many metrics showed substantial (BF: 0.1 - 0.3) support against inclusion of HIV status in the model, including occipital alpha power and peak frequency, somato-motor beta power and peak frequency, and frontal gamma power, suggesting evidence that these metrics do not differ between uninfected controls and PWH. Frontal delta power and frontal theta power only showed anecdotal (BF: 0.3 - 1) evidence against inclusion of HIV status.

Finally, examining the HIV by age interaction term, only occipital alpha power, and occipital alpha peak frequency showed substantial (BF: 0.1 - 0.3) support against inclusion in the model. Frontal gamma showed anecdotal (BF: 1 - 3) evidence for inclusion of the interaction in the model. All other metrics showed anecdotal (BF: 0.3 - 1) evidence against inclusion of the interaction term (Table 2).

No Effects of HAND and Epigenetic Age Advancement

No significant effects of HAND on oscillatory power were identified after splitting the PWH group by HAND status (Appendix B). Additionally, when examining epigenetic age advancement, no significant HIV by age advancement interactions were found (Appendix C). Such was also the case for alpha and beta peak frequency (Appendix D).

MEG Discussion

The current study examined the effects of age and HIV on resting state oscillatory power and peak frequencies. We identify increasing beta power with age in the somato-motor cortices, and decreasing delta power with age in the left posterior temporal cortex. We also found a decrease in peak alpha frequency with increasing age. For the effect of HIV however, we did not identify any significant differences between our samples of uninfected controls and virologically suppressed PWH. Post-hoc Bayes factor calculations supported no differences between groups in occipital alpha power, somato-motor beta power, and frontal gamma power. Additionally, peak frequency in both alpha and beta bands also showed evidence suggesting no effect of HIV status. Overall, our findings suggest a preservation of oscillatory function in adequately treated PWH, even in metrics that normally show changes with age.

The one HIV-related finding we did identify is an HIV by age interaction in frontal gamma power utilizing the region of interest analysis. This may fit in with HAND-status by age interactions identified in three task-based MEG studies.[107,109,110] However, notable differences led us to not focus on this specific finding. Firstly, this interaction did not appear to be driven by participants with HAND, and instead was driven by unimpaired PWH. This makes our interaction inconsistent with the previous task-based MEG studies which specifically found age interactions using PWH with HAND as a separate group. Secondly, resting state frontal gamma power has been shown to

have poor reliability in a longitudinal analysis of healthy control participants. This may be due to the low power and high degree of variability in resting state gamma activity.[170] Finally, within this study itself we found that our HIV by age effect was small in magnitude (anecdotal evidence on Bayesian analysis), and we did not identify any interactive effects on the whole brain analysis. Given these reasons, we believe further study is needed to validate this effect.

Our null results appear to be contradictory to previous studies that have identified differences in resting state oscillatory power in PWH. Notably, a series of three papers by Babiloni et al utilized EEG and consistently identified a reduction in alpha power in PWH.[93–95,171] This may be due to the relative health of the PWH included in this study. That is, two of the three studies showing reduced alpha power were performed in treatment naïve PWH,[94,95] and their third study showed that such reductions were mitigated in those with cART, and then further mitigated in those with cART and a CD4 count greater than 500 cells/µl.[93] Given our sample of PWH had a median current CD4 of 702, were all taking cART, and all had undetectable levels of HIV, we suspect that the reduced alpha power seen in treatment naïve PWH was not seen in this immunologically healthier sample. In fact, our data showed substantial evidence that HIV serostatus in our sample was not related to occipital alpha power, nor occipital alpha peak frequency. We therefore conclude that alpha oscillations are preserved with HIV infection, so long as adequate antiretroviral therapy is utilized. Further study is however needed to replicate these findings given differences with previous literature.

It is also worth discussing the potential differences between resting state oscillatory power, and spontaneous oscillatory power seen in the baseline of task based designs. Multiple studies have found increased spontaneous oscillatory power related to HIV and HAND during the baseline period of tasks.[84,86,87] These changes did not appear in our resting state data, and we suggest this may be due to a difference between the baseline of tasks, and a prolonged resting

state. That is, during cognitive processing, participants are primed and continually attentive to the task they are performing. Activity in regions and frequencies related to such cognitive processes may be elevated/depressed throughout the paradigm, such that it is different from resting state, but also not at the level of a full blown response in relation to a stimulus/response. In some sense, this is the principal of blocked task designs, where activity is averaged across the entire block under the assumption that activity related to the process of interest is elevated throughout the entire period of cognitive processing. This is not to say the baseline period utilized in these tasks is not "quiet," but rather is at a different stable baseline than that seen in eyes closed rest. In the context of HIV and HAND, this new task active baseline may be more relevant towards the cognitive dysfunction seen in some PWH and therefore show alterations not seen here. Of course further study is needed to examine these subtleties.

Our aging findings are however highly consistent with previous literature. Decreasing peak alpha frequency with age is now generally thought to be well established. Functionally, peak alpha frequency has been related to decreased working memory across the lifespan.[172] Increasing beta power in somato-motor cortices with age has previously been identified using MEG.[104] This increased resting beta has been speculated to be related to increased GABA activity in older adults, as previous studies have linked increased GABA concentration to increased somato-motor beta power.[173] Finally, our results of decreasing delta power with age is consistent with a number of studies identifying decreasing low frequency power with age. Delta activity has been broadly linked to multiple cognitive functions,[174] and decreases have been related to decreases in cognitive performance in older adults.[175] Our results expand upon these previous findings by showing the spatially specific distributions of these changes with age, as well as showing that these patterns are also present in PWH.

With respect to our finding of reduced alpha peak frequency with age, but not reduced alpha power, this may be due to the age range of our sample. A large study of resting EEG activity analyzed the alpha activity of 4651 patients across the full lifespan. They found that peak alpha frequency sharply increases until approximately age 20, remains stable until about age 45, and then gradually declines throughout older adulthood. Alpha power on the other hand decreased from infancy to approximately age 35, and then remained stable until about age 75 where amplitude increased slightly.[98] Our sample ranged in age from 22 to 72, which may have allowed us to detect the decrease in peak alpha frequency, but also largely placed us in the age range where alpha amplitude is stable.

The study has a number of limitations that must be considered. Firstly, as mentioned previously, our sample may not generalize well to a broader population of PWH that may have a variety of other complications and further study is needed to determine whether resting oscillatory activity may in fact be an indicator of more severe immunosuppression or other comorbidities. Additionally, as stated before, future studies should examine older adults (beyond age 72) and PWH with more severe diagnoses of HAND. Our study is also limited in its focus on resting state oscillatory power and peak frequency, and does not make any conclusions on potential changes in oscillatory functional connectivity. Similarly, oscillatory responses during cognitive processing may show differences that could not be detected in the resting state. Our study also only utilized eyes closed resting data, and may not directly translate to eyes open resting data, which would inherently show different spectral properties.

In conclusion, despite identified age related decreases in delta power, and alpha peak frequency, and increases in beta power, PWH did not show additional aberrations in these metrics, nor other oscillatory activity estimates. An HIV by age interaction was identified in frontal gamma power, however further study is needed given the small size of this effect.

CHAPTER 6 – Conclusions

We studied the structural and functional neural changes that occur with aging and HIV infection. Structural MRI showed broad decreases in grey matter volume and cortical thickness with age and HIV independently. Additionally, decreased grey matter volume related to increasing epigenetic age advancement specifically in PWH, showing that atrophy relates to molecular measurements of HIV related age advancement. Functional MRI examining resting state networks also showed independent effects of age and HIV in between network functional connectivity. These effects were in the same direction, suggesting that HIV-related increases in between-network functional connectivity may reflect a deficit that is similar to the aging process. These changes however did not relate to measurements of epigenetic age advancement, showing a separation of functional network changes from indices of molecular age advancement. Finally, resting state MEG measurements of oscillatory power and peak frequency showed no significant effects of HIV, with some measures showing explicit support for the null. This suggests a preservation of resting state oscillatory function in well-treated HIV infection, despite the changes seen in structure and network functional connectivity.

While we hypothesized that each neuroimaging metric would show alterations related to HIV, and that these alterations would each scale with age advancement, our results instead show an interesting independence and specificity of HIV-related aberrations. That is, only grey matter volume showed results that were fully in agreement with our hypotheses. Functional resting state networks on the other hand showed partial agreement, in that PWH showed an independent increase in between-network connectivity compared to uninfected controls, but this increase was not significantly associated with epigenetic age advancement. We speculate this difference is due to the more direct relationship between molecular aging and brain structure, compared to the more indirect relationship between molecular aging and network level brain function. Molecular

aging is inherently related to the cellular biological clock, and it therefore makes sense that inflammatory processes due to HIV lead to a poorer cellular aging profile, which manifests in more neuronal loss and/or synaptic pruning. Network level function on the other hand is a much more systems-level measure, one that can be influenced by aspects such as cognitive reserve, which may relate to compensatory activity that is not necessarily detrimental. Therefore, the mechanistic relationship between a molecular measurement of aging and functional network level activity is far more blurred, and may explain why we did not identify a relationship between HIV related increases in between-network functional connectivity and epigenetic age advancement.

Another aspect of specificity is the difference between the fMRI and MEG results. Although both are measures of brain function, oscillatory power and peak frequency are somewhat independent from fMRI measured resting state networks, not only in that they are measured in very different ways, but also that they are on different scales. That is, resting state networks are on the network level, where the relationships between distant brain regions are quantified, while our oscillatory metrics are observations at particular brain regions, examined without relating activity at such regions to others. We may therefore speculate that communication between brain regions is more affected by HIV infection, while raw oscillatory activity throughout the brain remains largely intact.

With these results we can look forward towards how this study could inform future studies and even treatments. Firstly, our results indicate that grey matter atrophy may be a useful marker of HIV-related age advancement. Brain aging is highly important to keep track of in a population that is affected by pathologic age advancement, and treatment of such pathologic aging may be just around the corner. In fact, an exciting new study in *Nature* successfully reversed cognitive aging in mice by blocking PGE_2 signaling (pro-inflammatory signaling) in microglia.[176] This

is the same kind of inflammaging that is thought to be related to HIV associated epigenetic advanced aging. Our results indicate that such a treatment may be useful to prevent brain atrophy, and thereby prevent or treat HIV-associated neurocognitive disorder. On the other hand, resting state oscillatory function may not be a useful indicator of HIV infection, and more specific task based paradigms may be necessary to probe the oscillatory differences that may be seen in PWH.

When examining the effect of HAND status, we identified a subset of effects that were specific to participants with HAND. We found that decreases in hippocampal and thalamic grey matter content, and increases in between-network functional connectivity with the ventral attention network were driven by participants with HAND. Thalamus and hippocampal atrophy would have clear implications in memory and cognitive function broadly, while connectivity with ventral attention network (sometimes called the salience network)[177] is critical in integrating sensory stimuli and switching between the default mode and executive networks.[178] These specific aspects of brain structure and function may be particularly sensitive to cognitive impairment, and ultimately we believe these alterations may have the ability to act as specific markers of cognitive impairment related to HIV infection. Future study should focus in on these aberrations given their more direct clinical relevance.

Many of our other HIV-related effects however were present both in PWH without cognitive impairment, and in those with HAND. As mentioned previously, this is still highly relevant as it shows alterations even in the absence of outright cognitive impairment. At the same time, further effects of HAND may not have been found due to the relatively broad definition of HAND. That is, a number of recent studies have called into question whether the prevalence of HAND has been overestimated.[152,153,179] Rather than the largely utilized Frascati criteria, these studies utilized a multivariate normative comparison, ultimately finding the prevalence of HAND

to be much smaller and less inclusive than reported by previous research criteria. A promising future direction might therefore be to examine neuropsychological function on a more continuous scale, or in specific cognitive domains. Such an approach may avoid the mixing of mild and severe neuropsychological impairment into one singular HAND group, which may have mitigated effects.

Numerous other future directions can be considered following our results. Firstly, while this study is multimodal in the sense that we examined the same research question with three separate modalities, we did not make an attempt to combine these data into one analysis. This was done because the metrics we computed (structure, network connectivity, and oscillatory activity) were relatively independent of one another. However, previous literature has successfully combined resting state fMRI functional connectivity with resting state MEG functional connectivity.[180] Methods to compute resting state MEG functional connectivity typically involve the computation of an othogonalized amplitude envelope correlation between source estimated signals.[181] While this additional analysis was outside of the scope of this study, future studies may be able to examine whether the HIV related aberrations we identified in between-network connectivity are also identifiable in neurophysiological data using these analyses. Alternatively, the data from the three methods could also be used to generate a more complex statistical model that incorporates all metrics. Such modeling could be used to examine potential mediations or moderations between structural and functional deficits related to HIV. Our work performed here with separate models is an important first step towards informing these more complex models, and future studies should continue to build upon this multimodal neuroimaging approach.

Additionally, we did not examine the potential effects of cART. It is therefore a possibility that the medications themselves may have contributed to some of the HIV-related alterations we have identified. Generally however, previous literature indicates that cART largely helps preserve

neural function by reducing viral load. The vast majority of antiretrovirals are not considered to be neurotoxic either. A notable exception to this however is efavirenz, which is relatively common given the use of Atripla (a cART pill that includes efavirenz, emtricitabine, and tenofovir disoproxil fumarate). Multiple studies have suggested that efavirenz can be neurotoxic[182,183] and may also affect functional neural activity.[108] We do not believe our results would have been solely due to efavirenz however, as only a portion of our large sample would have had it as a part of their current regimen. Efavirenz based regimens are being utilized less and less often, as INSTI based therapies are the current first line recommendations due to higher barriers to resistance and fewer serious side effects. Nevertheless, it may have been a contributing factor and future studies should examine this highly relevant question.

In conclusion, HIV infection is related to decreases in grey matter volume and increases in between-network functional connectivity, in a similar manner to, but independent of aging. Oscillatory activity on the other hand is largely preserved. HIV-associated reductions in grey matter volume also related to increases in epigenetic age advancement, while increases in between-network functional connectivity did not. This suggests that the HIV-related age advancement seen at the molecular level is tied to loss of grey matter, and that HIV-associated reorganization of resting state networks may be further removed from this measurement of the biological clock. These findings are a critical step towards characterizing the aging brain of PWH, which is crucial in understanding how to prevent and treat HIV-related neural deficits in an aging population.

APPENDICES

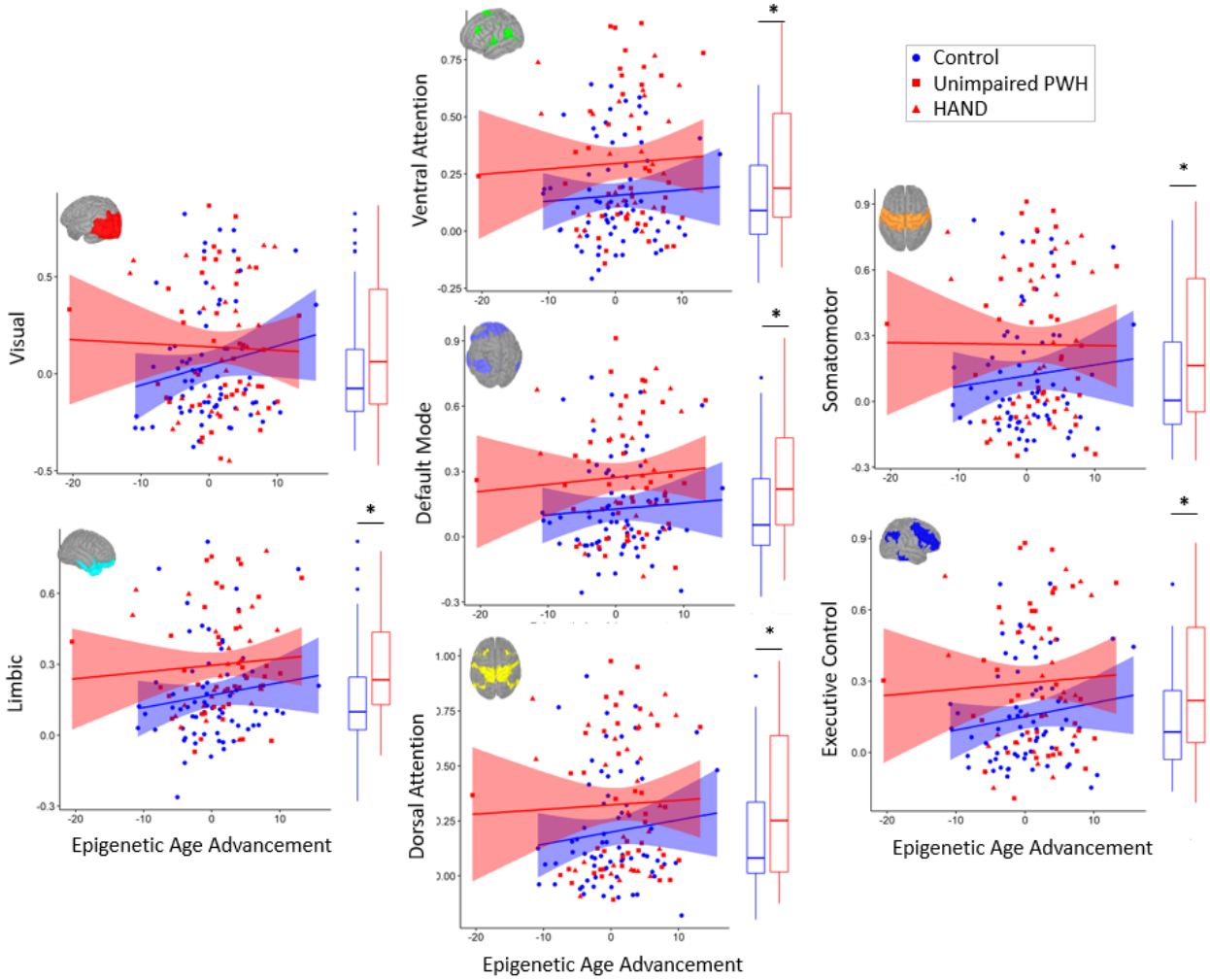

*Appendix A: Between-Network Functional Connectivity and Epigenetic Age Advancement. No HIV by age advancement effects were identified. Scatter plots display z values of each between-network functional connectivity metric by age, with uninfected controls in blue and PWH in red. HAND status is differentiated by shape for display purposes. Linear fits for each group are displayed with 95% confidence intervals. Boxplots displaying group differences are added to the right of each plot, and visual representations of each network are inset. * p<.05*

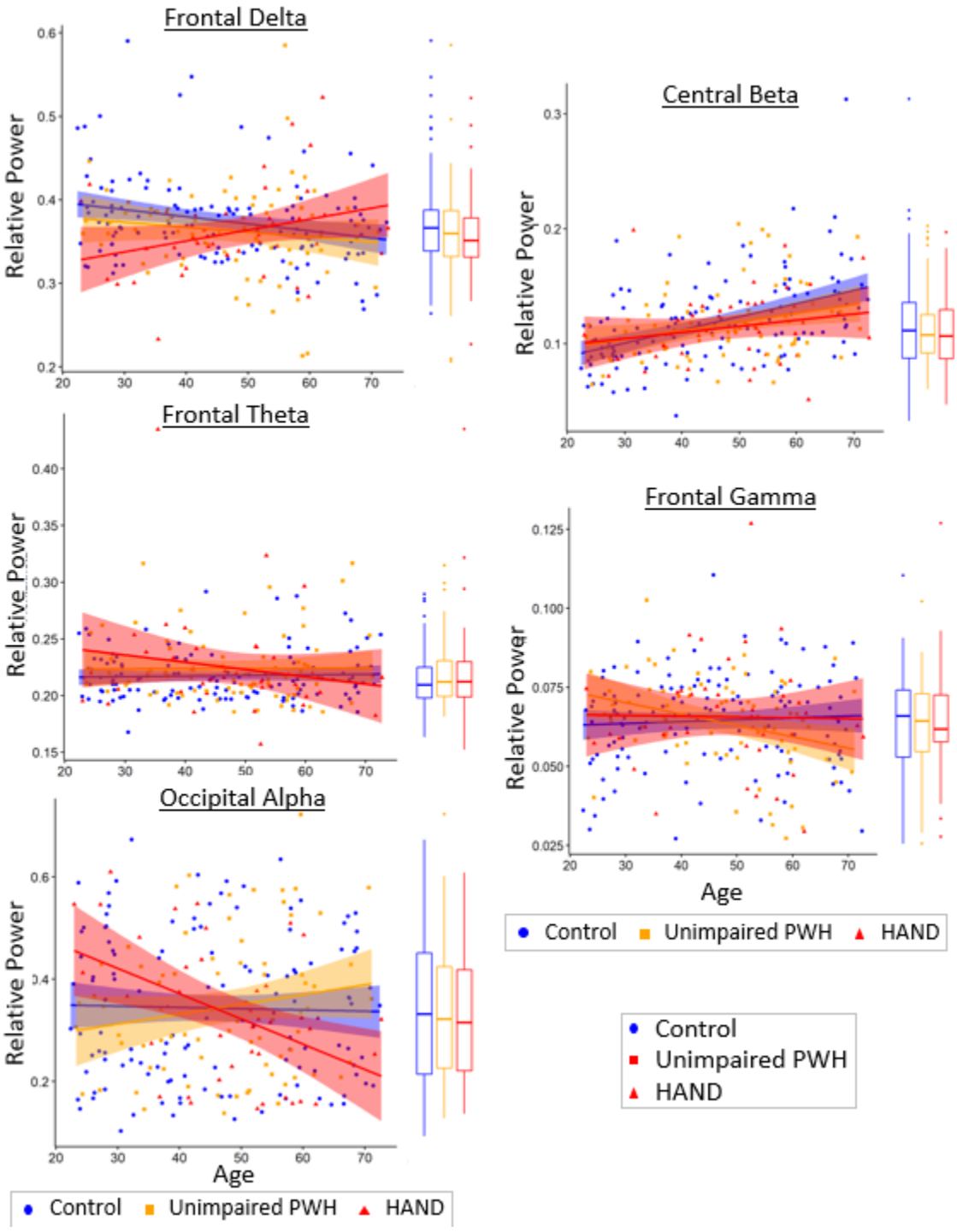

Appendix B: Oscillatory Power by Age and HAND Status. No effects of HAND were identified (all p>.05). Extracted power across pre-defined regions of interest are shown in scatter plots, displaying relative power values by age, with uninfected controls in blue, unimpaired PWH in orange, and PWH with HAND in red. Linear fits for each group are displayed with 95% confidence intervals. Boxplots displaying group differences are added to the right of each plot, ultimately displaying a lack of group differences.

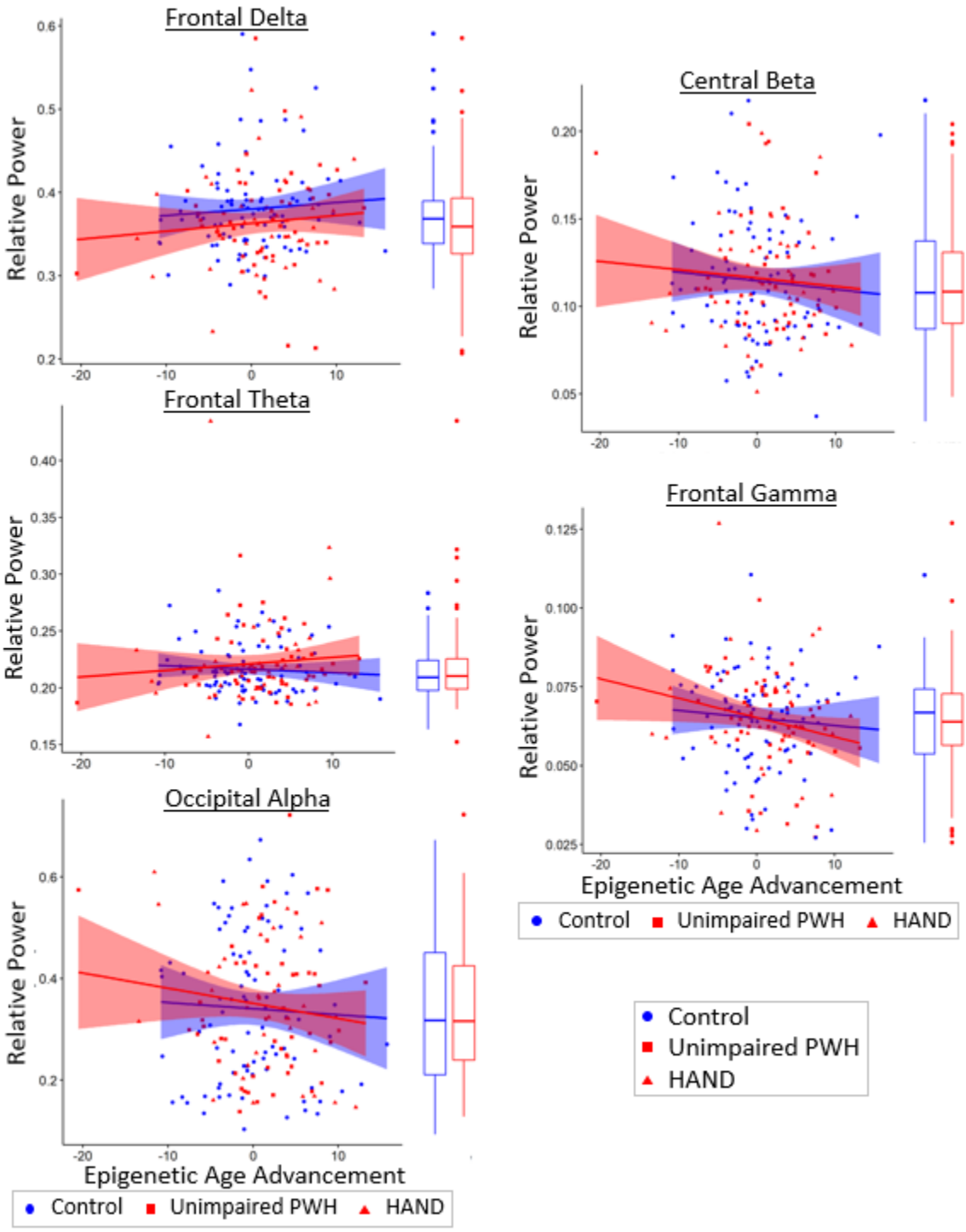

Appendix C: Oscillatory Power by HIV and Epigenetic Age Advancement. No HIV by age advancement effects were identified. Extracted power across pre-defined regions of interest are shown in scatter plots, displaying relative power values by age, with uninfected controls in blue and PWH in red. HAND status is differentiated by shape for display purposes. Linear fits for each group are displayed with 95% confidence intervals. Boxplots displaying group differences are added to the right of each plot, ultimately displaying a lack of group differences.

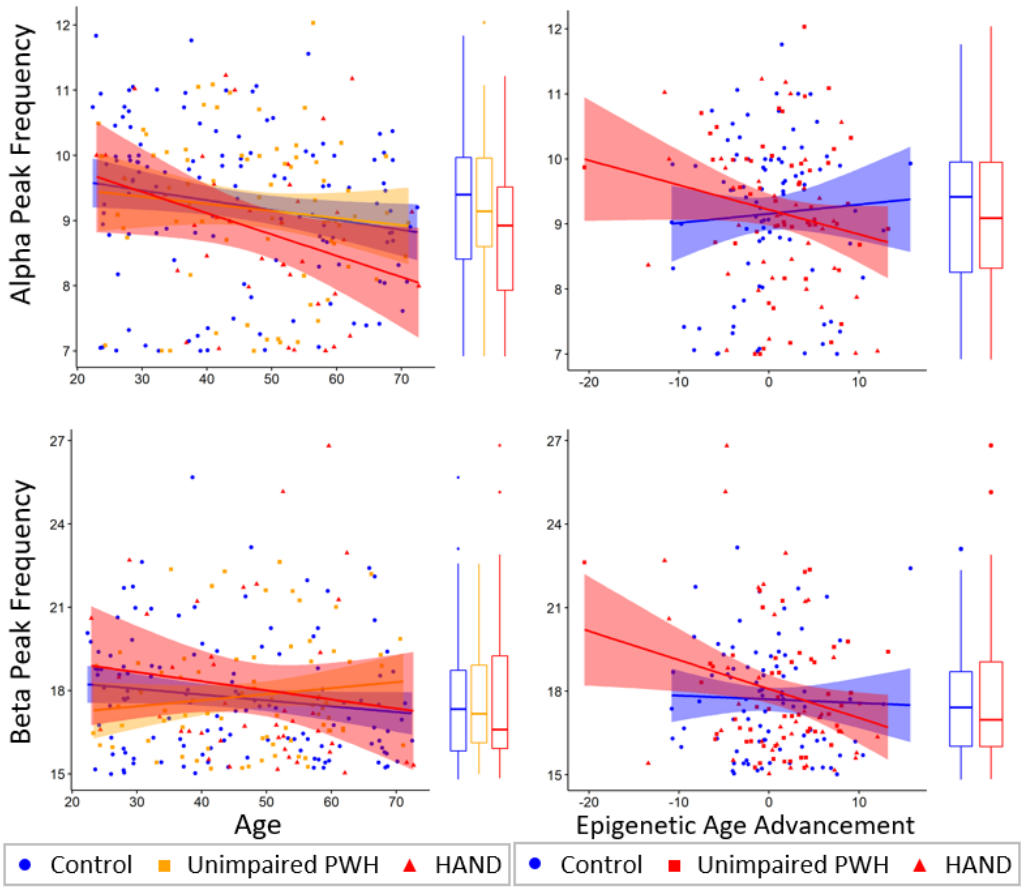

Appendix D: Alpha and Beta Peak Frequency with Age by HAND, and with Age Advancement. No effects of HAND or HIV by age advancement effects were identified. Extracted peak alpha (top) and beta (bottom) frequency across pre-defined regions of interest are shown in scatter plots, displaying peak frequency values by age (left), and by epigenetic age advancement (right). Linear fits for each group are displayed with 95% confidence intervals. Boxplots displaying group differences are added to the right of each plot, ultimately displaying a lack of group differences.

BIBLIOGRAPHY

1. Mahy M, Stover J, Stanecki K, Stoneburner R, Tassie J-M. Estimating the impact of antiretroviral therapy: regional and global estimates of life-years gained among adults. Sexually transmitted infections. The Medical Society for the Study of Venereal Disease; 2010;86:ii67–ii71.

2. Halkitis PN. The AIDS generation: Stories of survival and resilience. Oxford University Press; 2013.

3. Fauci AS. The human immunodeficiency virus: infectivity and mechanisms of pathogenesis. Science. American Association for the Advancement of Science; 1988;239:617–622.

4. A Timeline of HIV and AIDS [online]. HIV.gov 2016. Accessed at: https://www.hiv.gov/hiv-basics/overview/history/hiv-and-aids-timeline. Accessed February 3, 2021.

5. Samji H, Cescon A, Hogg RS, et al. Closing the Gap: Increases in Life Expectancy among Treated HIV-Positive Individuals in the United States and Canada. Okulicz JF, editor. PLoS ONE. 2013;8:e81355.

6. Ortblad KF, Lozano R, Murray CJL. The burden of HIV: insights from the Global Burden of Disease Study 2010. AIDS. 2013;27:2003–2017.

7. Rasmussen LD, May MT, Kronborg G, et al. Time trends for risk of severe age-related diseases in individuals with and without HIV infection in Denmark: a nationwide population-based cohort study. The Lancet HIV. 2015;2:e288–e298.

8. Wing EJ. HIV and aging. International Journal of Infectious Diseases. 2016;53:61–68.

9. Pathai S, Bajillan H, Landay AL, High KP. Is HIV a Model of Accelerated or Accentuated Aging? The Journals of Gerontology Series A: Biological Sciences and Medical Sciences. 2014;69:833–842.

10. Martin-Iguacel R, Llibre JM, Friis-Moller N. Risk of Cardiovascular Disease in an Aging HIV Population: Where Are We Now? Curr HIV/AIDS Rep. 2015;12:375–387.

11. Joshi D, O'Grady J, Dieterich D, Gazzard B, Agarwal K. Increasing burden of liver disease in patients with HIV infection. The Lancet. Elsevier; 2011;377:1198–1209.

12. Ando M, Tsuchiya K, Nitta K. How to manage HIV-infected patients with chronic kidney disease in the HAART era. Clin Exp Nephrol. 2012;16:363–372.

13. Heaton RK, Clifford DB, Franklin DR, et al. HIV-associated neurocognitive disorders persist in the era of potent antiretroviral therapy: CHARTER Study. Neurology. 2010;75:2087–2096.

14. Martin J, Volberding P. HIV and premature aging: a field still in its infancy. Annals of internal medicine. American College of Physicians; 2010;153:477–479.

15. Aung HL, Aghvinian M, Gouse H, et al. Is There Any Evidence of Premature, Accentuated and Accelerated Aging Effects on Neurocognition in People Living with HIV? A Systematic Review. AIDS and Behavior. Springer; Epub 2020.:1–44.

16. Gross AM, Jaeger PA, Kreisberg JF, et al. Methylome-wide analysis of chronic HIV infection reveals five-year increase in biological age and epigenetic targeting of HLA. Molecular cell. Elsevier; 2016;62:157–168.

17. Hannum G, Guinney J, Zhao L, et al. Genome-wide methylation profiles reveal quantitative views of human aging rates. Molecular cell. Elsevier; 2013;49:359–367.

18. Horvath S. DNA methylation age of human tissues and cell types. Genome biology. BioMed Central; 2013;14:3156.

19. Marioni RE, Shah S, McRae AF, et al. DNA methylation age of blood predicts all-cause mortality in later life. Genome biology. BioMed Central; 2015;16:25.

20. Horvath S, Levine AJ. HIV-1 infection accelerates age according to the epigenetic clock. The Journal of infectious diseases. Oxford University Press; 2015;212:1563–1573.

21. Levine AJ, Quach A, Moore DJ, et al. Accelerated epigenetic aging in brain is associated with pre-mortem HIV-associated neurocognitive disorders. Journal of neurovirology. Springer; 2016;22:366–375.

22. Horvath S, Stein DJ, Phillips N, et al. Perinatally acquired HIV infection accelerates epigenetic aging in South African adolescents. AIDS (London, England). NIH Public Access; 2018;32:1465.

23. Simioni S, Cavassini M, Annoni J-M, et al. Cognitive dysfunction in HIV patients despite long-standing suppression of viremia. Aids. LWW; 2010;24:1243–1250.

24. Heaton RK, Franklin DR, Ellis RJ, et al. HIV-associated neurocognitive disorders before and during the era of combination antiretroviral therapy: differences in rates, nature, and predictors. Journal of neurovirology. Springer; 2011;17:3–16.

25. Caruana G, Vidili G, Serra P, et al. The burden of HIV-associated neurocognitive disorder (HAND) in post-HAART era: a multidisciplinary review of the literature. Eur Rev Med Pharmacol Sci. 2017;21:2290–2301.

26. Dohgu S, Banks WA. Brain pericytes increase the lipopolysaccharide-enhanced transcytosis of HIV-1 free virus across the in vitro blood–brain barrier: evidence for cytokine-mediated pericyte-endothelial cell crosstalk. Fluids and Barriers of the CNS. BioMed Central; 2013;10:1–10.

27. González-Scarano F, Martín-García J. The neuropathogenesis of AIDS. Nature reviews immunology. Nature Publishing Group; 2005;5:69–81.

28. Kaul M, Zheng J, Okamoto S, Gendelman H, Lipton S. HIV-1 infection and AIDS: consequences for the central nervous system. Cell Death & Differentiation. Nature Publishing Group; 2005;12:878–892.

29. Baylis D, Bartlett DB, Patel HP, Roberts HC. Understanding how we age: insights into inflammaging. Longevity & healthspan. BioMed Central; 2013;2:1–8.

30. Franceschi C, Campisi J. Chronic inflammation (inflammaging) and its potential contribution to age-associated diseases. Journals of Gerontology Series A: Biomedical Sciences and Medical Sciences. Oxford University Press US; 2014;69:S4–S9.

31. Franceschi C, Garagnani P, Vitale G, Capri M, Salvioli S. Inflammaging and 'Garb-aging.' Trends in Endocrinology & Metabolism. Elsevier; 2017;28:199–212.

32. Holt JL, Kraft-Terry SD, Chang L. Neuroimaging studies of the aging HIV-1-infected brain. J Neurovirol. 2012;18:291–302.

33. Masters MC, Ances BM. Role of neuroimaging in HIV associated neurocognitive disorders (HAND). NIH Public Access; 2014. p. 89.

34. Moeller A, Backmund H. Ventricle brain ratio in the clinical course of HIV infection. Acta neurologica scandinavica. Wiley Online Library; 1990;81:512–515.

35. Hestad K, McArthur J, Pan GD, et al. Regional brain atrophy in HIV-1 infection: association with specific neuropsychological test performance. Acta Neurologica Scandinavica. Wiley Online Library; 1993;88:112–118.

36. DI SCLAFANI V, MACKAY RS, MEYERHOFF DJ, NORMAN D, WEINER MW, FEIN G. Brain atrophy in HIV infection is more strongly associated with CDC clinical stage than with cognitive impairment. Journal of the International Neuropsychological Society: JINS. NIH Public Access; 1997;3:276.

37. Becker JT, Sanders J, Madsen SK, et al. Subcortical brain atrophy persists even in HAART-regulated HIV disease. Brain imaging and behavior. Springer; 2011;5:77–85.

38. Clifford KM, Samboju V, Cobigo Y, et al. Progressive brain atrophy despite persistent viral suppression in HIV over age 60. Journal of acquired immune deficiency syndromes (1999). NIH Public Access; 2017;76:289.

39. Raz N, Lindenberger U, Rodrigue KM, et al. Regional Brain Changes in Aging Healthy Adults: General Trends, Individual Differences and Modifiers. Cerebral Cortex. 2005;15:1676–1689.

40. Taki Y, Thyreau B, Kinomura S, et al. Correlations among brain gray matter volumes, age, gender, and hemisphere in healthy individuals. PloS one. Public Library of Science; 2011;6.

41. Ances BM, Ortega M, Vaida F, Heaps J, Paul R. Independent Effects of HIV, Aging, and HAART on Brain Volumetric Measures: JAIDS Journal of Acquired Immune Deficiency Syndromes. 2012;59:469–477.

42. Cardenas V, Meyerhoff D, Studholme C, et al. Evidence for ongoing brain injury in human immunodeficiency virus–positive patients treated with antiretroviral therapy. J Neurovirol. 2009;15:324–333.

43. Chang L, Andres M, Sadino J, et al. Impact of apolipoprotein E ε4 and HIV on cognition and brain atrophy: Antagonistic pleiotropy and premature brain aging. NeuroImage. 2011;58:1017–1027.

44. Becker JT, Maruca V, Kingsley LA, et al. Factors affecting brain structure in men with HIV disease in the post-HAART era. Neuroradiology. 2012;54:113–121.

45. Pfefferbaum A, Rosenbloom MJ, Sassoon SA, et al. Regional Brain Structural Dysmorphology in Human Immunodeficiency Virus Infection: Effects of Acquired Immune Deficiency Syndrome, Alcoholism, and Age. Biological Psychiatry. 2012;72:361–370.

46. Towgood KJ, Pitkanen M, Kulasegaram R, et al. Mapping the brain in younger and older asymptomatic HIV-1 men: Frontal volume changes in the absence of other cortical or diffusion tensor abnormalities. Cortex. 2012;48:230–241.

47. Lake JE, Popov M, Post WS, et al. Visceral fat is associated with brain structure independent of human immunodeficiency virus infection status. Journal of neurovirology. Springer; 2017;23:385–393.

48. Van Zoest RA, Underwood J, De Francesco D, et al. Structural brain abnormalities in successfully treated HIV infection: associations with disease and cerebrospinal fluid biomarkers. The Journal of Infectious Diseases. Oxford University Press US; 2018;217:69–81.

49. Harris NS, Johnson AS, Huang Y-LA, et al. Vital signs: status of human immunodeficiency virus testing, viral suppression, and HIV preexposure prophylaxis—United States, 2013–2018. Morbidity and Mortality Weekly Report. Centers for Disease Control and Prevention; 2019;68:1117.

50. Drew PJ. Vascular and neural basis of the BOLD signal. Current opinion in neurobiology. Elsevier; 2019;58:61–69.

51. Logothetis NK, Wandell BA. Interpreting the BOLD signal. Annu Rev Physiol. Annual Reviews; 2004;66:735–769.

52. Arthurs OJ, Boniface S. How well do we understand the neural origins of the fMRI BOLD signal? TRENDS in Neurosciences. Elsevier; 2002;25:27–31.

53. Biswal B, Zerrin Yetkin F, Haughton VM, Hyde JS. Functional connectivity in the motor cortex of resting human brain using echo-planar MRI. Magnetic resonance in medicine. Wiley Online Library; 1995;34:537–541.

54. Fox MD, Snyder AZ, Vincent JL, Corbetta M, Van Essen DC, Raichle ME. The human brain is intrinsically organized into dynamic, anticorrelated functional networks. Proceedings of the National Academy of Sciences. National Acad Sciences; 2005;102:9673–9678.

55. Damoiseaux JS, Rombouts S, Barkhof F, et al. Consistent resting-state networks across healthy subjects. Proceedings of the national academy of sciences. National Acad Sciences; 2006;103:13848–13853.

56. Hakkers C, Arends J, Barth R, Du Plessis S, Hoepelman A, Vink M. Review of functional MRI in HIV: effects of aging and medication. Journal of neurovirology. Springer; 2017;23:20–32.

57. Chang L, Yakupov R, Nakama H, Stokes B, Ernst T. Antiretroviral treatment is associated with increased attentional load-dependent brain activation in HIV patients. Journal of Neuroimmune Pharmacology. Springer; 2008;3:95–104.

58. Chang L, Tomasi D, Yakupov R, et al. Adaptation of the attention network in human immunodeficiency virus brain injury. Annals of Neurology: Official Journal of the American Neurological Association and the Child Neurology Society. Wiley Online Library; 2004;56:259–272.

59. Chang L, Holt JL, Yakupov R, Jiang CS, Ernst T. Lower cognitive reserve in the aging human immunodeficiency virus-infected brain. Neurobiology of aging. Elsevier; 2013;34:1240–1253.

60. Chang L, Speck O, Miller EN, et al. Neural correlates of attention and working memory deficits in HIV patients. Neurology. AAN Enterprises; 2001;57:1001–1007.

61. Ernst T, Chang L, Jovicich J, Ames N, Arnold S. Abnormal brain activation on functional MRI in cognitively asymptomatic HIV patients. Neurology. AAN Enterprises; 2002;59:1343–1349.

62. Thames AD, Sayegh P, Terashima K, et al. Increased subcortical neural activity among HIV+ individuals during a lexical retrieval task. Neurobiology of disease. Elsevier; 2016;92:175–182.

63. Du Plessis S, Vink M, Joska JA, Koutsilieri E, Stein DJ, Emsley R. HIV infection and the fronto–striatal system: a systematic review and meta-analysis of fMRI studies. Aids. LWW; 2014;28:803–811.

64. Thomas JB, Brier MR, Snyder AZ, Vaida FF, Ances BM. Pathways to neurodegeneration: effects of HIV and aging on resting-state functional connectivity. Neurology. AAN Enterprises; 2013;80:1186–1193.

65. Ipser JC, Brown GG, Bischoff-Grethe A, et al. HIV infection is associated with attenuated frontostriatal intrinsic connectivity. Journal of the International Neuropsychological Society: JINS. NIH Public Access; 2015;21:203.

66. Ortega M, Brier MR, Ances BM. Effects of HIV and Combination Antiretroviral Therapy (cART) on cortico-striatal functional connectivity. AIDS (London, England). NIH Public Access; 2015;29:703.

67. Cole JH, Caan MWA, Underwood J, et al. No Evidence for Accelerated Aging-Related Brain Pathology in Treated Human Immunodeficiency Virus: Longitudinal Neuroimaging Results

From the Comorbidity in Relation to AIDS (COBRA) Project. Clinical Infectious Diseases. 2018;66:1899–1909.

68. Janssen MA, Hinne M, Janssen RJ, et al. Resting-state subcortical functional connectivity in HIV-infected patients on long-term cART. Brain Imaging and Behavior. Springer; 2017;11:1555–1560.

69. Ances BM, Vaida F, Yeh MJ, et al. HIV infection and aging independently affect brain function as measured by functional magnetic resonance imaging. The Journal of infectious diseases. The University of Chicago Press; 2010;201:336–340.

70. Juengst SB, Aizenstein HJ, Figurski J, Lopez OL, Becker JT. Alterations in the hemodynamic response function in cognitively impaired HIV/AIDS subjects. Journal of neuroscience methods. Elsevier; 2007;163:208–212.

71. Egbert AR, Biswal B, Karunakaran K, et al. Age and HIV effects on resting state of the brain in relationship to neurocognitive functioning. Behavioural Brain Research. Elsevier; 2018;344:20–27.

72. Betzel RF, Byrge L, He Y, Goñi J, Zuo X-N, Sporns O. Changes in structural and functional connectivity among resting-state networks across the human lifespan. Neuroimage. Elsevier; 2014;102:345–357.

73. Damoiseaux JS. Effects of aging on functional and structural brain connectivity. Neuroimage. Elsevier; 2017;160:32–40.

74. Spreng RN, Stevens WD, Viviano JD, Schacter DL. Attenuated anticorrelation between the default and dorsal attention networks with aging: evidence from task and rest. Neurobiology of aging. Elsevier; 2016;45:149–160.

75. Cao M, Wang J-H, Dai Z-J, et al. Topological organization of the human brain functional connectome across the lifespan. Developmental cognitive neuroscience. Elsevier; 2014;7:76–93.

76. Abidin AZ, DSouza AM, Schifitto G, Wismüller A. Detecting cognitive impairment in HIV-infected individuals using mutual connectivity analysis of resting state functional MRI. Journal of NeuroVirology. Springer; Epub 2020.:1–13.

77. Başar E, Başar-Eroglu C, Karakaş S, Schürmann M. Gamma, alpha, delta, and theta oscillations govern cognitive processes. International journal of psychophysiology. Elsevier; 2001;39:241–248.

78. Bosboom J, Stoffers D, Stam C, et al. Resting state oscillatory brain dynamics in Parkinson's disease: an MEG study. Clinical Neurophysiology. Elsevier; 2006;117:2521–2531.

79. Engels M, van Der Flier W, Stam C, Hillebrand A, Scheltens P, van Straaten E. Alzheimer's disease: the state of the art in resting-state magnetoencephalography. Clinical Neurophysiology. Elsevier; 2017;128:1426–1437.

80. Zeev-Wolf M, Levy J, Jahshan C, et al. MEG resting-state oscillations and their relationship to clinical symptoms in schizophrenia. NeuroImage: Clinical. Elsevier; 2018;20:753–761.

81. Wilson TW, Lew BJ, Spooner RK, Rezich MT, Wiesman AI. Aberrant brain dynamics in neuroHIV: Evidence from magnetoencephalographic (MEG) imaging. Progress in molecular biology and translational science. Elsevier; 2019;165:285–320.

82. Wilson TW, Heinrichs-Graham E, Robertson KR, et al. Functional brain abnormalities during finger-tapping in HIV-infected older adults: a magnetoencephalography study. Journal of Neuroimmune Pharmacology. Springer; 2013;8:965–974.

83. Wilson TW, Heinrichs-Graham E, Becker KM, et al. Multimodal neuroimaging evidence of alterations in cortical structure and function in HIV-infected older adults. Human brain mapping. Wiley Online Library; 2015;36:897–910.

84. Spooner RK, Wiesman AI, Mills MS, et al. Aberrant oscillatory dynamics during somatosensory processing in HIV-infected adults. NeuroImage: Clinical. Elsevier; 2018;20:85–91.

85. Wilson TW, Fox HS, Robertson KR, et al. Abnormal MEG oscillatory activity during visual processing in the prefrontal cortices and frontal eye-fields of the aging HIV brain. PLoS One. Public Library of Science; 2013;8:e66241.

86. Wiesman AI, O'Neill J, Mills MS, et al. Aberrant occipital dynamics differentiate HIV-infected patients with and without cognitive impairment. Brain. Oxford University Press; 2018;141:1678–1690.

87. Lew BJ, McDermott TJ, Wiesman AI, et al. Neural dynamics of selective attention deficits in HIV-associated neurocognitive disorder. Neurology. 2018;91:e1860–e1869.

88. Wilson TW, Proskovec AL, Heinrichs-Graham E, et al. Aberrant neuronal dynamics during working memory operations in the aging HIV-infected brain. Scientific reports. Nature Publishing Group; 2017;7:1–9.

89. Wiesman AI, O'Neill J, Mills MS, et al. Aberrant occipital dynamics differentiate HIV-infected patients with and without cognitive impairment. Brain. Oxford University Press; 2018;141:1678–1690.

90. Becker KM, Heinrichs-Graham E, Fox HS, et al. Decreased MEG beta oscillations in HIV-infected older adults during the resting state. Journal of neurovirology. Springer; 2013;19:586–594.

91. Becker JT, Fabrizio M, Sudre G, et al. Potential utility of resting-state magnetoencephalography as a biomarker of CNS abnormality in HIV disease. Journal of neuroscience methods. Elsevier; 2012;206:176–182.

92. Becker JT, Bajo R, Fabrizio M, et al. Functional connectivity measured with magnetoencephalography identifies persons with HIV disease. Brain imaging and behavior. Springer; 2012;6:366–373.

93. Babiloni C, Buffo P, Vecchio F, et al. Cortical sources of resting-state EEG rhythms in “experienced” HIV subjects under antiretroviral therapy. Clinical Neurophysiology. Elsevier; 2014;125:1792–1802.

94. Babiloni C, Pennica A, Del Percio C, et al. Abnormal cortical sources of resting state electroencephalographic rhythms in single treatment-naïve HIV individuals: A statistical z-score index. Clinical Neurophysiology. Elsevier; 2016;127:1803–1812.

95. Babiloni C, Vecchio F, Buffo P, et al. Cortical sources of resting-state EEG rhythms are abnormal in naïve HIV subjects. Clinical neurophysiology. Elsevier; 2012;123:2163–2171.

96. Barry RJ, De Blasio FM. EEG differences between eyes-closed and eyes-open resting remain in healthy ageing. Biological psychology. Elsevier; 2017;129:293–304.

97. Lodder SS, van Putten MJ. Automated EEG analysis: Characterizing the posterior dominant rhythm. Journal of neuroscience methods. Elsevier; 2011;200:86–93.

98. Aurlien H, Gjerde I, Aarseth J, et al. EEG background activity described by a large computerized database. Clinical Neurophysiology. Elsevier; 2004;115:665–673.

99. Knyazeva MG, Barzegaran E, Vildavski VY, Demonet J-F. Aging of human alpha rhythm. Neurobiology of aging. Elsevier; 2018;69:261–273.

100. Vysata O, Kukal J, Prochazka A, Pazdera L, Valis M. Age-related changes in the energy and spectral composition of EEG. Neurophysiology. Springer; 2012;44:63–67.

101. Babiloni C, Binetti G, Cassarino A, et al. Sources of cortical rhythms in adults during physiological aging: a multicentric EEG study. Human brain mapping. Wiley Online Library; 2006;27:162–172.

102. Gaál ZA, Boha R, Stam CJ, Molnár M. Age-dependent features of EEG-reactivity—Spectral, complexity, and network characteristics. Neuroscience letters. Elsevier; 2010;479:79–84.

103. Scally B, Burke MR, Bunce D, Delvenne J-F. Resting-state EEG power and connectivity are associated with alpha peak frequency slowing in healthy aging. Neurobiology of aging. Elsevier; 2018;71:149–155.

104. Heinrichs-Graham E, Wilson TW. Is an absolute level of cortical beta suppression required for proper movement? Magnetoencephalographic evidence from healthy aging. Neuroimage. Elsevier; 2016;134:514–521.

105. Rossiter HE, Davis EM, Clark EV, Boudrias M-H, Ward NS. Beta oscillations reflect changes in motor cortex inhibition in healthy ageing. Neuroimage. Elsevier; 2014;91:360–365.

106. Volf N, Gluhih A. Background cerebral electrical activity in healthy mental aging. Human Physiology. Springer; 2011;37:559–567.

107. Arif Y, Wiesman AI, O'Neill J, et al. The age-related trajectory of visual attention neural function is altered in adults living with HIV: A cross-sectional MEG study. EBioMedicine. Elsevier; 2020;61:103065.

108. Lew BJ, O'Neill J, Rezich MT, et al. Interactive effects of HIV and aging on neural oscillations: independence from neuropsychological performance. Brain Communications. Epub 2020.

109. Spooner RK, Wiesman AI, O'Neill J, et al. Prefrontal gating of sensory input differentiates cognitively impaired and unimpaired aging adults with HIV. Brain Communications. Oxford University Press; 2020;2:fcaa080.

110. Groff BR, Wiesman AI, Rezich MT, et al. Age-related visual dynamics in HIV-infected adults with cognitive impairment. Neurology-Neuroimmunology Neuroinflammation. AAN Enterprises; 2020;7.

111. Wiesman AI, Rezich MT, O'Neill J, et al. Epigenetic markers of aging predict the neural oscillations serving selective attention. Cerebral Cortex. Oxford University Press; 2020;30:1234–1243.

112. Doctor Klioze. MRI: Basic Physics & a Brief History [online]. Youtube. Accessed at: https://www.youtube.com/watch?v=djAxjtN_7VE.

113. Mechelli A, Price C, Friston K, Ashburner J. Voxel-Based Morphometry of the Human Brain: Methods and Applications. CMIR. 2005;1:105–113.

114. Logothetis NK, Pauls J, Augath M, Trinath T, Oeltermann A. Neurophysiological investigation of the basis of the fMRI signal. nature. Nature Publishing Group; 2001;412:150–157.

115. Yeo BT, Krienen FM, Sepulcre J, et al. The organization of the human cerebral cortex estimated by intrinsic functional connectivity. Journal of neurophysiology. American Physiological Society Bethesda, MD; Epub 2011.

116. Hansen P, Kringelbach M, Salmelin R. MEG: An Introduction to Methods. Oxford University Press; 2010.

117. Gaser C, Dahnke R. CAT-a computational anatomy toolbox for the analysis of structural MRI data. HBM. 2016;2016:336–348.

118. Manjón JV, Coupé P, Martí-Bonmatí L, Collins DL, Robles M. Adaptive non-local means denoising of MR images with spatially varying noise levels: Spatially Adaptive Nonlocal Denoising. J Magn Reson Imaging. 2010;31:192–203.

119. Rajapakse JC, Giedd JN, Rapoport JL. Statistical approach to segmentation of single-channel cerebral MR images. IEEE Trans Med Imaging. 1997;16:176–186.

120. Ashburner J, Friston KJ. Unified segmentation. Neuroimage. Elsevier; 2005;26:839–851.

121. Tohka J, Zijdenbos A, Evans A. Fast and robust parameter estimation for statistical partial volume models in brain MRI. NeuroImage. 2004;23:84–97.

122. Dahnke R, Yotter RA, Gaser C. Cortical thickness and central surface estimation. Neuroimage. Elsevier; 2013;65:336–348.

123. Yotter RA, Dahnke R, Thompson PM, Gaser C. Topological correction of brain surface meshes using spherical harmonics. Human brain mapping. Wiley Online Library; 2011;32:1109–1124.

124. Yotter RA, Thompson PM, Gaser C. Algorithms to improve the reparameterization of spherical mappings of brain surface meshes. Journal of Neuroimaging. Wiley Online Library; 2011;21:e134–e147.

125. Yan C-G, Wang X-D, Zuo X-N, Zang Y-F. DPABI: data processing & analysis for (resting-state) brain imaging. Neuroinformatics. Springer; 2016;14:339–351.

126. Power JD, Barnes KA, Snyder AZ, Schlaggar BL, Petersen SE. Spurious but systematic correlations in functional connectivity MRI networks arise from subject motion. Neuroimage. Elsevier; 2012;59:2142–2154.

127. Friston KJ, Williams S, Howard R, Frackowiak RS, Turner R. Movement-related effects in fMRI time-series. Magnetic resonance in medicine. Wiley Online Library; 1996;35:346–355.

128. Behzadi Y, Restom K, Liau J, Liu TT. A component based noise correction method (CompCor) for BOLD and perfusion based fMRI. Neuroimage. Elsevier; 2007;37:90–101.

129. Patel AX, Kundu P, Rubinov M, et al. A wavelet method for modeling and despiking motion artifacts from resting-state fMRI time series. Neuroimage. Elsevier; 2014;95:287–304.

130. Cordes D, Haughton VM, Arfanakis K, et al. Frequencies contributing to functional connectivity in the cerebral cortex in “resting-state” data. American Journal of Neuroradiology. Am Soc Neuroradiology; 2001;22:1326–1333.

131. Doucet GE, Lee WH, Frangou S. Evaluation of the spatial variability in the major resting-state networks across human brain functional atlases. Human brain mapping. Wiley Online Library; 2019;40:4577–4587.

132. Doucet GE, Rasgon N, McEwen BS, Micali N, Frangou S. Elevated body mass index is associated with increased integration and reduced cohesion of sensory-driven and internally guided resting-state functional brain networks. Cerebral Cortex. Oxford University Press; 2018;28:988–997.

133. Fonov VS, Evans AC, McKinstry RC, Almli C, Collins D. Unbiased nonlinear average age-appropriate brain templates from birth to adulthood. NeuroImage. Epub 2009.:S102.

134. Taulu S, Simola J. Spatiotemporal signal space separation method for rejecting nearby interference in MEG measurements. Physics in Medicine & Biology. IOP Publishing; 2006;51:1759.

135. Niso G, Tadel F, Bock E, Cousineau M, Santos A, Baillet S. Brainstorm Pipeline Analysis of Resting-State Data From the Open MEG Archive. Frontiers in neuroscience. Frontiers; 2019;13:284.

136. Ille N, Berg P, Scherg M. Artifact correction of the ongoing EEG using spatial filters based on artifact and brain signal topographies. Journal of clinical neurophysiology. LWW; 2002;19:113–124.

137. Uusitalo MA, Ilmoniemi RJ. Signal-space projection method for separating MEG or EEG into components. Medical and Biological Engineering and Computing. Springer; 1997;35:135–140.

138. Baillet S, Mosher JC, Leahy RM. Electromagnetic brain mapping. IEEE Signal processing magazine. Ieee; 2001;18:14–30.

139. Huang M, Mosher JC, Leahy R. A sensor-weighted overlapping-sphere head model and exhaustive head model comparison for MEG. Physics in Medicine & Biology. IOP Publishing; 1999;44:423.

140. Dale AM, Liu AK, Fischl BR, et al. Dynamic statistical parametric mapping: combining fMRI and MEG for high-resolution imaging of cortical activity. Neuron. Elsevier; 2000;26:55–67.

141. Aryee MJ, Jaffe AE, Corrada-Bravo H, et al. Minfi: a flexible and comprehensive Bioconductor package for the analysis of Infinium DNA methylation microarrays. Bioinformatics. Oxford University Press; 2014;30:1363–1369.

142. Riboli E, Hunt KJ, Slimani N, et al. European Prospective Investigation into Cancer and Nutrition (EPIC): study populations and data collection. Public health nutrition. Cambridge University Press; 2002;5:1113–1124.

143. Houseman EA, Accomando WP, Koestler DC, et al. DNA methylation arrays as surrogate measures of cell mixture distribution. BMC bioinformatics. Springer; 2012;13:86.

144. Antinori A, Arendt G, Becker J, et al. Updated research nosology for HIV-associated neurocognitive disorders. Neurology. AAN Enterprises; 2007;69:1789–1799.

145. Friston KJ, Holmes A, Poline J-B, Price CJ, Frith CD. Detecting activations in PET and fMRI: levels of inference and power. Neuroimage. Elsevier; 1996;4:223–235.

146. Roiser J, Linden D, Gorno-Tempinin M, Moran R, Dickerson B, Grafton S. Minimum statistical standards for submissions to Neuroimage: Clinical. NeuroImage: Clinical. Elsevier; 2016;12:1045.

147. Ge Y, Grossman RI, Babb JS, Rabin ML, Mannon LJ, Kolson DL. Age-related total gray matter and white matter changes in normal adult brain. Part I: volumetric MR imaging analysis. American journal of neuroradiology. Am Soc Neuroradiology; 2002;23:1327–1333.

148. Paul R, Cohen R, Navia B, Tashima K. Relationships between cognition and structural neuroimaging findings in adults with human immunodeficiency virus type-1. Neuroscience & Biobehavioral Reviews. Elsevier; 2002;26:353–359.

149. Thurnher MM, Judith Donovan Post M. The Uses of Structural Neuroimaging in the Brain in HIV-1-Infected Patients. The Spectrum of Neuro-AIDS Disorders: Pathophysiology, Diagnosis, and Treatment. Wiley Online Library; Epub 2008.:245–272.

150. O'connor E, Zeffiro TA, Zeffiro TA. Brain structural changes following HIV infection: meta-analysis. American Journal of Neuroradiology. Am Soc Neuroradiology; 2018;39:54–62.

151. Ghafouri M, Amini S, Khalili K, Sawaya BE. HIV-1 associated dementia: symptoms and causes. Retrovirology. BioMed Central; 2006;3:28.

152. Su T, Schouten J, Geurtsen GJ, et al. Multivariate normative comparison, a novel method for more reliably detecting cognitive impairment in HIV infection. Aids. LWW; 2015;29:547–557.

153. Wang Z, Molsberry SA, Cheng Y, et al. Cross-sectional analysis of cognitive function using multivariate normative comparisons in men with HIV disease. Aids. LWW; 2019;33:2115–2124.

154. Lemaitre H, Goldman AL, Sambataro F, et al. Normal age-related brain morphometric changes: nonuniformity across cortical thickness, surface area and gray matter volume? Neurobiology of Aging. 2012;33:617.e1-617.e9.

155. Ances BM, Hammoud DA. Neuroimaging of HIV-associated neurocognitive disorders (HAND): Current Opinion in HIV and AIDS. 2014;9:545–551.

156. Patel SH, Kolson DL, Glosser G, et al. Correlation between percentage of brain parenchymal volume and neurocognitive performance in HIV-infected patients. American journal of neuroradiology. Am Soc Neuroradiology; 2002;23:543–549.

157. Sanford R, Strain J, Dadar M, et al. HIV infection and cerebral small vessel disease are independently associated with brain atrophy and cognitive impairment: AIDS. 2019;33:1197–1205.

158. Sanford R, Ances BM, Meyerhoff DJ, et al. Longitudinal Trajectories of Brain Volume and Cortical Thickness in Treated and Untreated Primary Human Immunodeficiency Virus Infection. Clinical Infectious Diseases. 2018;67:1697–1704.

159. Fama R, Rosenbloom MJ, Sassoon SA, Rohlfing T, Pfefferbaum A, Sullivan EV. Thalamic volume deficit contributes to procedural and explicit memory impairment in HIV infection

with primary alcoholism comorbidity. Brain imaging and behavior. Springer; 2014;8:611–620.

160. Sanford R, Fellows LK, Ances BM, Collins DL. Association of Brain Structure Changes and Cognitive Function With Combination Antiretroviral Therapy in HIV-Positive Individuals. JAMA Neurol. 2018;75:72.

161. Horvath S, Zhang Y, Langfelder P, et al. Aging effects on DNA methylation modules in human brain and blood tissue. Genome Biol. 2012;13:R97.

162. Saad ZS, Gotts SJ, Murphy K, et al. Trouble at rest: how correlation patterns and group differences become distorted after global signal regression. Brain connectivity. Mary Ann Liebert, Inc. 140 Huguenot Street, 3rd Floor New Rochelle, NY 10801 USA; 2012;2:25–32.

163. Weissenbacher A, Kasess C, Gerstl F, Lanzenberger R, Moser E, Windischberger C. Correlations and anticorrelations in resting-state functional connectivity MRI: a quantitative comparison of preprocessing strategies. Neuroimage. Elsevier; 2009;47:1408–1416.

164. Chaganti JR, Heinecke A, Gates TM, Moffat KJ, Brew BJ. Functional Connectivity in Virally Suppressed Patients with HIV-Associated Neurocognitive Disorder: A Resting-State Analysis. AJNR Am J Neuroradiol. 2017;38:1623–1629.

165. Guha A, Wang L, Tanenbaum A, et al. Intrinsic network connectivity abnormalities in HIV-infected individuals over age 60. Journal of neurovirology. Springer; 2016;22:80–87.

166. Ng KK, Lo JC, Lim JK, Chee MW, Zhou J. Reduced functional segregation between the default mode network and the executive control network in healthy older adults: a longitudinal study. Neuroimage. Elsevier; 2016;133:321–330.

167. Damoiseaux JS, Greicius MD. Greater than the sum of its parts: a review of studies combining structural connectivity and resting-state functional connectivity. Brain Structure and Function. Springer; 2009;213:525–533.

168. Clyde MA, Ghosh J, Littman ML. Bayesian adaptive sampling for variable selection and model averaging. Journal of Computational and Graphical Statistics. Taylor & Francis; 2011;20:80–101.

169. Wetzels R, Matzke D, Lee MD, Rouder JN, Iverson GJ, Wagenmakers E-J. Statistical evidence in experimental psychology: An empirical comparison using 855 t tests. Perspectives on Psychological Science. Sage Publications Sage CA: Los Angeles, CA; 2011;6:291–298.

170. Lew BJ, Fitzgerald EE, Ott, Lauren R., Penhale SH, Wilson TW. Three-year reliability of MEG resting state oscillatory power. in prep.

171. Fernández-Cruz AL, Fellows LK. The electrophysiology of neuroHIV: a systematic review of EEG and MEG studies in people with HIV infection since the advent of highly-active antiretroviral therapy. Clinical Neurophysiology. Elsevier; 2017;128:965–976.

172. Clark CR, Veltmeyer MD, Hamilton RJ, et al. Spontaneous alpha peak frequency predicts working memory performance across the age span. International journal of psychophysiology. Elsevier; 2004;53:1–9.

173. Muthukumaraswamy SD, Myers JF, Wilson SJ, et al. The effects of elevated endogenous GABA levels on movement-related network oscillations. Neuroimage. Elsevier; 2013;66:36–41.

174. Harmony T. The functional significance of delta oscillations in cognitive processing. Frontiers in integrative neuroscience. Frontiers; 2013;7:83.

175. Vlahou EL, Thurm F, Kolassa I-T, Schlee W. Resting-state slow wave power, healthy aging and cognitive performance. Scientific reports. Nature Publishing Group; 2014;4:1–6.

176. Minhas PS, Latif-Hernandez A, McReynolds MR, et al. Restoring metabolism of myeloid cells reverses cognitive decline in ageing. Nature. Nature Publishing Group; Epub 2021.:1–7.

177. Webb TW, Igelström KM, Schurger A, Graziano MS. Cortical networks involved in visual awareness independent of visual attention. Proceedings of the National Academy of Sciences. National Acad Sciences; 2016;113:13923–13928.

178. Menon V. Salience network. Elsevier; Epub 2015.

179. Meyer A-CL, Boscardin WJ, Kwasa JK, Price RW. Is it time to rethink how neuropsychological tests are used to diagnose mild forms of HIV-associated neurocognitive disorders? Impact of false-positive rates on prevalence and power. Neuroepidemiology. Karger Publishers; 2013;41:208–216.

180. Tewarie P, Hillebrand A, van Dellen E, et al. Structural degree predicts functional network connectivity: a multimodal resting-state fMRI and MEG study. NeuroImage. Elsevier; 2014;97:296–307.

181. Brookes MJ, Hale JR, Zumer JM, et al. Measuring functional connectivity using MEG: methodology and comparison with fcMRI. Neuroimage. Elsevier; 2011;56:1082–1104.

182. Ciavatta VT, Bichler EK, Speigel IA, et al. In vitro and ex vivo neurotoxic effects of efavirenz are greater than those of other common antiretrovirals. Neurochemical research. Springer; 2017;42:3220–3232.

183. Apostolova N, Blas-Garcia A, Galindo MJ, Esplugues JV. Efavirenz: what is known about the cellular mechanisms responsible for its adverse effects. European journal of pharmacology. Elsevier; 2017;812:163–173.